DISSERTATION

Elastoplastic instabilities of lamellar structures

ausgeführt zum Zwecke der Erlangung des akademischen Grades eines
Doktors der technischen Wissenschaften unter der Leitung von

O. Univ. Prof. Dipl.-Ing. Dr.techn. Franz G. RAMMERSTORFER
E317
Institut für Leichtbau und Struktur-Biomechanik

eingereicht an der Technischen Universität Wien
Fakultät für Maschinenbau und Betriebswissenschaften

von

Dipl.-Ing. Benedikt DAUM
Matrikelnummer: 0017473
Haidingergasse 17/3
A-1030 Wien

Wien, im Juli 2015   Benedikt Daum

Abstract

The present work investigates local bucking in layered structures comprising a thin elastic layer (lamella) embedded in a comparatively thick matrix under in-layer-plane loading. The matrix is considered to be in an elastoplastic state at the initiation of the lamella-buckling. As an application, this setup can be thought to represent the microstructure of certain alloys at the level of an individual metal-grain, although the presented results are not limited to such a setup.

The presence of inelastic deformations in the matrix requires that stability of the loading process is investigated rather then the stability of isolated equilibrium states. For irreversible deformations these two concepts of stability do not coincide. A deformation process following an equilibrium path involving inelastic deformations may become nonunique and can bifurcate even while the individual states that comprise the path are in stable equilibrium when considered isolated. The theory that allows for the treatment of inelastic bifurcations is reviewed from the literature and the present problem is formulated in its context.

The implications resulting from the theory of inelastic instabilities, with particular regard for the post buckling behaviour, are demonstrated using a simplified model that allows for analytical treatment of the problem. Taking advantage of the homogeneous prebuckling stress distribution the governing equations for plane strain J_2-plasticity are solved in a simplified manner for more refined models, and approximate analytical results for the bifurcation load where obtained.

Analytical considerations are complemented by numerical simulations to validate the results. For the simulations a suitable unit cell-model was developed and verified by independent simulations. Comparison of analytical predictions and numerical results are in good accordance for the case of ideal plasticity in the matrix and provide some insight in the underlying mechanisms for the case of a hardening matrix. For both cases an analytical interpretation of the obtained buckling mode is given.

Kurzfassung

Ziel der vorliegenden Arbeit ist die Untersuchung lokaler Beulmodi in geschichteten Strukturen aus dünnen, elastischen Lamellen eingebettet in eine vergleichsweise dickwandige Matrixschicht unter Belastung in Richtung der Lamellenebene. Dabei wird von elastoplastischem Materialverhalten in der Matrixschicht ausgegangen. Die in der Arbeit gewonnenen Erkenntnisse lassen sich unter gewissen Annahmen auf die mikrostrukturierte Metalllegierungen anwenden, sind jedoch nicht auf diese beschränkt.

Die Lösung des Stabilitätsproblems in Gegenwart pfadabhängigen Materialverhaltens bildet das Kernthema der Arbeit wobei ein weiter gefasster Stabilitätsbegriff aus der Literatur Anwendung findet. Unter anderem ist eine Unterscheidung zwischen der Stabilität von Gleichgewichtslagen und der physischen Realisierbarkeit von Belastungspfaden die aus diesen Gleichgewichtszuständen gebildet sind zu treffen. Die entsprechende Theorie wird überblicksartig dargestellt und auf das vorliegende Problem angewandt.

Zur Beschreibung des Problems wurden mehrere analytische Modelle mit unterschiedlichen Abstraktionsgraden entwickelt. Ein stark vereinfachtes, einführendes Modell dient zur ersten Annäherung an das Problem und erlaubt die Demonstration der gegenüber dem rein elastisch gebetteten Beulproblem substanziell unterschiedlichen Systemverhalten, insbesondere im Nachbeulbereich. Ein weiteres Modell für den Sonderfall der idealen Von Mises-Plastizität erlaubt die Angabe eines analytischen Ausdrucks für die Beullast. Allgemeinere Fälle werden ebenfalls in stark vereinfachter Weise behandelt.

Die analytischen Betrachtungen werden zur Validierung durch numerische Untersuchen ergänzt. Dazu wurden geeignete Einheitszellenmodelle entwickelt. Durch Vergleich von analytischen Vorhersagen mit numerischen Ergebnissen wird gezeigt, dass für den idealplastischen Sonderfall eine gute quantitative Übereinstimmung gegeben ist, und im allgemeineren Fall die analytische Methoden eine Interpretation des Systemverhaltens ermöglichen.

Acknowledgments

Contents

Contents

1 Introduction

Microscopic material testing is a common method in modern material research [Kiener et al., 2009] as it allows the determination of local mechanical properties at a very high spatial resolution. These test are commonly performed as compression tests, due to the more complicated sample preparation and test setup for micro-tensile testing. Samples for compressive testing are typically prepared by using the focused ion beam milling technique to remove surrounding material so that a rather short and stocky 'micropillar' remains. This micropillar can be tested by compressing it with an microscopic loading device. These tests frequently extend deep into the elastoplastic regime and the compressive loading may give rise to several instability phenomena, for instance, beam-like buckling of the pillar was reported in [Zhang et al., 2006, Rester et al., 2011] in spite of the relatively low aspect ratio, i.e. pillar height to the sample diameter. It is of interest for the experimenter in how far buckling as a phenomenon inherent to the structure of the sample rather than its pure material stiffness affect the test-results, and to which degree test results reflect actual material properties. The author investigated the effect of beam-like global buckling of micropillar compression samples in [Daum et al., 2013]. The circumstance that the material is in whole or partially in an yielding state is crucial for this purpose as it requires treatment of the problem by the theory of stability for path-dependent processes, first developed by Hill [Hill, 1958]. In the presence of plasticity even structures that are not susceptible to instability in the elastic range might buckle, as is the case for the low aspect ratio pillar.

At the microscopic scale material properties are often inhomogeneous, either due to the presence of different material phases or because they comprise multiple grains. In case of small grains the Hall-Petch size-effects might also contribute to inhomogeneity. This inhomogeneous stiffness distribution can trigger additional buckling modes which are local to the microstructure as opposed to the global beam-like buckling mode. It is these local forms of instabilities that the present work is concerned with, and the author strifes to investigate the effect of microstructural inhomogeneity on the apparent stiffness. The local buckling due local inhomogeneities is of course not limited to micropillar compression tests and can occur in bulk material as well. For the actual microstructure, however, only a particular scenario is considered here which is a lamellar compound of hard and thin elastic lamellae embedded in a rather soft, yielding matrix. Such lamellar structures appear, for instance, in certain kinds of Titanium-Aluminide alloys that have their manufacturing conditions controlled in a way that generates thin and hard α_2-Ti$_3$Al-lamella embedded in a matrix of the γ-TiAl phase by crystal-twinning, cf. Fig. 1.1(a). The yield-stress in the individual phases differs, and is affected by the crystal-orientation, possibly a Hall-Petch size effect in the thin lamellae [Maruyama et al., 2004, Edalati et al., 2012] and other mechanisms. This usually leads to a much higher yield-stress in the lamella. So for

the example of the lamellar Titanium-Aluminide alloy or for any other generic lamellar compound where there is a strong disparity of yield strength between the lamella and the matrix material in conjunction with a greatly reduced material stiffness in the elastoplastic regime, buckling of the lamella might occur when the matrix is in an yielding state. The study of the effects lamella buckling in an elastoplastic matrix on the apparent stiffness-properties of the matrix-lamella-compound is the principal interest of the present work.

The present work is mainly concerned with lamellar structures on a microscopic level. Even though, no length scale is involved and the results apply to macroscopic bodies as well as microscopic ones, it is shown by the investigations that ep-instabilities in lamellar structures often require very high stresses. In a macroscopic structures, like e.g. a sandwich structure, this stress is likely exceed the lamella yield stress before any ep-instabilities become relevant. On a microscopic level, however, size effects might be present and cause strengthening for very thin lamella to such an extend that they remain elastic even at very high levels of stress.

For microscopic samples, the matrix might constitute few crystals or even a single crystal. In that case crystal plasticity usually must be applied to accurately capture the behaviour of the matrix. The present work uses J_2-plasticity, however, and, therefore, additional considerations are required to check the applicability of this simplification. In some cases the application of J_2-plasticity can give sufficiently accurate results even for single crystals. For instance, if the deformation mechanism is dominated by twinning

For instance, when the actual irreversible deformation mechanism is dominated by twinning, cf. e.g. [Rester et al., 2011] for details regarding the case of Titanium Aluminides, several twin systems are may be activated simultaneously, and the resulting behaviour can be expected to be nearly isotropic. A further reason for using von Mises plasticity is the fact that crystal plasticity requires material data for the critical resolved shear stress, critical resolved twin stress and hardening parameters for the respective slip systems that are difficult to obtain or choose in a meaningful way. This data set is compacted by a global yield stress and the hardening parameter(s) in the case of von Mises plasticity.

It is the foremost intend of this work to point out the underlying mechanisms behind the phenomena, and for this reason analytical considerations seem to be indispensable. However, due to to the involved nature of the present problem, an exact and general description is out of reach and analytical solutions are limited to certain assumptions and simplifications. Nevertheless, even approximations can help to give an interpretation to more precise results obtained by numerical methods e.g. by finite element analysis. The structure of the present work follows this philosophy by starting off with a presentation of the plasticity formulation used and a literature-review on the subject of inelastic stability and uniqueness. This provides the foundation for a highly simplified model with incompatible deformation modes. The simplicity allows for an in-depth examination that is inaccessible for a more faithful model. Throughout the work the expressions 'horizontal', 'vertical' are used to refer to the 1 and 2-direction respectively, while 'left'/'right' and 'top'/'bottom' are used along the same line. Numerical results are given in generic units such as force units [F] or length units [L]. Where possible material parameters are chosen so that that they are of a similar magnitude as some real materials for Newtons and Millimeters as base units, however, no effort is made to represent a particular material.
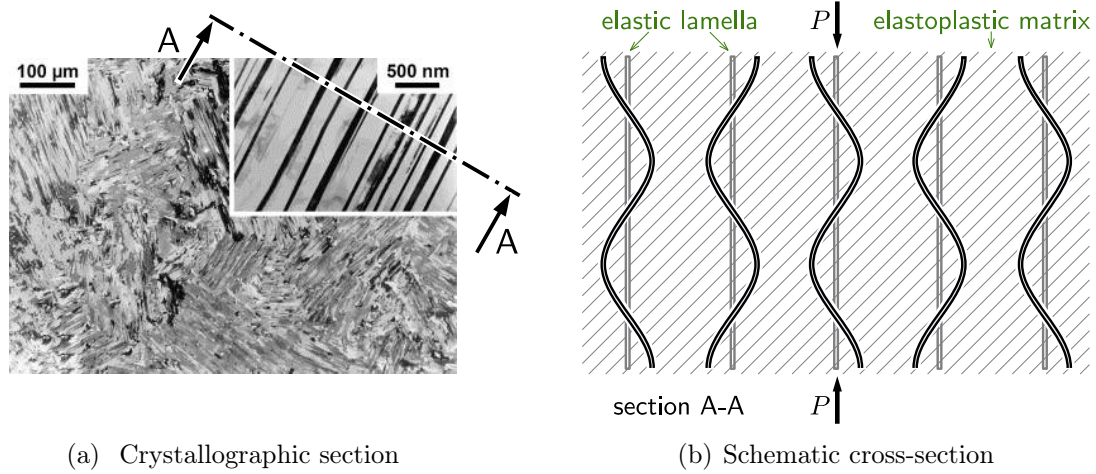
(a) Crystallographic section (b) Schematic cross-section

Figure 1.1: Microscope image of an array of Ti$_3$Al-lamella in a TiAl-matrix [Clemens et al., 2006] and it idealized representation. The lamella spacing is assumed constant and the hypothetical buckling mode is shown in the right picture

The analytical calculations where aided by the computer algebra program 'Mathematica' in the version 9 by Wolfram Research, Inc. For the numerical simulations the commercial finite element program 'Abaqus' by Dassault Systmes Simulia Corp. was used. Plots where either created directly in Mathematica or using the Python-library 'matplotlib'.

2 Plasticity formulation for bifurcation and stability analysis

The present chapter serves to discuss the plasticity formulation used in the subsequent considerations. The plasticity model used is a standard phenomenological isotropic-hardening Von-Mises model and the resulting equations are well known. It is necessary, however, to embed this model in a formulation that allows for the treatment of problems involving bifurcation and stability phenomena. Some complication arises from the need to account for the effect of stress in a preloaded state on the stiffness and for this purpose a finite strain formulation is required. Nevertheless, the state that is checked for either stability or bifurcation is supposed to be known, and only infinitesimal close neighbour states need to be considered. Initial and current state can thus be identified with each other and this results in some simplification over the fully nonlinear case.

It is well known that elastoplastic materials are path dependent and the constitutive law can not relate stress and strain directly, but rather only rates thereof. This path-dependence is the cause of some remarkable effects and require that a distinction between the concepts of bifurcation and instability is made. This is a prominent feature of elasto-plasticity without equivalent in a purely elastic structure, cf. chapter 3.

In the present work only quasi-static deformation processes are considered. Loading is controlled by a common proportionality factor, changing only indefinitely slow with respect to actual time. The rate of some quantity taken with respect to the load proportionality factor is indicated by a solid dot over the symbol.

An other important aspect is that for elastic metal structures the stresses are usually low in comparison to the elastic moduli, and their destabilizing effect are essentially connected to rotations. When plasticity is present, however, the stresses can reach the same order of magnitude as the incremental moduli, and deformation modes without rotations can be relevant as well.

The notation used prefers capital letters for Lagrangian or mixed, i.e. two-point, quantities, while lower case letters are used for Eulerian quantities, where feasible. The same applies to the capitalization of indices.

2.1 Strain rate decomposition

For the purpose of formulating the flow rule it is necessary to refer to the finite strain equivalent of the plastic strain rate. The approach used by [McMeeking and Rice, 1975] in the context of bifurcation analysis is based on a straightforward adaptation of the Prandtl-Reuss equations to Eulerian strain rates. Starting with the additive decomposition of the velocity and its gradient, $\underset{\sim}{l}$, into elastic and plastic contributions the symmetric part of the velocity gradient, the rate of deformation tensor $\underset{\sim}{d}$, can be split additively as well. The symbol $\underset{\sim}{w}$ refers to the spin tensor and superscript e or p indicate the elastic and plastic part, respectively.

$$
\begin{aligned}
\underset{\sim}{l} &= \operatorname{grad} \underset{\sim}{v} = \underset{\sim}{l}^{e} + \underset{\sim}{l}^{p} \\
\underset{\sim}{d} &= \operatorname{sym}(\underset{\sim}{l}^{e}) + \operatorname{sym}(\underset{\sim}{l}^{p}) = \underset{\sim}{d}^{e} + \underset{\sim}{d}^{p} \tag{2.1_1} \\
\underset{\sim}{w} &= \operatorname{skw}(\underset{\sim}{l}^{e}) + \operatorname{skw}(\underset{\sim}{l}^{p}) = \underset{\sim}{w}^{e} + \underset{\sim}{w}^{p} \tag{2.1_2}
\end{aligned}
$$

This decomposition is, however, not the only one possible and the proper separation of elastic and plastic deformation is a subject of research in finite strain plasticity. As a counter example suppose a multiplicative decomposition of the deformation gradient $\underset{\sim}{F} = \underset{\sim}{F}^{e}\underset{\sim}{F}^{p}$, as introduced by Lee [Lee, 1981], with $\underset{\sim}{F}^{e} = \underset{\sim}{v}^{e}\underset{\sim}{R}^{e}$ as the deformation gradient between an unloaded intermediate configuration and the spatial configuration. The rotation $\underset{\sim}{R}^{e}$ is ambiguous in this decomposition and is set to $\underset{\sim}{1}$ by definition. The symbol $\underset{\sim}{v}^{e}$ stands for the elastic part of the Eulerian stretch tensor. This gives the following expressions for the rate of deformation- and spin-tensors [Wu, 2004]:

$$
\begin{aligned}
\underset{\sim}{d} &= \underset{\sim}{d}^{e} + \operatorname{sym}(\underset{\sim}{v}^{e}\underset{\sim}{d}^{p}\underset{\sim}{v}^{e-1}) + \operatorname{sym}(\underset{\sim}{v}^{e}\underset{\sim}{w}^{p}\underset{\sim}{v}^{e-1}) \tag{2.2_1} \\
\underset{\sim}{w} &= \underset{\sim}{w}^{e} + \operatorname{skw}(\underset{\sim}{v}^{e}\underset{\sim}{d}^{p}\underset{\sim}{v}^{e-1}) + \operatorname{skw}(\underset{\sim}{v}^{e}\underset{\sim}{w}^{p}\underset{\sim}{v}^{e-1}) \tag{2.2_2}
\end{aligned}
$$

For (2.2) and (2.1) to coincide the elastic strain has to be assumed small, i.e. $\underset{\sim}{v}^{e} \to \underset{\sim}{1}$. Nevertheless, for the purpose of analysing bifurcation and stability the current configuration will be identified with the material configuration, and (2.1) holds without additional assumptions.

The additive strain rate decomposition, together with the restriction to small elastic stretch, is also used in the finite element simulation software Abaqus, which was used for the simulations presented in this work [Hibbitt et al., 1997].

2.2 Eulerian tangent material stiffness

The material properties relate to the Cauchy stress, the constitutive law is, thus, given in terms of Eulerian quantities in the first place. Again following [McMeeking and Rice, 1975] a straightforward method to obtain the Eulerian tangent material stiffness for an additive decomposition scheme is to use a finite strain analogon to the classical Prandtl-Reuss equations. The equations are adapted by replacing the rates of small strain by the

rate of deformation tensor. With the elastic response taken to be the same as in linear elasticity the rate of Cauchy stress is:

$$\dot{\underset{\sim}{\sigma}} = \underset{\approx}{\mathbb{E}} : (\underset{\sim}{\mathbf{d}} - \underset{\sim}{\mathbf{d}}^{\mathrm{p}}) \tag{2.3}$$

With $\underset{\approx}{\mathbb{E}}$ as the small strain elasticity tensor:

$$\underset{\approx}{\mathbb{E}} = (\lambda \delta_{ij}\delta_{kl} + \mu \delta_{ik}\delta_{jl} + \mu \delta_{il}\delta_{jk}) \, \underline{\mathbf{e}}_i \otimes \underline{\mathbf{e}}_j \otimes \underline{\mathbf{e}}_k \otimes \underline{\mathbf{e}}_l \tag{2.4}$$

The usual Lamé parameters are alternatively used as parameters for elasticity:

$$\lambda = \frac{\nu E}{(1 - 2\nu)(1 + \nu)}$$
$$\mu = \frac{\nu E}{2(1 + \nu)}$$

The Prandtl-Reuss equations in index notation:

$$\dot{\sigma}_{ij} = \lambda \delta_{ij} d_{kk} + 2\mu d_{ij} - 2\mu d_{ij}^{\mathrm{p}} \qquad\qquad i, j, k = 1, 2, 3 \tag{2.5}$$

The inverse relation is:

$$d_{ij} = \frac{1}{2\mu} \left[\dot{\sigma}_{ij} - \frac{\lambda}{3\lambda + 2\mu} \dot{\sigma}_{kk} \delta_{ij} \right] + d_{ij}^{\mathrm{p}} \qquad\qquad i, j, k = 1, 2, 3 \tag{2.6}$$

In the present work only classical Von Mises-plasticity with an associated plastic flow potential is considered. Together with an appropriate objective stress rate this allows for the existence of a rate potential which, as will be discussed below, is crucial for the theory invoked to investigate bifurcation and stability. The deviatoric stress tensor needed to formulate the yield function is indicated by an overscript chevron.

$$\hat{\underset{\sim}{\sigma}} = \underset{\sim}{\sigma} - \frac{1}{3} \underset{\sim}{\mathbf{1}} \operatorname{tr}(\underset{\sim}{\sigma}) \tag{2.7}$$

With the positive quantity κ, equal to $\sqrt{2/3}$ of the uniaxial yield stress, the Von Mises yield function is given as:

$$\mathcal{F} = \hat{\underset{\sim}{\sigma}} : \hat{\underset{\sim}{\sigma}} - \kappa^2 = 0 \tag{2.8}$$

Using a associated flow rule gives an expression that relates the plastic part of the rate of deformation tensor and the plastic consistency parameter, ϕ:

$$\underset{\sim}{\mathbf{d}}^{\mathrm{p}} = \frac{1}{2} \phi \frac{\partial \mathcal{F}}{\partial \underset{\sim}{\sigma}} = \phi \hat{\underset{\sim}{\sigma}} \tag{2.9}$$

2 Plasticity formulation for bifurcation and stability analysis

The consistency condition is given below, with the last equality due to the vanishing trace of $\hat{\underline{\sigma}}$:

$$\dot{\mathcal{F}} = 2\hat{\underline{\sigma}} : \dot{\hat{\underline{\sigma}}} - 2\kappa\dot{\kappa} = 2\hat{\underline{\sigma}} : \dot{\underline{\sigma}} - 2\kappa\dot{\kappa} = 0 \tag{2.10}$$

As hardening law only isotropic hardening is considered. Thus the rate of κ, proportional to the rate of the increase in uniaxial yield stress by the factor of $\sqrt{2/3}$, can be expressed by the product of a positive hardening factor θ and the magnitude of the rate of deformation tensor. Via normality and the yield condition $\mathcal{F} = 0$ this becomes:

$$\dot{\kappa} = \theta\|\underline{d}^{\mathrm{p}}\| = \theta\phi\|\hat{\underline{\sigma}}\| = \theta\phi\sqrt{\hat{\underline{\sigma}} : \hat{\underline{\sigma}}} = \theta\phi\kappa \tag{2.11}$$

The factor θ is related to the tangent modulus, E_t, by (2.12), both are in the following assumed constant. It can be related to the tangent modulus by considering the uniaxial case:

$$\|\underline{d}^{\mathrm{p}}\| = \sqrt{3/2}\,d_{11}^{\mathrm{p}} \qquad \dot{\kappa} = \sqrt{2/3}\,\dot{\sigma}_y \qquad d_{11}^{\mathrm{p}} = \dot{\sigma}_y\left(\frac{1}{E_t} - \frac{1}{E}\right)$$

$$\theta = \frac{2}{3}\frac{E_t E}{E - E_t} \tag{2.12}$$

Using the consistency condition (2.10), the elastic response (2.3) and the evolution equation for the isotropic hardening (2.11) the consistency parameter is obtained:

$$\hat{\underline{\sigma}} : \underline{\underline{\mathbb{E}}} : \underline{d} - \hat{\underline{\sigma}} : \underline{\underline{\mathbb{E}}} : \hat{\underline{\sigma}}\phi - \kappa^2\theta\phi = 0$$

$$\phi = \frac{\hat{\underline{\sigma}} : \underline{\underline{\mathbb{E}}} : \underline{d}}{\hat{\underline{\sigma}} : \underline{\underline{\mathbb{E}}} : \hat{\underline{\sigma}} + \kappa^2\theta} \tag{2.13}$$

The Eulerian elastoplastic tangent material stiffness tensor $\underline{\underline{\mathbb{L}}}^{\mathrm{p}}$ is thus:

$$\dot{\underline{\sigma}} = \underline{\underline{\mathbb{E}}} : \underline{d} - \underline{\underline{\mathbb{E}}} : \hat{\underline{\sigma}}\phi$$

$$\dot{\underline{\sigma}} = \left[\underline{\underline{\mathbb{E}}} - \frac{\underline{\underline{\mathbb{E}}} : \hat{\underline{\sigma}} \otimes \hat{\underline{\sigma}} : \underline{\underline{\mathbb{E}}}}{\hat{\underline{\sigma}} : \underline{\underline{\mathbb{E}}} : \hat{\underline{\sigma}} + \kappa^2\theta}\right] : \underline{d}$$

$$\underline{\underline{\mathbb{L}}}^{\mathrm{p}} = \underline{\underline{\mathbb{E}}} - \frac{\underline{\underline{\mathbb{E}}} : \hat{\underline{\sigma}} \otimes \hat{\underline{\sigma}} : \underline{\underline{\mathbb{E}}}}{\hat{\underline{\sigma}} : \underline{\underline{\mathbb{E}}} : \hat{\underline{\sigma}} + \kappa^2\theta} \tag{2.14}$$

The elastic tangent material stiffness tensor is, of course, symmetric. The elastoplastic tangent modulus for an associated flow rule is symmetric as well. The symmetry property will be of fundamental importance in chapter 3, since it allows for the introduction of a rate potential.

$$\underline{\underline{\mathbb{L}}} = \begin{cases} \underline{\underline{\mathbb{E}}} & : & \phi = 0 \\ \underline{\underline{\mathbb{L}}}^{\mathrm{p}} & : & \phi > 0 \end{cases} \tag{2.15}$$

2.3 Mixed tangent material stiffness

[Hill, 1958, Lubliner, 2008]; In the previous section the Eulerian tangent material stiffness was formulated. To obtain the Lagrangian form, customary in solid mechanics, a transformation is required. The Cauchy, Kirchhoff and first Piola-Kirchhoff (PK1) stress tensors are related according to (2.16) below. The symbol J stands for $\det(\underset{\sim}{\mathsf{F}})$, $\underset{\sim}{\boldsymbol{\tau}}$ and $\underset{\sim}{\mathsf{P}}$ are the Kirchhoff and the PK1-stress, respectively. It is advantageous to continue with the Kirchhoff stress, rather than the Cauchy stress, for reasons that become apparent further below.

$$\mathsf{J}\underset{\sim}{\boldsymbol{\sigma}} = \underset{\sim}{\boldsymbol{\tau}} = \underset{\sim}{\mathsf{P}}\underset{\sim}{\mathsf{F}}^{\mathsf{T}} \tag{2.16}$$

The quasi-static rates required for the formulation of the tangent are obtained by taking the material time derivative of (2.16).

$$\dot{\underset{\sim}{\boldsymbol{\tau}}} = \dot{\underset{\sim}{\mathsf{P}}}\underset{\sim}{\mathsf{F}}^{\mathsf{T}} + \underset{\sim}{\mathsf{P}}\dot{\underset{\sim}{\mathsf{F}}}^{\mathsf{T}} = \dot{\underset{\sim}{\mathsf{P}}}\underset{\sim}{\mathsf{F}}^{\mathsf{T}} + \underset{\sim}{\boldsymbol{\tau}}\underset{\sim}{\mathsf{F}}^{-\mathsf{T}}\dot{\underset{\sim}{\mathsf{F}}}^{\mathsf{T}} = \dot{\underset{\sim}{\mathsf{P}}}\underset{\sim}{\mathsf{F}}^{\mathsf{T}} + \underset{\sim}{\boldsymbol{\tau}}\underset{\sim}{\mathsf{l}}^{\mathsf{T}}$$

$$\dot{\underset{\sim}{\mathsf{P}}}\underset{\sim}{\mathsf{F}}^{\mathsf{T}} = \dot{\underset{\sim}{\boldsymbol{\tau}}} - \underset{\sim}{\boldsymbol{\tau}}\underset{\sim}{\mathsf{l}}^{\mathsf{T}} \tag{2.17}$$

The material time derivate of Kirchhoff-stress $\dot{\underset{\sim}{\boldsymbol{\tau}}}$ is a nonobjective quantity, i.e. it does not obey the standard tensor-transformation rule for a rigid body rotation superimposed on the spatial configuration. Therefore, it can not be used to formulate a constitutive relation. A remedy is provided by performing a pull back operation on $\underset{\sim}{\boldsymbol{\tau}}$ which yields the second Piola-Kirchhoff (PK2) stress tensor $\underset{\sim}{\mathsf{S}}$. The PK2-stress tensor is intrinsically independent of any rigid body rotations, since it is a total Lagrangian quantity and, therefore, its material time derivative $(\underset{\sim}{\mathsf{S}})^{\boldsymbol{\cdot}}$ is unaffected by any rigid body rotations on the spatial configuration. Performing the derivation on $\underset{\sim}{\mathsf{S}}$ and a subsequent push forward completes the operation and yields the objective Oldroyd-rate of Kirchhoff-stress, $\overset{\triangle}{\underset{\sim}{\boldsymbol{\tau}}}$. The pull back-derive-push forward process is called a Lie derivative.

$$\overset{\triangle}{\underset{\sim}{\boldsymbol{\tau}}} = \underset{\sim}{\mathsf{F}}(\underset{\sim}{\mathsf{F}}^{-1}\underset{\sim}{\boldsymbol{\tau}}\underset{\sim}{\mathsf{F}}^{-\mathsf{T}})^{\boldsymbol{\cdot}}\underset{\sim}{\mathsf{F}}^{\mathsf{T}} = \dot{\underset{\sim}{\boldsymbol{\tau}}} - \underset{\sim}{\mathsf{l}}\underset{\sim}{\boldsymbol{\tau}} - \underset{\sim}{\boldsymbol{\tau}}\underset{\sim}{\mathsf{l}}^{\mathsf{T}} \tag{2.18}$$

Other objective, but approximate, stress rates can be defined by using kinematic simplifications, e.g. by substituting the velocity gradient $\underset{\sim}{\mathsf{l}}$ in (2.18) by the spin tensor $\underset{\sim}{\boldsymbol{w}}$ the corotational Zaremba Jaumann-rate (ZJ-rate, $\overset{\circ}{\underset{\sim}{\boldsymbol{\tau}}}$) is obtained. For plasticity-problems the ZJ-rate is popular for some advantageous mathematical properties. It is important, however, to take the ZJ-rate of Kirchhoff stress, rather than Cauchy stress.

$$\overset{\circ}{\underset{\sim}{\boldsymbol{\tau}}} = \dot{\underset{\sim}{\boldsymbol{\tau}}} - \underset{\sim}{\boldsymbol{w}}\underset{\sim}{\boldsymbol{\tau}} + \underset{\sim}{\boldsymbol{\tau}}\underset{\sim}{\boldsymbol{w}} \tag{2.19}$$

Since an objective stress rate has been established, the constitutive relation can be formed by relating it to the rate of deformation tensor $\underset{\sim}{\boldsymbol{d}}$ via the Eulerian tangent material stiffness tensor $\underset{\approx}{\mathbb{L}}$.

$$\overset{\circ}{\underset{\sim}{\boldsymbol{\tau}}} = \underset{\approx}{\mathbb{L}} : \underset{\sim}{\boldsymbol{d}} \tag{2.20}$$

Equations (2.19) and (2.20) can be combined to eliminate $\dot{\underset{\approx}{\tau}}$ from (2.17):

$$\dot{\underline{P}}\underline{F}^{\mathsf{T}} = \underset{\approx}{\mathbb{L}} : \underline{d} + \underline{w}\underline{\tau} - \underline{\tau}\underline{w} - \underline{\tau}\underline{l}^{\mathsf{T}} = \underset{\approx}{\mathbb{L}} : \underline{d} + \underline{w}\underline{\tau} - \underline{\tau}\underline{w} - \underline{\tau}(\underline{d}^{\mathsf{T}} + \underline{w}^{\mathsf{T}})$$

$$\dot{\underline{P}}\underline{F}^{\mathsf{T}} = \underset{\approx}{\mathbb{L}} : \underline{d} + \underline{w}\underline{\tau} - \underline{\tau}\underline{d} \tag{2.21}$$

The rate of the PK1-stress is related to the rate of the deformation gradient by the mixed Eulerian-Lagrangian fourth-order tangent material stiffness tensor $\underset{\approx}{\mathbb{C}}$ (Eq. (2.22)). It can be determined by eliminating $(\underline{P})^{\bullet}$ from Eq. (2.21)

$$\dot{\underline{P}} = \underset{\approx}{\mathbb{C}} : \dot{\underline{F}} \tag{2.22}$$

$$\dot{\underline{P}}\underline{F}^{\mathsf{T}} = (\underset{\approx}{\mathbb{C}} : \dot{\underline{F}})\underline{F}^{\mathsf{T}} = \left(\underset{\approx}{\mathbb{C}} : (\dot{\underline{F}}\underline{F}^{-1}\underline{F})\right)\underline{F}^{\mathsf{T}} = \left(\underset{\approx}{\mathbb{C}} : (\underline{l}\underline{F})\right)\underline{F}^{\mathsf{T}}$$

$$\left(\underset{\approx}{\mathbb{C}} : (\underline{l}\underline{F})\right)\underline{F}^{\mathsf{T}} = \underset{\approx}{\mathbb{L}} : \underline{d} + \underline{w}\underline{\tau} - \underline{\tau}\underline{d} \tag{2.23}$$

Assuming minor symmetry $\mathbb{L}_{ijkl} = \mathbb{L}_{ijlk}$ on the Eulerian tangent material stiffness allows for the following substitution:

$$\mathbb{L}_{ijkl}d_{kl} = \tfrac{1}{2}\mathbb{L}_{ijkl}(l_{kl} + l_{lk}) = \tfrac{1}{2}\mathbb{L}_{ijkl}l_{kl} + \tfrac{1}{2}\mathbb{L}_{ijlk}l_{lk} = \mathbb{L}_{ijlk}l_{lk}$$

$$\left(\underset{\approx}{\mathbb{C}} : (\underline{l}\underline{F})\right)\underline{F}^{\mathsf{T}} = \underset{\approx}{\mathbb{L}} : \underline{l} + \underline{w}\underline{\tau} - \underline{\tau}\underline{d} \tag{2.24}$$

Translating Eq. (2.24) to index-notation:

$$\mathbb{C}_{iJkL}l_{km}F_{mL}F_{jJ} = \mathbb{L}_{ijkl}l_{kl} + w_{im}\tau_{mj} - \tau_{im}d_{mj}$$

Inserting the definition of $\underline{l}$, $\underline{d}$ and $\underline{w}$ into the last expression allows $\underline{v}$ to be eliminated. After some algebra (2.25) is obtained:

$$\mathbb{C}_{iJkL}F_{jJ}F_{lL} = \mathbb{L}_{ijkl} + \tfrac{1}{2}(\tau_{jl}\delta_{ik} - \tau_{jk}\delta_{il} - \tau_{ik}\delta_{jl} - \tau_{il}\delta_{jk}) \tag{2.25}$$

By choosing the reference state to be instantaneously coincident with the current state the deformation gradient and the Jacobian assume identity.

$$\underline{F} \to \underline{1} \qquad J \to 1$$

$$\mathbb{C}_{ijkl} = \mathbb{L}_{ijkl} + \tfrac{1}{2}(\sigma_{jl}\delta_{ik} - \sigma_{jk}\delta_{il} - \sigma_{ik}\delta_{jl} - \sigma_{il}\delta_{jk}) \tag{2.26}$$

Because of this identification $\underline{x}$ and $\underline{X}$, $\underline{l}$ and $\dot{\underline{F}}$, etc. coincide. The symbols $\underline{X}$ and $\dot{\underline{F}}$ are generally used in the remainder of the thesis. It is apparent from (2.26) that the mixed tangent material stiffness $\underset{\approx}{\mathbb{C}}$ consists of two contributions: A stiffness arising directly from the material properties, represented by $\underset{\approx}{\mathbb{L}}$, and extra terms dependent on current stress. For the case of elasticity the material stiffness usually exceeds the absolute value of the stress components by orders of magnitude, and they predominantly effect stability via rotations. In the elastoplastic regime, however the moduli are much reduced and possibly of the same order of magnitude as the stresses. All contribution from the stress terms should, therefore, be taken into account [Hill, 1958].

With respect to symmetry of the mixed material stiffness tensor it can be noted that the transformation (2.26) maintains the major symmetry property, provided that $\mathbb{L}_{ijkl} = \mathbb{L}_{ijlk}$. If, however, in (2.20) the ZJ-rate of Kirchhoff stress is replaced by the ZJ-rate of Cauchy stress an additional term $\sigma_{ij}\delta_{kl}$ is introduced on the right hand side of (2.25) and major symmetry is lost.

2.4 Specialization for assumed initial loading

Suppose a macroscopic body with a laminated microstructure under possibly very general loading. Areas of the body where the loading direction coincides with the lamella plane are candidates for lamella buckling. Further assuming that the characteristic lamella spacing is sufficiently small compared to the overall dimensions of the body, the lamella can be considered on a separate micro scale on which the macroscopic stress/strain gradients can be neglected. By neglecting the Poisson-effect of the lamella the body is assumed to be subject to plane strain conditions in transverse-in-plane direction. Expansion in out-of-plane direction is thought to be unobstructed. These assumptions are appropriate only for certain macroscopic configurations, but facilitates both analytical and numerical treatment of the problem and seems necessary to limit the scope of the present work. The
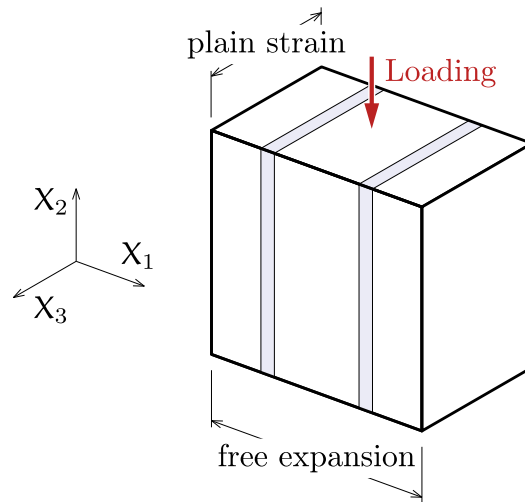

Figure 2.1: Loading on the micro-level

constitutive equations can then be evaluated further for a biaxially preloaded reference state in an unbuckled configuration. This reference state will be tested for uniqueness and stability in the following chapters. Thus the Cauchy-stress tensor and the deviatoric Cauchy-stress tensor evaluated at the reference state are given by Eq. (2.27) and Eq. (2.28) respectively.

$$\underset{\sim}{\boldsymbol{\sigma}} = \begin{bmatrix} 0 & 0 & 0 \\ 0 & \sigma_{22} & 0 \\ 0 & 0 & \sigma_{33} \end{bmatrix} \tag{2.27}$$

$$\underset{\sim}{\hat{\boldsymbol{\sigma}}} = \begin{bmatrix} \frac{1}{3}\left(-\sigma_{22} - \sigma_{33}\right) & 0 & 0 \\ 0 & \sigma_{22} + \frac{1}{3}\left(-\sigma_{22} - \sigma_{33}\right) & 0 \\ 0 & 0 & \frac{1}{3}\left(-\sigma_{22} - \sigma_{33}\right) + \sigma_{33} \end{bmatrix} \tag{2.28}$$

The Eulerian tangent material stiffness tensor generally depends on the current stress, cf. (2.14). However, introducing the simplification that the plastic part of the strain rate in transverse in-plane direction vanishes separately, i.e. the elastic contribution to the transverse in-plane strain is negligible small, in addition to the overall strain, the Eulerian tangent material stiffness becomes constant. This simplification provides an approximate relation of σ_{22} and σ_{33} directly from the flow rule.

$$\frac{\partial \mathcal{F}}{\partial \sigma_{33}} = \frac{1}{3}\left(-2\sigma_{22} + 4\sigma_{33}\right) \doteq 0$$

$$\sigma_{33} \doteq \frac{1}{2}\sigma_{22}$$

Substituting this relation into the yield function gives the current stress state in terms of κ, proportional to the yield-stress.

$$\mathcal{F} = \frac{1}{3}\left(2\sigma_{22}^2 - 2\sigma_{22}\sigma_{33} + 2\sigma_{33}^2\right) - \kappa^2 = 0$$

$$\sigma_{22} = -\sqrt{2}\,\kappa$$

$$\sigma_{33} = -\frac{1}{\sqrt{2}}\kappa$$

This approximation holds well for monotonous loading sufficiently far beyond the point of initial yielding, cf. numerical results in Fig. 2.2. It is shown when discussing numerical results in later chapters that elastoplastic buckling usually requires high levels of stresses and strains that usually exceed the yield-stress by far. Therefore, this approximation seems justified at least for the numerical examples included in this work. Thus the stresses in a plate loaded homogeneously in direction-2, freely expanding in direction-1, with zero strain in direction-3 are approximately given by Eq. (2.27) and (2.30), provided, the current stress state is sufficiently far beyond the initial yielding point. The Cauchy-stress tensor and its deviator are thus:

$$\underset{\sim}{\boldsymbol{\sigma}} = \frac{\kappa}{\sqrt{2}} \begin{bmatrix} 0 & 0 & 0 \\ 0 & -2 & 0 \\ 0 & 0 & -1 \end{bmatrix} \tag{2.29}$$
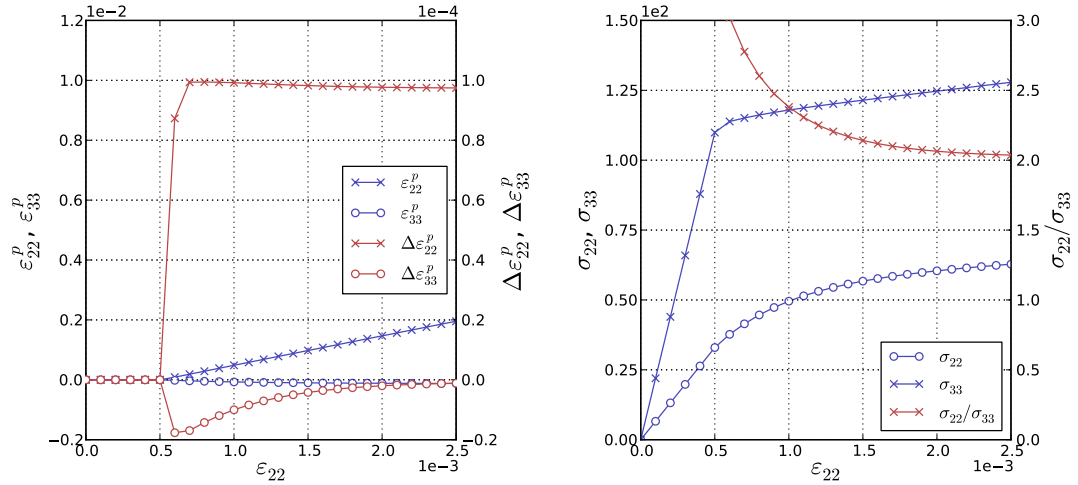
(a) $\nu = 0.30$, $E_t = 5\,\mathrm{GPa}$
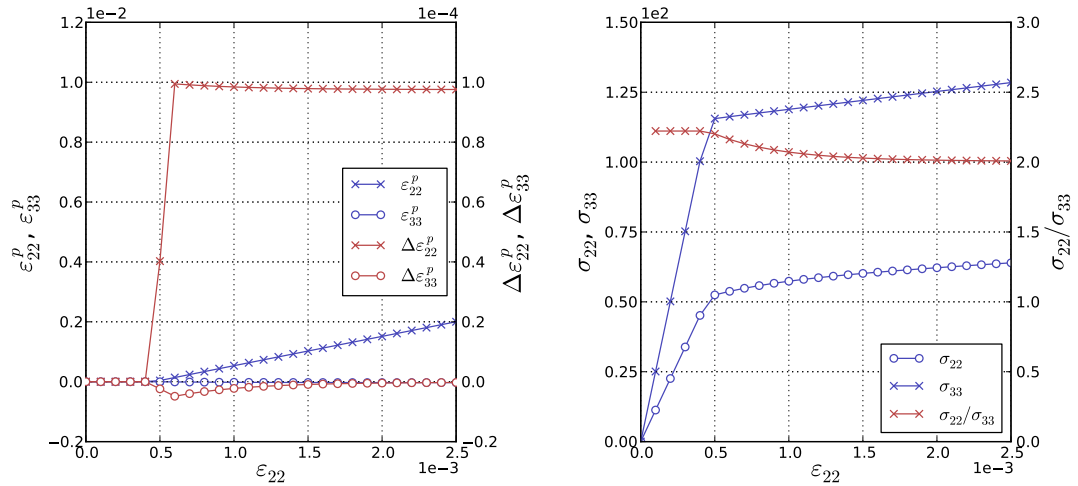
(b) $\nu = 0.45$, $E_t = 5\,\mathrm{GPa}$

Figure 2.2: Plastic strains, plastic strain rates and stresses obtained from FEM-analysis for monotonic loading of an element constrained to plane strain, $E = 200\,\mathrm{GPa}$, $\sigma_y = 100\,\mathrm{MPa}$

$$\hat{\underset{\sim}{\sigma}} = \frac{\kappa}{\sqrt{2}} \begin{bmatrix} 1 & 0 & 0 \\ 0 & -1 & 0 \\ 0 & 0 & 0 \end{bmatrix} \tag{2.30}$$

The consistency parameter can be evaluated via Eq. (2.13) and the plastic part of the rate of deformation tensor becomes:

$$\varphi = \frac{\sqrt{2}\,\mu(d_{11} - d_{22})}{\kappa(2\mu + \theta)} \tag{2.31}$$

$$\underset{\sim}{d}^p = \frac{\mu(d_{11} - d_{22})}{2\mu + \theta} \begin{bmatrix} 1 & 0 & 0 \\ 0 & -1 & 0 \\ 0 & 0 & 0 \end{bmatrix} \tag{2.32}$$

The so obtained relations between total and plastic strain rate are referenced in the following. From Eq (2.33) it can be seen that no plastic shear occurs at the instance of buckling and before. No restriction on the total shear is in place, though.

$$d_{11}^p = \frac{\mu(d_{11} - d_{22})}{2\mu + \theta} = -d_{22}^p \tag{2.33_1}$$

$$d_{12}^p = 0 \tag{2.33_2}$$

From Eq. (2.14) the plane strain tangent material stiffness of the matrix for the current simplifications can be assembled. The variable κ cancels out and the only remaining constants are the Lamé-parameters and the hardening factor θ.

$$\begin{aligned} \underset{\approx}{\mathbb{L}}^p &= (\lambda\delta_{ij}\delta_{kl} + \mu\delta_{ik}\delta_{jl} + \mu\delta_{il}\delta_{jk})\, \underline{e}_i \otimes \underline{e}_j \otimes \underline{e}_k \otimes \underline{e}_l \\ &\quad - \frac{2\mu^2}{2\mu + \theta}\,(\underline{e}_1 \otimes \underline{e}_1 - \underline{e}_2 \otimes \underline{e}_2) \otimes (\underline{e}_1 \otimes \underline{e}_1 - \underline{e}_2 \otimes \underline{e}_2) \end{aligned} \tag{2.34}$$

The following abbreviations are introduced, where ξ stand for a switch function assuming 0 when $\varphi = 0$ and 1 when $\varphi > 0$:

$$F_1 = \underset{\approx}{\mathbb{L}}_{1111} = \underset{\approx}{\mathbb{L}}_{2222} = \lambda + 2\mu - \frac{2\mu^2}{\theta + 2\mu}\xi \tag{2.35_1}$$

$$F_2 = \underset{\approx}{\mathbb{L}}_{1122} = \underset{\approx}{\mathbb{L}}_{2211} = \lambda + \frac{2\mu^2}{\theta + 2\mu}\xi \tag{2.35_2}$$

The full 3-axial material tangent for the assumed plane strain condition is written out in Eq. (2.36) using a matrix containing matrices as elements. The first two indices denoting the row, respectively column, in the outer matrix, and the last two indices denoting row and column in the inner matrix. The first and the last pair of indices can be interchanged

because of the major symmetry of $\underset{\approx}{\mathbb{L}}$. The sub-matrices are symmetric as well.

$$\underset{\approx}{\mathbb{L}} = \begin{bmatrix} \begin{bmatrix} F_1 & 0 & 0 \\ 0 & F_2 & 0 \\ 0 & 0 & \lambda \end{bmatrix} & \begin{bmatrix} 0 & \mu & 0 \\ \mu & 0 & 0 \\ 0 & 0 & 0 \end{bmatrix} & \begin{bmatrix} 0 & 0 & \mu \\ 0 & 0 & 0 \\ \mu & 0 & 0 \end{bmatrix} \\ \begin{bmatrix} 0 & \mu & 0 \\ \mu & 0 & 0 \\ 0 & 0 & 0 \end{bmatrix} & \begin{bmatrix} F_2 & 0 & 0 \\ 0 & F_1 & 0 \\ 0 & 0 & \lambda \end{bmatrix} & \begin{bmatrix} 0 & 0 & 0 \\ 0 & 0 & \mu \\ 0 & \mu & 0 \end{bmatrix} \\ \begin{bmatrix} 0 & 0 & \mu \\ 0 & 0 & 0 \\ \mu & 0 & 0 \end{bmatrix} & \begin{bmatrix} 0 & 0 & 0 \\ 0 & 0 & \mu \\ 0 & \mu & 0 \end{bmatrix} & \begin{bmatrix} \lambda & 0 & 0 \\ 0 & \lambda & 0 \\ 0 & 0 & \lambda+2\mu \end{bmatrix} \end{bmatrix} \tag{2.36}$$

In (2.36) all indices run from 1 to 3. However, due to the plane strain assumption all third elements can be dropped to obtain (2.37).

$$\underset{\approx}{\mathbb{L}} = \begin{bmatrix} \begin{bmatrix} F_1 & 0 \\ 0 & F_2 \end{bmatrix} & \begin{bmatrix} 0 & \mu \\ \mu & 0 \end{bmatrix} \\ \begin{bmatrix} 0 & \mu \\ \mu & 0 \end{bmatrix} & \begin{bmatrix} F_2 & 0 \\ 0 & F_1 \end{bmatrix} \end{bmatrix} \tag{2.37}$$

3 Stability and uniqueness of elastoplastic structures

Conflicting theories about the nature of instability phenomena in elastoplastic structures had been put forward in the first half of the 20th century [Johnston, 1983, Bažant and Cedolin, 2010]. A source of confusion arose from the circumstance that some researchers considered stability of an equilibrium at constant loading while others allowed for variable load in their theories. On account of the activation of different constitutive branches they arrived at different results. The problem has been finally resolved by R. Hill [Hill, 1958, Hill, 1959, Hill, 1978], who showed that the key aspect of the problem lies in the fact that the concepts of stability and uniqueness do not coincide for path-dependent problems as they do for elasticity. Perturbation of a given equilibrium state, at constant loading, typically causes unloading in some parts of the previously plastic structure and thus stiffness and the critical load depend on some combination of the elastic and plastic modulus. Bifurcation from the primary loading path usually starts much earlier, however. The variable loading allows for compensation of any unloading taking place and typically results in a much lower stiffness and, therefore, critical load. Nevertheless, careful investigation of the equilibrium *state* at the bifurcation point reveals it to be stable. Consequently, an elastoplastic structure can bifurcate without becoming unstable, and a distinction between those two concepts needs to be made.

The present chapter strives to give an overview of the definitions and criteria for both stability and uniqueness that have been established in the literature adequate for the problem at hand. Even though the theory available in the literature allows treatment of elastoplastic uniqueness and stability problems in a very general manner, only those aspects that apply to the present problem of buckling of lamellae embedded in an elastoplastic matrix are taken into account, i.e. follower loads are excluded. The limitations are stated in detail in section 3.1 below. The present work is concerned with the buckling behaviour of elastic lamellae embedded in an elastoplastic matrix. Term 'buckling' is used to denote the transition from a previously homogeneous deformation mode to a new inhomogeneous one, i.e. by this definition buckling essentially means bifurcation.

3.1 Rate boundary value problem

Before the question of stability and bifurcation can be posed, the problem under consideration has to be defined. The starting point is given by the classical local static equilibrium conditions formulated for a body occupying the Volume V in the material configuration

and bounded by the surface S, (3.1). The unit normal vector, the traction per surface area and the body forces, all with respect to the material configuration, are denoted by $\underline{N}$, $\underline{T}$ and $\underline{B}$ respectively.

$$
\begin{aligned}
&\text{in V:} \quad \mathrm{Div}(\underline{\underline{P}}) + \underline{B} = \underline{0} \\
&\text{on S:} \quad \underline{\underline{P}} \cdot \underline{N} = \underline{T}
\end{aligned}
\tag{3.1}
$$

Due to the incremental nonlinearity of the constitutive law the problem must be formulated in rate form. Rates are denoted by an overscript dot in the likeness of a time derivative, however, all deformations are thought to occur in a quasi static manner. Taking the time derivate of (3.1) immediately yields a condition of continuing equilibrium:

$$
\begin{aligned}
&\text{in V:} \quad \mathrm{Div}(\dot{\underline{\underline{P}}}) + \dot{\underline{B}} = \underline{0} \\
&\text{on S:} \quad \dot{\underline{\underline{P}}} \cdot \underline{N} = \dot{\underline{T}}
\end{aligned}
\tag{3.2}
$$

Thus, the weak form of the local continuing equilibrium for a proper test function $\underline{\eta}$ is obtained as:

$$
\int_V \left(\mathrm{Div}(\dot{\underline{\underline{P}}}) + \dot{\underline{B}} \right) \cdot \underline{\eta} \, \mathrm{d}V = 0
\tag{3.3}
$$

The scalar product of the divergence with the test function in the previous equation adheres to an identity similar to the product rule.

$$
\mathrm{Div}(\dot{\underline{\underline{P}}}) \cdot \underline{\eta} = -\dot{\underline{\underline{P}}} : \mathrm{Grad}(\underline{\eta}) + \mathrm{Div}(\dot{\underline{\underline{P}}}^{\mathsf{T}} \underline{\eta})
\tag{3.4}
$$

Using the identity to transform the weak form in the usual way allows a reference to the boundary conditions (BCs) being made.

$$
-\int_V \dot{\underline{\underline{P}}} : \mathrm{Grad}\,\underline{\eta} \, \mathrm{d}V + \int_S \dot{\underline{T}} \cdot \underline{\eta} \, \mathrm{d}S + \int_V \dot{\underline{B}} \cdot \underline{\eta} \, \mathrm{d}V = 0
\tag{3.5}
$$

The BCs are given in the form of prescribed Surface tractions, $\dot{\underline{T}}$, on some part of the surface of the body S_T and prescribed velocities, i.e. displacement rates, $\bar{\underline{v}}$, on the complementary surface $S_u = S \setminus S_T$ as a function of the loading parameter λ. Only conservative loading controlled independently of the deformation of the body is considered. Prescribed quantities are furnished with an overbar. The body load is generally assumed to be a controlled quantity. To exclude rigid body displacements from the following considerations it will be generally assumed that: $S_u \neq \{\emptyset\}$. The loading is thought to be governed by a load proportionality factor λ which uniformly controls the quasi static development of the BCs.

From here on let the symbol $\underline{v}$ be reserved for kinematically admissible velocity fields during the deformation process and it is assumed to be continuously differentiable. Pre-

scribed velocities are denoted by $\bar{\underline{v}}$ and any $\underline{v}$ conforms to the kinematic BCs on $\mathsf{S_u}$ by assuming the prescribed values there.

$$\underline{v} = \bar{\underline{v}} \quad \text{on } \mathsf{S_u} \tag{3.6}$$

A second class of velocity fields will be indicated by the symbol $\underline{w}$. It is defined as the infinitesimal variation of the velocity field $\underline{v}$ at some frozen state of the load proportionality factor and, hence, vanishes on $\mathsf{S_u}$.

$$\underline{w} = \delta\underline{v}$$
$$\underline{w} = \underline{0} \quad \text{on } \mathsf{S_u} \tag{3.7}$$

The rate form of the virtual work principle is obtained for $\underline{\eta} = \underline{w}$. In equation (3.8) the virtual work $\delta\mathcal{A}$ vanishes if $\underline{v}$ is a solution to the boundary value problem. Here $(\bar{\mathbf{T}})^{\boldsymbol{\cdot}}$, $(\bar{\underline{\mathbf{B}}})^{\boldsymbol{\cdot}}$ are given external quantities, in general nonzero. A solution for $\underline{v}$ could be obtained via, e.g. , a discretization scheme.

$$\delta\mathcal{A}(\underline{v}) = -\int_V \dot{\underset{\sim}{\mathbf{P}}}(\underline{v}) : \operatorname{Grad}\underline{w}\,\mathrm{d}V + \int_{\mathsf{S_T}} \dot{\bar{\mathbf{T}}}\cdot\underline{w}\,\mathrm{d}S + \int_V \dot{\bar{\mathbf{B}}}\cdot\underline{w}\,\mathrm{d}V = 0 \tag{3.8}$$

$$\underline{w} = \underline{0} \quad \text{on } \mathsf{S_u}, \text{ arbitrary otherwise}$$

For the so defined rate boundary value problem stability and bifurcation is analyzed in the following sections.

3.2 Stability of equilibrium

In elasto-statics a stable equilibrium state for a purely elastic body under conservative loading is usually defined via the Lagrange-Dirichlet theorem, i.e. a given equilibrium state is stable if it assigns an strict minimum to the associated potential energy of the load-structure system consisting of the body and the loading device [Leine, 2010]. Then, any perturbation by a kinetic energy of vanishingly small amplitude is confined to infinitesimally close neighbor configurations.

The path dependence introduced by plasticity, however, precludes the existence of an elastic potential and the Lagrange-Dirichlet theorem can not be invoked directly [Bažant and Cedolin, 2010]. As a remedy, the work of a system is analyzed instead. The work released by the complete load-structure system, indicated by the symbol $\mathcal{A}$, is split into a part representing the work released by the deformation of the body, called the internal work $\mathcal{A}_{\mathrm{int}}$, and the work released by the loading device, called the external work $\mathcal{A}_{\mathrm{ext}}$. The internal work can also be thought of as the negative of the work supplied to the body to realize a certain deformation.

$$\mathcal{A} = \mathcal{A}_{\mathrm{int}} + \mathcal{A}_{\mathrm{ext}}$$

According to [Hill, 1959], a given equilibrium state perturbed by supplying some kinetic energy $\Delta\mathcal{T}$, the system can at most attain any configuration associated with the work $-\Delta\mathcal{A} = \Delta\mathcal{T}$. The magnitude of the perturbation is thought to be infinitesimal and only configurations reached by a direct path, i.e. those paths activating only one constitutive branch, are considered. The deformation will, in general, involve dissipation due to plasticity, and it is assumed that the plastic work on a indirect path is not smaller than that on the direct path leading to the same final configuration. Then, for a given value of plastic work, any indirect or oscillating path will lead to a configuration closer to the initial configuration, or at most the same configuration, than the direct path. If then, $\Delta\mathcal{A}$ decreases monotonically from zero along every direct path from the initial configuration the motion following a vanishingly small perturbation $\Delta\mathcal{T}$ will vanish itself in the limit, and the equilibrium is called stable in analogy to the Lagrange-Dirichlet theorem for systems with an elastic potential.

The work done by the perturbation can be approximated by a Maclaurin series expansion. In the series $\Delta\mathcal{A}$ is stationary up to first order terms, as required for equilibrium. Thus, stability is decided by the second order terms of the series, provided they are not identically zero themselves, which will be excluded from the following considerations, and higher order terms can be truncated.

$$\Delta\mathcal{A} = +\dot{\mathcal{A}}\Delta t + \ddot{\mathcal{A}}\tfrac{1}{2}\Delta t^2 + \mathcal{O}(\Delta t^3) \tag{3.9}$$
$$\dot{\mathcal{A}} = 0$$

The internal work rate in general includes dissipation due to plasticity and the stress increments depend on stain increments in a nonlinear manner. Second order terms are obtained by derivation. In this section the gradient of $\underline{w}$ is denoted by $\mathrm{Grad}(\underline{w})$ instead of the symbol $(\underline{\underline{F}})^{\bullet}$ in order to emphasise the kinematic restrictions in place.

$$\dot{\mathcal{A}}_{\mathrm{int}}(\underline{w}) = -\int_V \underline{\underline{P}}(\underline{w}) : \mathrm{Grad}\,\underline{w}\,\mathrm{d}V$$
$$\ddot{\mathcal{A}}_{\mathrm{int}}(\underline{w}) = -\int_V \left(\dot{\underline{\underline{P}}}(\underline{w}) : \mathrm{Grad}\,\underline{w} + \underline{\underline{P}}(\underline{w}) : \mathrm{Grad}\,\dot{\underline{w}}\right)\mathrm{d}V \tag{3.10}$$

The external work is the work done by the loading device and assumed to be conservative. It can be seen, therefore, as the negative change in the potential of the external forces

$$\dot{\mathcal{A}}_{\mathrm{ext}}(\underline{w}) = +\int_S \underline{T}\cdot\underline{w}\,\mathrm{d}S \qquad\qquad +\int_V \bar{\underline{B}}\cdot\underline{w}\,\mathrm{d}V$$
$$\ddot{\mathcal{A}}_{\mathrm{ext}}(\underline{w}) = +\int_S \left(\dot{\underline{T}}\cdot\underline{w} + \underline{T}\cdot\dot{\underline{w}}\right)\mathrm{d}S + \int_V \left(\dot{\bar{\underline{B}}}\cdot\underline{w} + \bar{\underline{B}}\cdot\dot{\underline{w}}\right)\mathrm{d}V \tag{3.11}$$

Stability is understood as a property of an equilibrium state, i.e. it is investigated at a given instant of an ongoing deformation process. Therefore, the load proportionality factor λ controlling the process remains frozen for the purpose of establishing stability. Deformation dependent loading has been excluded from any considerations before. So regardless of the actual dependence of the prescribed tractions and displacements on the

load proportionality factor all admitted loads can be considered dead loads.

$$
\left.
\begin{aligned}
\text{in V:} \quad & \bar{\underline{B}} \sim \lambda \\
\text{on } S_T: \quad & \bar{\underline{T}} \sim \lambda \\
\text{on } S_u: \quad & \bar{\underline{u}} \sim \lambda
\end{aligned}
\right\} \quad \lambda = \text{const.} \quad
\left\{
\begin{aligned}
& \dot{\bar{\underline{B}}} = \underline{0} \\
& \dot{\bar{\underline{T}}} = \underline{0} \\
& \bar{\underline{w}} = \underline{0}
\end{aligned}
\right.
\tag{3.12}
$$

The expression for the external work can thus be simplified, and the remaining terms can be transformed to a volume integral via Gauss's theorem and local equilibrium.

$$
\ddot{\mathcal{A}}_{\text{ext}} = + \int_{S_T} \bar{\underline{T}} \cdot \dot{\underline{w}} \, dS + \int_V \bar{\underline{B}} \cdot \dot{\underline{w}} \, dV = + \int_S \underline{T} \cdot \dot{\underline{w}} \, dS + \int_V \bar{\underline{B}} \cdot \dot{\underline{w}} \, dV
$$

$$
= + \int_V \left(\text{Div}(\underline{\underline{P}}(\underline{w})^\mathsf{T} \dot{\underline{w}}) - \text{Div}(\underline{\underline{P}}(\underline{w})) \cdot \dot{\underline{w}} \right) dV
$$

$$
\ddot{\mathcal{A}}_{\text{ext}} = + \int_V \underline{\underline{P}}(\underline{w}) : \text{Grad } \dot{\underline{w}} \, dV
\tag{3.13}
$$

The external work cancels the second term of the internal work and the work done by an infinitesimal perturbation does not depend on accelerations.

$$
\Delta \mathcal{A} = -\tfrac{1}{2} \Delta t^2 \int_V \dot{\underline{\underline{P}}}(\underline{w}) : \text{Grad } \underline{w} \, dV + \mathcal{O}(\Delta t^3)
\tag{3.14}
$$

From (3.14) it can be seen that stability of equilibrium is decided by a functional $\mathcal{I}(\underline{w})$, as defined below. This stability functional was introduced by R. Hill [Hill, 1958, Hill, 1959]. A sufficient criterion for stability is provided, if $\mathcal{I}(\underline{w})$ is positive for every nonzero kinematically admissible velocity field $\underline{w}$, i.e. any velocity field that conforms to the frozen displacements at S_u by vanishing there.

$$
\mathcal{I}(\underline{w}) := \int_V \dot{\underline{\underline{P}}}(\underline{w}) : \text{Grad } \underline{w} \, dV
$$

$$
\mathcal{I}(\underline{w}) > 0 \qquad \text{for every } \underline{w}, \ \underline{w} \neq \underline{0}, \ \underline{w} \text{ vanishes on } S_u \qquad \implies \text{stable}
\tag{3.15}
$$

3.3 Hill's criterion of uniqueness

As has been suggested in the introduction to this chapter stability and uniqueness are two apart concepts for bodies under plastic deformations. A sufficient criterion for uniqueness of the solution for a boundary-value problem in rate-form was given by R. Hill in [Hill, 1958, Hill, 1959], and an excerpt of the literature on the subject is included here to point out the most important differences and their implications.

In order to investigate uniqueness, suppose that two distinct velocity solutions $\underline{v}^*$ and $\underline{v}$ to the rate-form boundary value problem exist, and let the respective quantities be indicated by a present or missing superscript asterisk. Differences in quantities between

both solutions shall be denoted by the prefix Δ. The stress rates for each solution are constitutively related to the gradient of the respective velocity field. Here $\mathrm{Grad}(\underline{v})$ is used instead of $(\underline{\underline{F}})^{\boldsymbol{\cdot}}$ to emphasise the different kinematic constraints as opposed to the previous section.

$$\Delta\underline{v} = \underline{v}^* - \underline{v}$$

$$\mathrm{Grad}\,\Delta\underline{v} = \mathrm{Grad}\,\underline{v}^* - \mathrm{Grad}\,\underline{v}$$

$$\Delta\dot{\underline{\underline{P}}} = \dot{\underline{\underline{P}}}^* - \dot{\underline{\underline{P}}} = \underline{\underline{\mathbb{C}}}(\mathrm{Grad}\,\underline{v}^*) : \mathrm{Grad}\,\underline{v}^* - \underline{\underline{\mathbb{C}}}(\mathrm{Grad}\,\underline{v}) : \mathrm{Grad}\,\underline{v}$$

If both velocity fields are solutions, they share the prescribed body forces per reference volume, $\bar{\underline{B}}$, the prescribed tractions per reference area, $\bar{\underline{T}}$, on the surface S_u and the prescribed velocities, $\bar{\underline{v}}$, on the complementary surface and the respective rates. Therefore, differences in the rates of prescribed quantities are zero on their particular domain.

$$
\begin{aligned}
\text{in } V: \quad & \mathrm{Div}(\dot{\underline{\underline{P}}}^*) = \mathrm{Div}(\dot{\underline{\underline{P}}}) = -\dot{\bar{\underline{B}}} \\
& \mathrm{Div}(\dot{\underline{\underline{P}}}^*) - \mathrm{Div}(\dot{\underline{\underline{P}}}) = \Delta\big(\mathrm{Div}(\dot{\underline{\underline{P}}})\big) = \mathrm{Div}(\Delta\dot{\underline{\underline{P}}}) = -\Delta\dot{\bar{\underline{B}}} = \underline{0} \\
\text{on } S_T: \quad & \Delta\dot{\bar{\underline{T}}} = \underline{0} \\
\text{on } S_u: \quad & \Delta\dot{\bar{\underline{v}}} = \underline{0}
\end{aligned}
\tag{3.16}
$$

Since the differences in the controlled quantities vanish the following statements hold:

$$\int_S \Delta\dot{\underline{T}}\cdot\Delta\underline{v}\,\mathrm{d}S = \int_{S_T} \Delta\dot{\underline{T}}\cdot\Delta\underline{v}\,\mathrm{d}S + \int_{S_u} \Delta\dot{\underline{T}}\cdot\Delta\bar{\underline{v}}\,\mathrm{d}S = 0 \tag{3.17}$$

$$\int_V \Delta\dot{\bar{\underline{B}}}\cdot\Delta\underline{v}\,\mathrm{d}V = 0 \tag{3.18}$$

The last two equations can be combined with the divergence theorem and the local equilibrium conditions to yield a relation for the volume integral of the differences of the double contraction on PK1-stress with the deformation gradient:

$$\int_S \Delta\dot{\underline{T}}\cdot\Delta\underline{v}\,\mathrm{d}S + \int_V \Delta\dot{\bar{\underline{B}}}\cdot\Delta\underline{v}\,\mathrm{d}V = 0$$

$$\int_V \big(\mathrm{Div}(\Delta\dot{\underline{\underline{P}}}^\mathsf{T}\Delta\underline{v}) - \mathrm{Div}(\Delta\dot{\underline{\underline{P}}})\cdot\Delta\underline{v}\big)\,\mathrm{d}V = 0$$

$$\int_V \Delta\dot{\underline{\underline{P}}} : \mathrm{Grad}\,\Delta\underline{v}\,\mathrm{d}V = 0 \tag{3.19}$$

To facilitate further references, the functional $\mathcal{H}$, as defined below, is introduced as an abbreviation. The condition (3.19), respectively (3.17), necessary for nonuniqueness, can be inverted to give a sufficient condition for uniqueness by replacing equality with nonequality. The condition can be weakened further and uniqueness is implied a fortiori if the left hand side of (3.19) takes only positive values for any pair of kinematically admissible

velocity fields. A sufficient condition for uniqueness is, therefore, that the uniqueness condition (3.21) holds for all pairs of continuously differentiable velocity fields taking the values prescribed on S_u [Hill, 1959].

$$\mathcal{H}(\underline{v}^*, \underline{v}) := \int_V \Delta\dot{\underline{P}} : \operatorname{Grad} \Delta\underline{v} \, dV = \int_S \Delta\dot{\underline{T}} \cdot \Delta\underline{v} \, dS \tag{3.20}$$

$$\mathcal{H}(\underline{v}^*, \underline{v}) > 0 \qquad \text{for every } \underline{v}^*, \underline{v} \text{ and } \underline{v}^* \neq \underline{v} \qquad \Longrightarrow \text{ unique and stable} \tag{3.21}$$

If uniqueness condition (3.21) holds, stability is implied because of (3.22). The converse, however, is not true in general, and uniqueness is not implied by $\mathcal{I}(\underline{w}) > 0$ for every nonzero $\underline{w}$ in the presence of inelastic material behaviour. Uniqueness and stability are separate concepts for elastoplastic rate boundary value problems.

$$\mathcal{H}(\underline{0}, \underline{w}) \equiv \mathcal{I}(\underline{w}) \tag{3.22}$$

Taking into account the considerations regarding stability stated in section 3.2 it can further be remarked that although $\mathcal{H} \neq 0$ for all admissible pairs is sufficient for uniqueness, the equilibrium is probably unstable if $\mathcal{H} < 0$ for all admissible velocity pairs. This case is excluded from any further considerations and (3.21) provides a condition sufficient for both uniqueness and stability. If a solution $\underline{v}$ is known, it can be taken as a member in the criterion. Hill's uniqueness condition requires to prove the property $\mathcal{H} > 0$ for all admissible pairs $\underline{v}^*, \underline{v}$ and is, therefore, difficult to apply in practice. It can, however, be extended further for materials that admit a rate potential, as is the case for the material obeying the normality flow rule that is considered in the present work.

3.4 Rate potential

Limiting all further considerations to materials that allow for the existence of a rate potential $\mathcal{U}$, the results from the previous sections can be specified further [Hill, 1958, Hill, 1959, Hill, 1978]. Deferring the requirements for such a potential to exist for the moment, the rate potential takes the form in (3.23). It is, in general, a function homogeneous of degree two in $\dot{\underline{F}}$ and reverts to a quadratic form for the special case of elasticity.

$$\mathcal{U}(\dot{\underline{F}}) = \frac{1}{2} \dot{\underline{P}} : \dot{\underline{F}} \tag{3.23}$$

Via applying Euler's theorem for homogeneous functions, cf. (7.17), the rate of PK1-stress can be related to the partial derivative of $\mathcal{U}$ by comparison with (3.23):

$$2 \cdot \mathcal{U}(\dot{\underline{F}}) = \frac{\partial \mathcal{U}}{\partial \dot{\underline{F}}} : \dot{\underline{F}} \qquad\qquad \Rightarrow \dot{\underline{P}}(\dot{\underline{F}}) = \frac{\partial \mathcal{U}}{\partial \dot{\underline{F}}} \tag{3.24}$$

3 Stability and uniqueness of elastoplastic structures

The relation of the rate of the PK1-stress, $\dot{\mathbf{P}}$, to the rate of the deformation gradient, $\dot{\mathbf{F}}$, is nonlinear in the plastic regime on account of the possibility to activate different constitutional branches, but homogeneous of degree one. Applying Euler's theorem again and comparison with (2.22) relates the mixed material stiffness to the partial derivatives of $\mathcal{U}$.

$$1 \cdot \dot{\mathbf{P}}(\dot{\mathbf{F}}) = \frac{\partial \dot{\mathbf{P}}}{\partial \dot{\mathbf{F}}} : \dot{\mathbf{F}} = \frac{\partial^2 \mathcal{U}}{\partial \dot{\mathbf{F}} \partial \dot{\mathbf{F}}} : \dot{\mathbf{F}} \qquad \Rightarrow \mathbb{C}(\dot{\mathbf{F}}) = \frac{\partial^2 \mathcal{U}}{\partial \dot{\mathbf{F}} \partial \dot{\mathbf{F}}} \tag{3.25}$$

Because of the symmetry of the second derivatives in the second equation in (3.25), major symmetry of the material stiffness is required for the rate potential to exist via the Schwarz integrability condition. In the present case a Von Mises-yield function with an associated flow rule where adopted in chapter 2, and the material tangent moduli $\mathbb{L}$ and $\mathbb{C}$ possess the major symmetry property.

The existence of the rate potential implies a so-called reciprocal relation for the variations. Therefore, the variation of the rate potential is given by (3.26) [Hill, 1978, Lubarda, 2002]:

$$\delta\dot{\mathbf{P}} : \dot{\mathbf{F}} = \dot{\mathbf{P}} : \delta\dot{\mathbf{F}}$$
$$\delta\mathcal{U} = \dot{\mathbf{P}} : \delta\dot{\mathbf{F}} = \delta\dot{\mathbf{P}} : \dot{\mathbf{F}} \tag{3.26}$$

The uniqueness condition was developed by Hill [Hill, 1959] into an extremum principle for materials that allow for the existence of a rate potential. A velocity field $\mathbf{v}$ is a solution to the rate boundary value problem as defined in section 3.1 if and only if it assigns to the functional $\mathcal{J}(\mathbf{v})$ as defined in (3.27) a stationary value, i.e. the first variation of the functional vanishes for all $\mathbf{w}$. This stationary condition is equivalent to the virtual work principle in rate form (3.8) due to (3.26).

$$\mathcal{J}(\mathbf{v}) = \int_V \mathcal{U}(\text{Grad}(\mathbf{v})) \, dV - \int_{S_T} \dot{\mathbf{T}} \cdot \mathbf{v} \, dS - \int_V \dot{\mathbf{B}} \cdot \mathbf{v} \, dV \tag{3.27}$$

$$\delta\mathcal{J}(\mathbf{v}, \mathbf{w}) = 0 \qquad \text{for every } \mathbf{w} \tag{3.28}$$

The uniqueness condition (3.21) can be rewritten as:

$$\delta\mathcal{J}(\mathbf{v}^*, \mathbf{v}^* - \mathbf{v}) - \delta\mathcal{J}(\mathbf{v}, \mathbf{v}^* - \mathbf{v}) > 0 \qquad \text{for every } \mathbf{v}^*, \mathbf{v} \text{ and } \mathbf{v}^* \neq \mathbf{v} \tag{3.29}$$

This is the condition of strict convexity of the functional $\mathcal{J}$. Therefore, if the uniqueness condition (3.21) holds, the unique solution $\mathbf{v}^0$ assigns to $\mathcal{J}(\mathbf{v})$ a strict and absolute minimum [Hill, 1959, Hill, 1978]:

$$\mathcal{J}(\mathbf{v}) > \mathcal{J}(\mathbf{v}^0) \qquad \text{for every } \mathbf{v} \text{ and } \mathbf{v} \neq \mathbf{v}^0 \tag{3.30}$$

3.5 Linear comparison material

The uniqueness condition (3.21) is difficult to apply to an actual problem, because it requires to prove $\mathcal{H}(\underline{v}^*, \underline{v}) > 0$ for all admissible velocity fields $\underline{v}^*, \underline{v}$. In practice the first bifurcation point is usually sought-after. A possible approach would be to take the known primary solution, say $\underline{v}^0$, as a member of the pair so that only the remaining arbitrary but admissible velocity field $\underline{v}$ has to be considered in the criterion [Hill, 1978].

An other approach, applicable for materials that allow for a rate potential, was introduced by Hill: The actual incrementally nonlinear material is thought to be replaced by a linear comparison material for the purpose of determining uniqueness. The actual material, nonlinear on account of being piecewise linear in the loading and the unloading direction, is mentally replaced by a linear comparison material. Suppose the fundamental, i.e. unbuckled, deformation path that is to be investigated and the respective velocity solution $\underline{v}^0$ following this path is known. Then the corresponding comparison material $\underset{\approx}{\mathbb{C}}^0$ is obtained by disregarding the unloading branch of the constitutive relation and linearly extending the loading branch in both directions in those regions that are currently yielding on the fundamental path. In currently elastic regions the material is already incrementally linear and no change is necessary. The material tangent of the comparison material then no longer depends on the gradient of the velocity field.

Because in the actual material the stiffer unloading branch might be active in some parts, the comparison material has a lower stiffness or is at most as stiff as the actual material. The actual rate potential of the material is as convex or more convex than the potential of the comparison material which is a quadratic form with $\underset{\approx}{\mathbb{C}}^0$. The resulting inequality is known as the relative convexity property, (3.31), and it can generally be assumed for classic elastoplastic solids.

$$(\dot{\underline{P}}^* - \dot{\underline{P}}) : (\dot{\underline{F}}^* - \dot{\underline{F}}) \geqslant (\dot{\underline{F}}^* - \dot{\underline{F}}) : \underset{\approx}{\mathbb{C}}^0 : (\dot{\underline{F}}^* - \dot{\underline{F}}) \qquad \text{for every } \dot{\underline{F}}, \dot{\underline{F}}^* \tag{3.31}$$

The relative convexity property can be used in the uniqueness condition to obtain a lower bound to $\mathcal{H}(\underline{v}^*, \underline{v})$ in (3.20). By this procedure the uniqueness problem for the actual solid is transformed to a stability of the comparison solid.

$$\mathcal{H}(\underline{v}^*, \underline{v}) \geqslant \int_V \left(\dot{\underline{F}}^* - \dot{\underline{F}} \right) : \underset{\approx}{\mathbb{C}}^0 : \left(\dot{\underline{F}}^* - \dot{\underline{F}} \right) \, \mathrm{d}V$$

$$\dot{\underline{F}}^* - \dot{\underline{F}} = \operatorname{Grad} \underline{v}^* - \operatorname{Grad} \underline{v} = \operatorname{Grad} \underline{w}$$

$$\mathcal{H}(\underline{v}^*, \underline{v}) \geqslant \int_V \operatorname{Grad} \underline{w} : \underset{\approx}{\mathbb{C}}^0 : \operatorname{Grad} \underline{w} \, \mathrm{d}V = \mathcal{I}^0(\underline{w}) \tag{3.32}$$

It can be seen that a sufficient condition for uniqueness of the solution $\underline{v}^0$ following the fundamental deformation path is that the stability-functional calculated for the linear comparison solid, $\mathcal{I}^0(\underline{w})$, is strictly positive [Hill, 1958, Hill, 1959]. Because (3.33) guarantees uniqueness of $\underline{v}^0$, $\mathcal{I}^0(\underline{w})$ is called the exclusion functional.

$$\mathcal{I}^0(\underline{w}) > 0 \qquad \text{for every } \underline{w} \neq \underline{0} \qquad\qquad \Longrightarrow \text{ uniqueness of } \underline{v}^0 \tag{3.33}$$

Condition (3.33) is a sufficient condition for uniqueness. For discretized systems, however, references [Petryk, 1991, Petryk and Thermann, 1992] show that it is also necessary for uniqueness, cf. section 3.7, provided (3.15) holds.

3.6 Discretized systems

In the following chapters elastoplastic stability problems are considered in a discretized form and deformations are approximated by shape functions. This applies to both, analytical- and FEM-models. Critical loads calculated for discretized systems are, possibly close, upper bounds for critical loads of the continuous system.

In this section relevant quantities are reformulated for discretized systems, following the notation used in [Petryk and Thermann, 1992]. For ease of manipulation the generalized coordinates (GCs), respectively their rates, are collected in an algebraic vector $\underline{\mathbf{V}}$. The indices are assigned to the GCs in such a way that the uninterrupted sequence of GCs from 1 to some number $\mathfrak{m}$ is load controlled, while the remaining sequence from $\mathfrak{m}+1$ to $\mathfrak{n}$ is under displacement control. The velocity field $\underline{\mathbf{v}}$ is approximated using shape functions, $\underline{\boldsymbol{\phi}}_i$, associated with the respective GC-rate.

$$\underline{\mathbf{V}} := \left[\ \overbrace{\dot{q}_1 \ \ldots \ \dot{q}_m}^{\text{GCs under load control}} \ \underbrace{\dot{q}_{m+1} \ \ldots \ \dot{q}_n}_{\text{GCs under displacement control}} \ \right]^{\mathsf{T}}$$

$$\underline{\mathbf{v}} = \left[\ \underline{\boldsymbol{\phi}}_1 \ \ldots \ \underline{\boldsymbol{\phi}}_m \ \underline{\boldsymbol{\phi}}_{m+1} \ \ldots \ \underline{\boldsymbol{\phi}}_n \ \right] \begin{bmatrix} \dot{q}_1 \\ \vdots \\ \dot{q}_m \\ \dot{q}_{m+1} \\ \vdots \\ \dot{q}_n \end{bmatrix}$$

To approximate the velocity field conforming to homogeneous displacement BCs, $\underline{\mathbf{w}}$, a different algebraic vector, $\underline{\mathbf{W}}$, is defined:

$$\underline{\mathbf{W}} := \left[\ \overbrace{\dot{q}_1 \ \ldots \ \dot{q}_m}^{\text{GCs under load control}} \ \underbrace{0 \ \ 0 \ \ 0}_{\text{GCs under displacement control}} \ \right]^{\mathsf{T}}$$

$$\underline{\mathbf{w}} = \left[\ \underline{\boldsymbol{\phi}}_1 \ \ldots \ \underline{\boldsymbol{\phi}}_m \ \underline{\boldsymbol{\phi}}_{m+1} \ \ldots \ \underline{\boldsymbol{\phi}}_n \ \right] \begin{bmatrix} \dot{q}_1 \\ \vdots \\ \dot{q}_m \\ 0 \\ \vdots \\ 0 \end{bmatrix}$$

In order to clearly point out the range of the indices involved, summation is in the following explicitly stated by the summation symbol, even for repeated indices. The rates of the deformation gradient and the PK1-stress tensor are thus rewritten in terms of the discrete GC-rates as follows:

$$\dot{\underset{\sim}{\mathbf{F}}} = \sum_{j=1}^{n} \dot{q}_j \, \mathrm{Grad} \, \underline{\boldsymbol{\phi}}_j$$

$$\dot{\underset{\sim}{\mathbf{P}}}(\underline{\mathbf{v}}) = \sum_{j=1}^{n} \dot{q}_j \, \underset{\approx}{\mathbb{C}}(\underline{\mathbf{v}}) : \mathrm{Grad} \, \underline{\boldsymbol{\phi}}_j$$

Upon substituting the discretization into the rate form virtual work principle, (3.8), the negative of the first volume integral on the left hand side is pertinently defined as the product of the rate of the internal force vector components, $(Q_i)^{\bullet}$, and the GC-rates, $\dot{q}_i$. The internal force rate vector components are then:

$$\dot{Q}_i(\underline{\mathbf{v}}) = + \int_V \dot{\underset{\sim}{\mathbf{P}}}(\underline{\mathbf{v}}) : \mathrm{Grad} \, \underline{\boldsymbol{\phi}}_i \, dV \qquad\qquad i = 1 \ldots n$$

$$\dot{Q}_i(\underline{\mathbf{v}}) = + \sum_{j=1}^{n} \dot{q}_j \int_V \mathrm{Grad} \, \underline{\boldsymbol{\phi}}_j : \underset{\approx}{\mathbb{C}}(\underline{\mathbf{v}}) : \mathrm{Grad} \, \underline{\boldsymbol{\phi}}_i \, dV \qquad i = 1 \ldots n \qquad (3.34)$$

In analogy, the rate of the external force vector components $(P_i)^{\bullet}$ is formed by the last two terms on the right hand side of (3.8). The index i extends only up to m, because the remaining GC-rates are directly controlled.

$$\dot{P}_i = \int_V \dot{\underline{\mathbf{B}}} \cdot \underline{\boldsymbol{\phi}}_i \, dV + \int_{S_T} \dot{\underline{\mathbf{T}}} \cdot \underline{\boldsymbol{\phi}}_i \, dS \qquad\qquad i = 1 \ldots m \qquad (3.35)$$

The $\mathcal{J}$-functional for discretized systems takes the form:

$$\mathcal{J}(\underline{\mathbf{v}}) = \frac{1}{2} \sum_{i=1}^{n} \dot{Q}_i(\underline{\mathbf{v}}) \dot{q}_i - \sum_{i=1}^{m} \dot{P}_i \dot{q}_i \qquad\qquad (3.36)$$

The rate form virtual work principle for discretized systems is given below. On account of $\dot{q}_i$ being arbitrary where GC-rates are not directly controlled this reverts back to the equation of continuing equilibrium, i.e. equilibrium of the internal and external force rates.

$$\delta\mathcal{J}(\underline{\mathbf{v}}, \underline{\mathbf{w}}) = -\delta\mathcal{A}(\underline{\mathbf{v}}, \underline{\mathbf{w}}) = \sum_{i=1}^{m} \left(+ \dot{Q}_i(\underline{\mathbf{v}}) \dot{q}_i - \dot{P}_i \dot{q}_i \right) = 0 \qquad (3.37)$$

$$\dot{Q}_i(\underline{\mathbf{v}}) = \dot{P}_i \qquad\qquad i = 1 \ldots m \qquad (3.38)$$

The system's tangent stiffness matrix is the change of the net force-rate with respect to the GC-rate. When excluding deformation dependent loading the controlled external

force rates do not depend on the GC-rates.

$$
\mathsf{K}_{ij}(\underline{v}) = \frac{\partial}{\partial \dot{q}_j}\big(\dot{Q}_i(\underline{v}) - \dot{P}_i\big) = \frac{\partial}{\partial \dot{q}_j}\big(\dot{Q}_i(\underline{v})\big)
$$

$$
\mathsf{K}_{ij}(\underline{v}) = \int_V \operatorname{Grad} \underline{\phi}_j : \underset{\approx}{\mathbb{C}}(\underline{v}) : \operatorname{Grad} \underline{\phi}_i \, dV \qquad\qquad i,j = 1 \ldots n \qquad (3.39)
$$

The systems stiffness matrix is also linked to the second derivatives of $\mathcal{J}$:

$$
\begin{aligned}
\frac{\partial^2 \mathcal{J}(\underline{v})}{\partial \dot{q}_k \partial \dot{q}_l} &= \frac{\partial^2}{\partial \dot{q}_k \partial \dot{q}_l}\Big(\frac{1}{2}\sum_{i=1}^{n}\dot{Q}_i(\underline{v})\dot{q}_i - \sum_{i=1}^{m}\dot{P}_i \dot{q}_i\Big) \\
&= \frac{1}{2}\frac{\partial}{\partial \dot{q}_l}\Big(\sum_{i=1}^{n}\frac{\partial \dot{Q}_i}{\partial \dot{q}_k}\dot{q}_i + \sum_{i=1}^{n}\dot{Q}_i\delta_{ik} - \sum_{i=1}^{m}\dot{P}_i\delta_{ik}\Big)
\end{aligned}
$$

$$
\frac{\partial^2 \mathcal{J}(\underline{v})}{\partial \dot{q}_i \partial \dot{q}_j} = \frac{\partial \dot{Q}_i(\underline{v})}{\partial \dot{q}_j} = \mathsf{K}_{ij}(\underline{v}) \qquad\qquad (3.40)
$$

3.7 Energy interpretation and path-stability

In [Petryk, 1991, Petryk and Thermann, 1992] an extended theory for inelastic bifurcation problems was introduced on the basis of an energy interpretation. It is assumed, that the material under consideration allows a rate potential. The references define an energy functional $\mathcal{E}$ of the system consisting of the deformable body and the loading device as the sum of the energy contained in the body and the potential of the loading device, $\mathcal{V}$. The energy of the deformable body is equal to the negative work of the internal forces, $\mathcal{A}_{\text{int}}$, which is used here instead.

$$
\mathcal{E} = -\mathcal{A}_{\text{int}} + \mathcal{V} \qquad\qquad (3.41)
$$

The cited references consider discretized systems and energy expressions are given in terms of generalized forces and displacements, respectively their rates.

$$
-\mathcal{A}_{\text{int}} = +\sum_{i=1}^{n}\int_0^t Q_i \dot{q}_i \, dt \qquad\qquad (3.42)
$$

The external forces are assumed to allow for a potential, $\mathcal{V}$, it is in general not equal to the negative of their work $-\mathcal{A}_{\text{ext}}$, unless the external forces are dead loads.

$$
\mathcal{V} = -\sum_{i=1}^{m} P_i q_i \qquad\qquad (3.43)
$$

For equilibrium, the first time derivative of the energy functional does not depend on the rate of the free GCs $\dot{q}_i, i = 1..m$. The GC-rates $\dot{q}_i, i = m + 1..n$ and the rate of the external forces $(P_i)^\bullet$ are prescribed.

$$
\begin{aligned}
\dot{\mathcal{E}}(\underline{v}) &= \sum_{i=1}^{n} Q_i \dot{q}_i - \sum_{i=1}^{m} (\dot{P}_i q_i + P_i \dot{q}_i) \\
&= \sum_{i=1}^{m} (Q_i - P_i) \dot{q}_i + \sum_{i=m+1}^{n} Q_i \dot{q}_i - \sum_{i=1}^{m} \dot{P}_i q_i
\end{aligned}
\tag{3.44}
$$

For an equilibrium state the second time derivative of the energy functional is:

$$
\ddot{\mathcal{E}}(\underline{v}) = \sum_{i=1}^{n} \dot{Q}_i \dot{q}_i - 2 \sum_{i=1}^{m} \dot{P}_i \dot{q}_i + \sum_{i=m+1}^{n} Q_i \ddot{q}_i - \sum_{i=1}^{m} \ddot{P}_i q_i
\tag{3.45}
$$

The second time derivatives of q_i and P_i are prescribed quantities for $i = m + 1..n$ and $i = 1..m$ respectively. So for any pair of velocity fields $\underline{v}^{(1)}$ and $\underline{v}^{(2)}$ at an equilibrium state there is the identity [Petryk, 1985]:

$$
\tfrac{1}{2} \ddot{\mathcal{E}}(\underline{v}^{(1)}) - \tfrac{1}{2} \ddot{\mathcal{E}}(\underline{v}^{(2)}) = \mathcal{J}(\underline{v}^{(1)}) - \mathcal{J}(\underline{v}^{(2)})
\tag{3.46}
$$

For an equilibrium state under constant loading, as has been considered in section 3.2, the first time derivative of the energy functional (3.44) vanishes. The additional energy required to move the system form the equilibrium state in an arbitrary, but kinematically admissible, direction, at constant loading, is then given by $\ddot{\mathcal{E}}(\underline{w})$:

$$
\ddot{\mathcal{E}}(\underline{w}) = \sum_{i=1}^{m} \dot{Q}_i(\underline{w}) \dot{q}_i
\tag{3.47}
$$

The last equation is used in [Petryk, 1991, Petryk and Thermann, 1992] to introduce the notion of directional stability, i.e. if spontaneous departure from an equilibrium state along a direct path $\underline{w}$ is prevented by an energy barrier in every admissible direction the equilibrium is said to be directionally stable. For directional stability it is required that:

$$
\sum_{i=1}^{m} \dot{Q}_i(\underline{w}) \dot{q}_i > 0 \qquad \text{for every } \underline{w} \neq \underline{0}
\tag{3.48}
$$

Under the limitations stated in section 3.2 the stability criteria (3.15) and (3.48) are equivalent, with the latter given for discretized systems. With regard to the existence and uniqueness of a solution to (3.38) [Petryk and Thermann, 1992] states three theorems. Quantities with a superscript 0 refer to the fundamental (primary) deformation path.

Theorem 1: The system of equations (3.38) at a directionally stable equilibrium state has a solution which assigns to $\mathcal{J}$ it absolute minimum value in $\underline{V}$.

Theorem 2: For uniqueness of a solution $\underset{\sim}{\boldsymbol{v}}$ to (3.38) at a directionally stable equilibrium state it is necessary that $\underset{\sim}{\boldsymbol{v}}$ assigns to $\mathcal{J}$ a strict and absolute minimum value.

$$\mathcal{J}(\underset{\sim}{\boldsymbol{v}}) < \mathcal{J}(\underset{\sim}{\boldsymbol{v}}^*) \qquad \text{for every } \underset{\sim}{\boldsymbol{v}} \neq \underset{\sim}{\boldsymbol{v}}^* \tag{3.49}$$

A necessary condition for a $\mathcal{J}(\underset{\sim}{\boldsymbol{v}})$ to attain a minimum is positive semidefiniteness of $\underset{\sim}{\mathbf{K}}(\underset{\sim}{\boldsymbol{v}})$, cf. (3.40).

$$\dot{q}_i K_{ij}(\underset{\sim}{\boldsymbol{v}}) \dot{q}_j \geqslant 0 \qquad \text{for every } \underset{\sim}{\boldsymbol{w}} \tag{3.50}$$

These theorems lead to the corollary:

Corollary 1: The solution in velocities is nonunique at every point on a solution path along which (3.48) holds but (3.50) does not: This means that the bifurcation points are then not isolated but form a continuous nonuniqueness range.

Theorem 3: If there exists a solution $\underset{\sim}{\boldsymbol{v}}^0$ to (3.38) such that:
  (i) the respective tangent stiffness matrix $\underset{\sim}{\mathbf{K}}^0$ is positive definite, and
  (ii) the stress and deformation rates $(\underset{\sim}{\mathbf{P}}^0)^{\bullet}$ and $(\underset{\sim}{\mathbf{F}}^0)^{\bullet}$ corresponding to $\underset{\sim}{\boldsymbol{v}}^0$ satisfy the constitutive inequality (3.51)
  then the solution $\underset{\sim}{\boldsymbol{v}}^0$ is unique.

$$\dot{\underset{\sim}{\mathbf{P}}}^0 : \dot{\underset{\sim}{\mathbf{F}}} - \dot{\underset{\sim}{\mathbf{P}}} : \dot{\underset{\sim}{\mathbf{F}}}^0 \geqslant 0 \qquad \text{for every } \dot{\underset{\sim}{\mathbf{F}}} \tag{3.51}$$

The constitutive inequality (3.51) is not more restrictive than the relative convexity property (3.31) and holds for classic J_2-plasticity. The theorems 2 and 3 lead to a second corollary:

Corollary 2: If (3.48) and (3.51) hold along a deformation path then positive definiteness of the tangent stiffness matrix $\underset{\sim}{\mathbf{K}}^0$ is necessary and sufficient for uniqueness of the first- and second-order solutions.

This leaves the question which path is followed when uniqueness is lost. On the basis of the first corollary it could be argued that once the system encounters the first bifurcation point it can no longer be followed because because there nonuniqueness would persist in a continuous interval. In [Petryk and Thermann, 1992] a criterion to exclude unstable *paths* is given by appealing to energy considerations: Along a stable path the actual deformation increment must minimize the value of the increment of the energy functional $\mathcal{E}$ calculated with accuracy to second-order therms, within the class of all kinematically admissible deformation increments. Because the first oder term $\mathcal{E}$ is independent of the deformation mode for equilibrium states, as shown in (3.44), path-stability is decided by the second order term. This definition can be regarded as a specification of the intuitive engineering hypothesis that a real deformation mode in metals exhibits a tendency to minimize the energy consumption. Due to the identity (3.46) this means that a stable deformation path

also necessarily minimizes $\mathcal{J}$. Therefore, on the actually followed solution $\underline{\boldsymbol{v}}$ there is the relation:

$$\mathcal{J}(\underline{\boldsymbol{v}}^*) \geqslant \mathcal{J}(\underline{\boldsymbol{v}}) \qquad \text{for every } \underline{\boldsymbol{v}}^* \tag{3.52}$$

3.8 Example: axially loaded beam

As a demonstration the bifurcation behaviour of a rectangular beam-like structure of length L and height H, under axial compressive loading, P, is investigated. The out-of-plane dimension of the structure is one unit-length and no out-of-plane displacements are permitted. The only deformation modes allowed in the model are sinusoidal deflection and axial shortening and the respective GCs are q_1 and q_2. The load P is considered to be controlled by the load proportionality factor λ.
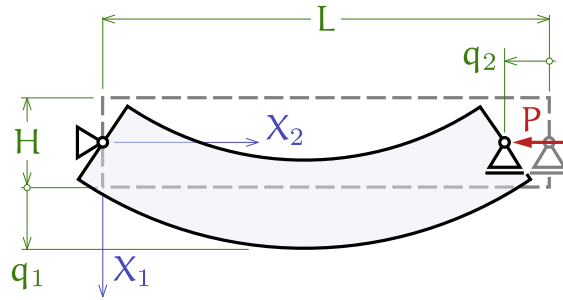

Figure 3.1: Assumed deformation mode

The kinematic assumptions are the same as for the Euler-Bernoulli beam theory. The quasi-static deformation rates v_i for these assumptions are:

$$v_1 = \sin\left(\frac{\pi X_2}{L}\right)\dot{q}_1 \tag{3.53$_1$}$$

$$\begin{aligned}
v_2 &= -\frac{X_2}{L}\dot{q}_2 - \frac{\partial v_1}{\partial X_2}X_1 \\
&= -\frac{X_2}{L}\dot{q}_2 - \frac{\pi X_1}{L}\cos\left(\frac{\pi X_2}{L}\right)\dot{q}_1
\end{aligned} \tag{3.53$_2$}$$

The coefficients of the GC-rates form the shape function vectors, (3.54), their spatial gradients are given in (3.55).

$$\underline{\boldsymbol{\Phi}}_1 = \begin{bmatrix} \sin(\frac{\pi X_2}{L}) \\ -\frac{\pi X_1}{L}\cos(\frac{\pi X_2}{L}) \end{bmatrix} \tag{3.54$_1$}$$

$$\underline{\boldsymbol{\Phi}}_2 = \begin{bmatrix} 0 \\ -\frac{X_2}{L} \end{bmatrix} \tag{3.54$_2$}$$

$$\text{Grad } \underline{\boldsymbol{\phi}}_1 = \begin{bmatrix} 0 & \frac{\pi}{L}\cos\frac{\pi X_2}{L} \\ -\frac{\pi}{L}\cos\frac{\pi X_2}{L} & +\frac{\pi^2}{L^2}\sin\frac{\pi X_2}{L} \end{bmatrix} \tag{3.55_1}$$

$$\text{Grad } \underline{\boldsymbol{\phi}}_2 = \begin{bmatrix} 0 & 0 \\ 0 & -\frac{1}{L} \end{bmatrix} \tag{3.55_2}$$

For simplicity the assumption is made that the structure is monotonically loaded to some point beyond the initial yielding load along the primary equilibrium path. Instability and bifurcation in the purely elastic regime or immediately upon yielding are excluded. Quantities evaluated at the primary loading path are indicated by right superscript 0. With regards to the constitutive behavior only the modulus $\mathbb{L}_{2222}$ is considered, which is equal to the tangent modulus E_t on the primary loading path. The current stress σ_{22} equals $-P/H$ and is homogeneous over the entire cross-section, thus the linear comparison material is obtained from (2.26):

$$\underset{\approx}{\mathbb{C}}^0 = \begin{bmatrix} \begin{bmatrix} 0 & 0 \\ 0 & 0 \end{bmatrix} & \begin{bmatrix} 0 & -\frac{P}{2H} \\ +\frac{P}{2H} & 0 \end{bmatrix} \\ \begin{bmatrix} 0 & +\frac{P}{2H} \\ +\frac{P}{2H} & 0 \end{bmatrix} & \begin{bmatrix} 0 & 0 \\ 0 & E_t + \frac{P}{H} \end{bmatrix} \end{bmatrix} \tag{3.56}$$

Using the mixed material tangent of the linear comparison material in (3.34) yields the internal force rates on the fundamental path. The beam-like structure is thought to have a high ratio of L to H, so H^2 can be reasonably neglected over L^2.

$$\dot{Q}_1(\underline{v}^0) = \frac{\pi^2}{24L^3}\left(\pi^2 E_t H^3 + (\pi^2\cancel{H^2} - 12L^2)P\right)\dot{q}_1 \tag{3.57_1}$$

$$\dot{Q}_2(\underline{v}^0) = \frac{HE_t + P}{L}\dot{q}_2 \tag{3.57_2}$$

The system tangent stiffness matrix on the fundamental path is:

$$\underset{\sim}{K}(\underline{v}^0) = \begin{bmatrix} \frac{\pi^4 E_t H^3}{24L^3} - \frac{\pi^2 P}{2L} & 0 \\ 0 & \frac{E_t H}{L} + \frac{P}{L} \end{bmatrix} \tag{3.58}$$

The tangent stiffness matrix is initially positive definite, but with increasing load the eigenvalues decrease and at some critical load, P^0 it will become singular. The load can be obtained from setting the determinant to zero.

$$\left(\pi^2 E_t H^3 - 12L^2 P^0\right)\left(E_t H + P^0\right) = 0$$

$$(P^0)_1 = \frac{\pi^2 E_t H^3}{12L^2} \tag{3.59_1}$$

$$(P^0)_2 = -E_t H \tag{3.59_2}$$

The solution then resembles the elastic buckling load of the beam but has the Young's modulus exchanged for the tangent modulus. The similarity is superficial, though, as both loss of uniqueness and stability coincide for the elastic Euler-buckling. In the present case, however, $(\mathsf{P}^0)_1$ merely marks the end of the uniqueness of $\underline{\underline{v}}^0$. If the load is increased further the system will deviate from the fundamental path. Stability, on the other hand, is decided by (3.52) and has to be considered for a fixed value of the load proportionality factor. At constant load $\mathbb{L}_{2222}$ is equal to $\mathsf{E_t}$ only parts of the cross-section experiencing further loading and equals the elastic modulus E in the unloaded ones, (3.56) does not apply. The internal force rates $(\mathsf{Q_i}(\underline{\underline{w}}))^{\bullet}$ and the tangent stiffness matrix $\underset{\sim}{\mathsf{K}}(\underline{\underline{w}})$ are rather involved for this scenario and it is more conveniently considered for a further simplified problem known as Shanley's column, cf. below.

3.9 Example: Shanley's column

A classical introductory example is known as Shanley's column in the literature [Bažant and Cedolin, 2010]. As a further simplification over the previous problem a two degrees of freedom-system consisting of rigid T-bars attached to vertical trusses is considered, cf. Fig. 3.2. The homogeneity of stress and strain in the trusses allows for a more convenient handling of the problem. Again, the load P is considered to be controlled.
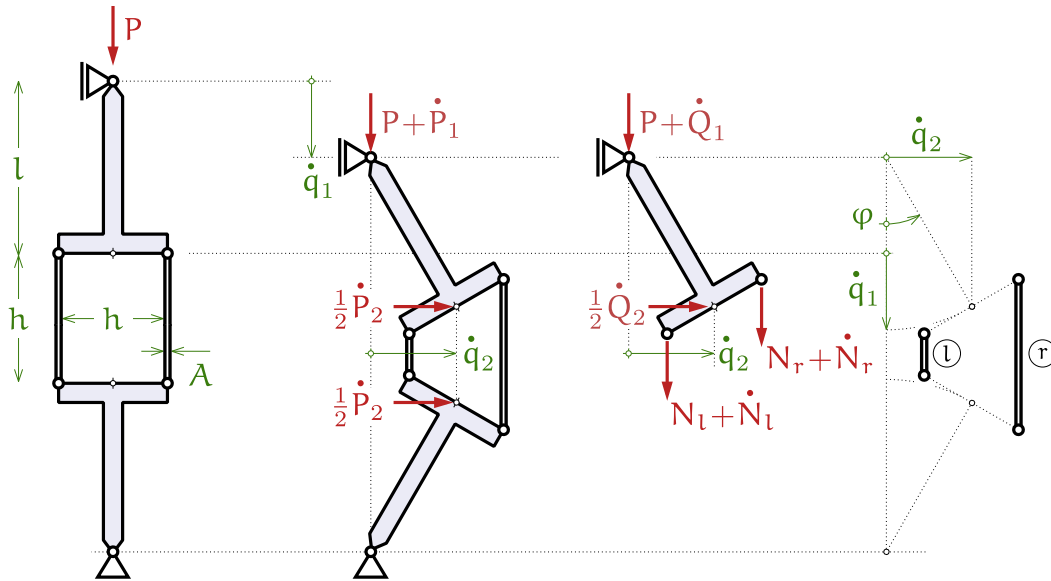

Figure 3.2: Shanley's column

The change in length of the trusses, as a function of the T-bar rotation angle φ, is given in (3.60).

$$\Delta \mathfrak{l}_{\mathfrak{l},r} = -\mathsf{q}_1 \mp 2\frac{\mathsf{h}}{2}\sin(\varphi) + 2(1-\cos(\varphi))\mathfrak{l} \tag{3.60}$$

Only first order accuracy is required, so the trigonometric functions are substituted by the first element of their series expansion in the following.

$$\dot{\varepsilon}_{l,r} = \frac{\Delta l_{l,r}}{h} = -\frac{\dot{q}_1}{h} \mp \frac{\dot{q}_2}{l} + \mathcal{O}(\dot{q}_i^2) \tag{3.61}$$

For the rate of the truss forces the incremental nonlinearity needs to be taken into account by allowing different constitutive branches to be active in the left and right truss. The tangent moduli are E_l and E_r, respectively, and they can assume either the tangent modulus, E_t, for loading or the elastic modulus, E, for the case of unloading.

$$\dot{N}_{l,r} = E_{l,r} A \left(-\frac{\dot{q}_1}{h} \mp \frac{\dot{q}_2}{l} \right) \tag{3.62}$$

Since the structure forms a statically determinate system the internal forces can be obtained directly from equilibrium. Force equilibrium in vertical direction and taking into account that the non rate terms of the reference configuration are already balanced yields the first internal force:

$$\dot{Q}_1 = -\dot{N}_l - \dot{N}_r = (E_l + E_r)\frac{A}{h}\dot{q}_1 + (E_l - E_r)\frac{A}{l}\dot{q}_2 \tag{3.63_1}$$

The equilibrium of moments gives after some algebra the second internal force:

$$\dot{Q}_2 = (E_l - E_r)\frac{A}{l}\dot{q}_1 + (E_l + E_r)\frac{Ah}{l^2}\dot{q}_2 - 2P\dot{q}_2 \tag{3.63_2}$$

Via (3.39) the system tangent stiffness matrix is obtained as:

$$\underset{\sim}{\mathbf{K}}(\underline{v}) = \begin{bmatrix} \dfrac{(E_l + E_r)A}{h} & \dfrac{(E_l - E_r)A}{l} \\ \dfrac{(E_l - E_r)A}{l} & \dfrac{(E_l + E_r)Ah}{l^2} - \dfrac{2P}{l} \end{bmatrix} \tag{3.64}$$

In order to find the first bifurcation load the tangent stiffness matrix is evaluated for the primary equilibrium path, i.e. $\underline{v} = \underline{v}^0 = \begin{bmatrix} \dot{q}_1 & 0 \end{bmatrix}^\mathsf{T}$. It is apparent from (3.61) that for this path both trusses are in the loading branch, thus the tangent stiffness matrix takes the form:

$$\underset{\sim}{\mathbf{K}}^0(\underline{v}^0) = \begin{bmatrix} \dfrac{2E_t A}{h} & 0 \\ 0 & \dfrac{2E_t Ah}{l^2} - \dfrac{2P}{l} \end{bmatrix} \tag{3.65}$$

Other tangent stiffness matrices corresponding to other constitutive branches need not be considered here, because of the arguments presented in section 3.5. Assuming the system was loaded into the elastoplastic regime and neither instability nor bifurcation occurred in the elastic regime or on the transition to the plastic regime, then $\underset{\sim}{\mathbf{K}}^0$ is still positive

$$\mathtt{E} = 10 \times 10^3 \, [\mathrm{FL}^{-2}] \quad \mathtt{E_t} = 5 \times 10^3 \, [\mathrm{FL}^{-2}] \quad \mathtt{h} = 1 \, [\mathrm{L}] \quad \mathtt{l} = 10 \, [\mathrm{L}] \quad \mathtt{A} = 1 \, [\mathrm{L}^2]$$

Table 3.1: Parameters used to generate the Figs. 3.3(a), 3.4(a), 3.4(b) and 3.5(a).

definite. The functional $\mathcal{J}$ calculated for this scenario by (3.36) is depicted in Fig. 3.3(a). Further loading will, however, decrease the lowest eigenvalue and at a certain level of the loading parameter $\underset{\sim}{\mathbf{K}}^0$ will become singular. Then the primary loading path no longer minimizes $\mathcal{J}$ and bifurcation occurs at load $\mathtt{P}^{*0}$.

$$\mathtt{P}^{*0} = \frac{\mathtt{E_t A h}}{\mathtt{l}} \tag{3.66}$$

Instability, however, is not implied by bifurcation and needs to be evaluated separately by the means of (3.48), i.e. the presence or absence of an energy barrier. When calculating the internal forces the tangent stiffness has to be taken in the direction of $\underset{\sim}{\mathbf{w}}$ rather then $\underline{\mathbf{v}}^0$, and the respectively active constitutive branch has to be taken into account. The result calculated at the bifurcation load $\mathtt{P}^{*0}$ is presented as a contour plot, Fig. 3.4(b). Note that there are 4 possible combinations of activated branches, resulting in a patch of surfaces of piecewise constant curvature. The contours represent states that can be reached by monotonic radial displacement from the origin for a given amount of work done on the system. All contours form closed curves around the origin, and the work is positive everywhere but the origin. Consequently the equilibrium state at $\mathtt{P}^{*0}$ is still stable in the energy sense as discussed in section 3.7.

Bifurcation at the primary bifurcation point can be prevented by additional constraints, e.g. when the bifurcation load is lower than the yield load. If this additional constraint is removed, bifurcation occurs at a secondary bifurcation point. If the stability criterion is still met, secondary bifurcation will occur in a quasi-static manner i.e. without sudden unloading, cf. Fig. 3.5(a).
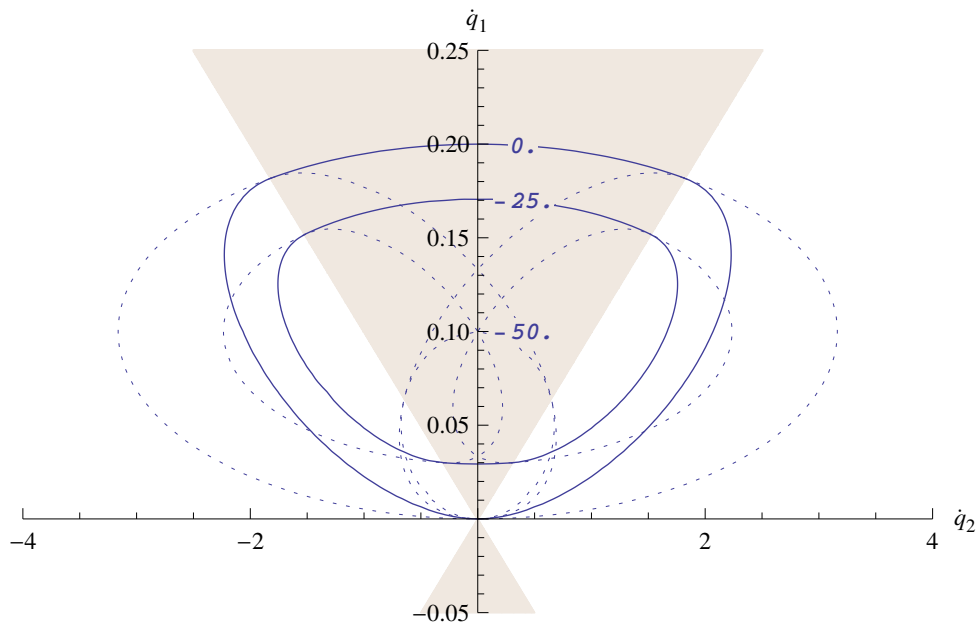
(a) Contour plot of $\mathcal{J}$. The surface consist of three patches (solid lines); The dashed lines are a continuation of the patches beyond their range of validity
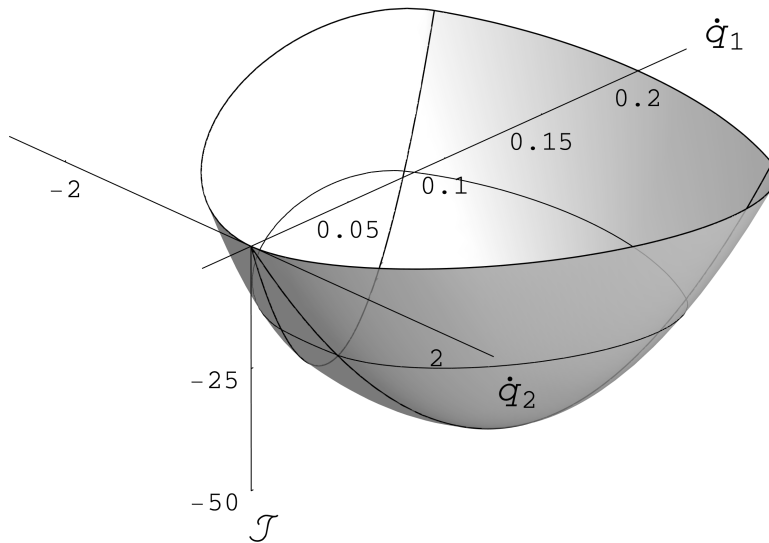

(b) Axonometric view of the surface generated by $\mathcal{J}$. Only the part $\mathcal{J} < 0$ is shown.

Figure 3.3: Functional $\mathcal{J}(\dot{q}_1, \dot{q}_2, \dot{P} = 10^3)$ evaluated according to (3.36) at 90% of the primary bifurcation load P^{*0}. $\mathcal{J}$ is minimized on the fundamental loading path $\dot{q}_2 = 0$. In the shaded cone above the origin both trusses are yielding; in the one below both are unloading. In the unshaded areas only one truss is loading, while the other is unloading.
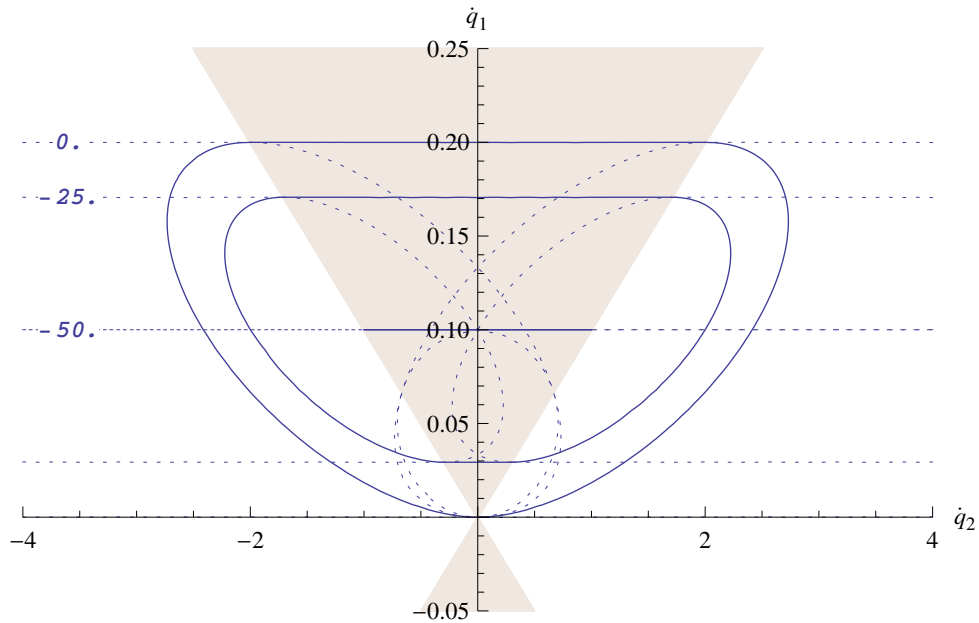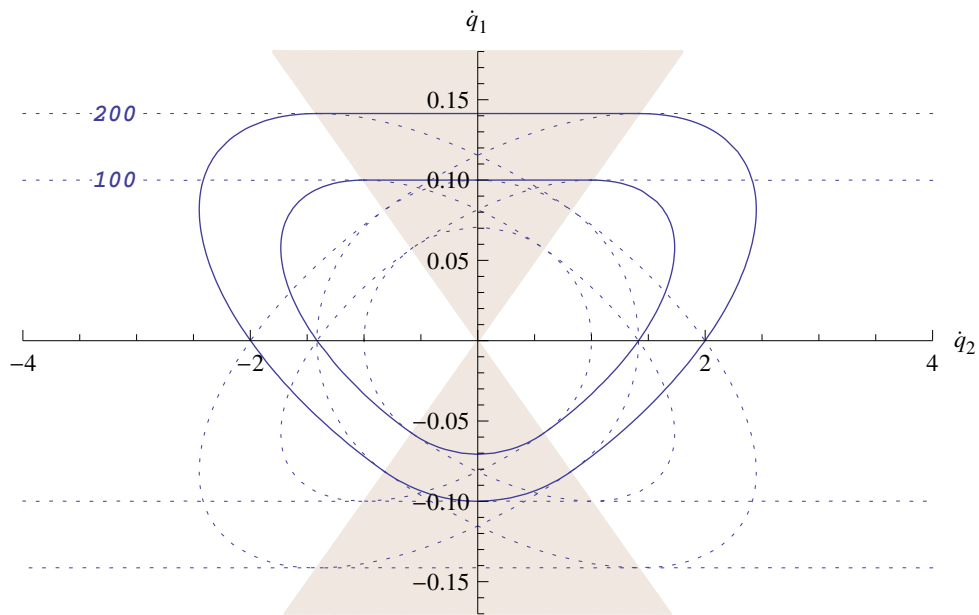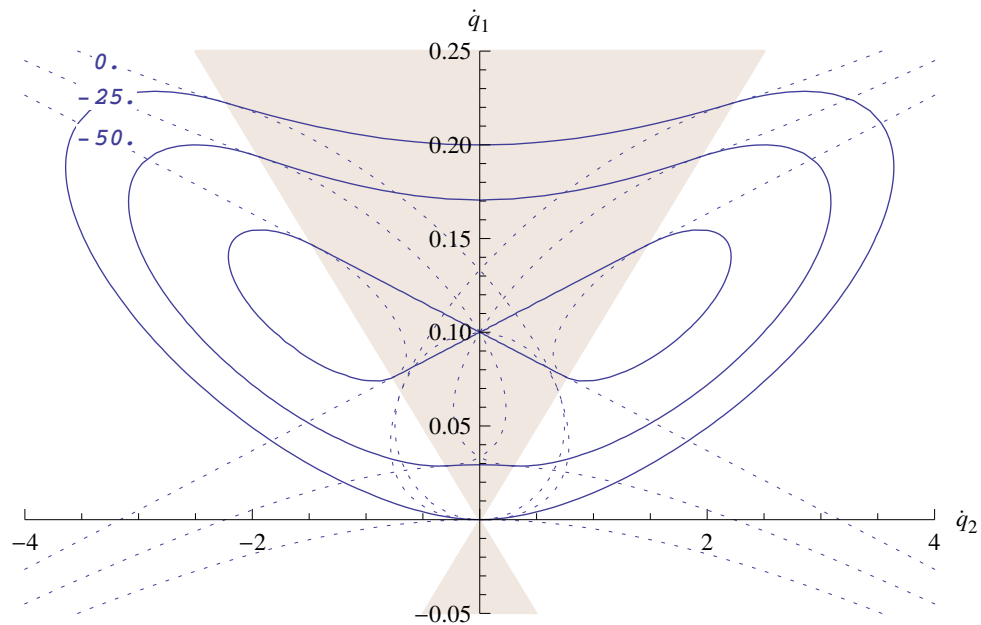
(a) Contour plot of $\mathcal{J}$

(b) Contour plot of $\mathcal{I}$; Load control over all GCs is assumed, then $\underline{W} = \underline{V} = \begin{bmatrix} \dot{q}_1 & \dot{q}_2 \end{bmatrix}^{\mathsf{T}}$

Figure 3.4: Functionals $\mathcal{J}(\dot{q}_1, \dot{q}_2, \dot{P} = 10^3)$ and $\mathcal{I}(\dot{q}_1, \dot{q}_2)$ evaluated according to (3.36) and (3.15) at the primary bifurcation load P^{*0}. The fundamental loading path no longer strictly minimizes $\mathcal{J}$ and $\dot{q}_2$ is not forced to zero at increasing load $(P)^{\bullet}$, cf. Fig. 3.4(a). On the other hand for $(P)^{\bullet} = 0$ the perturbation work $\mathcal{I}$ is still positive for all $\dot{q}_1, \dot{q}_2$, cf. Fig. 3.4(b).
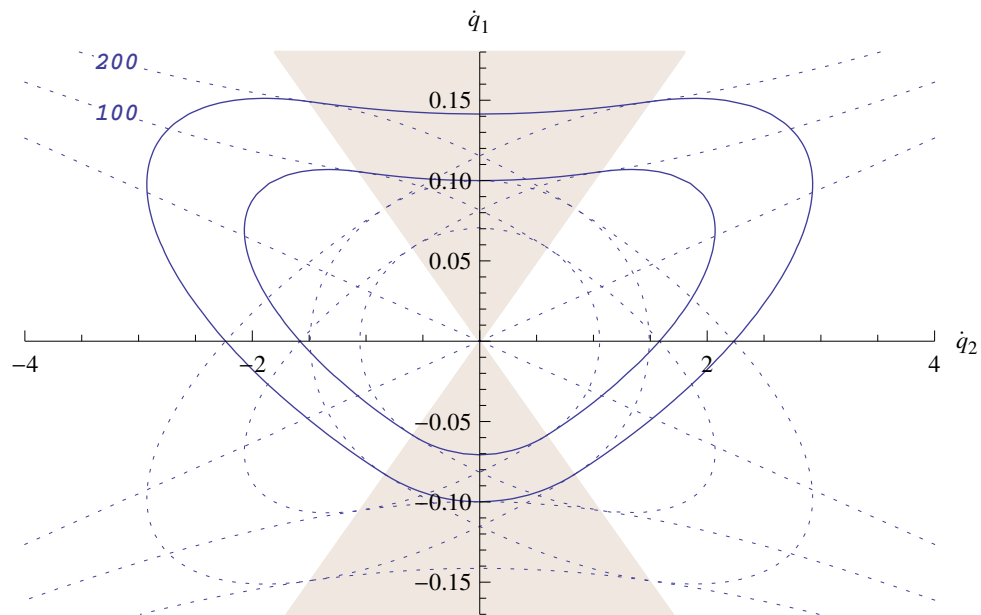
(a) Contour plot of $\mathcal{J}$

(b) Contour plot of $\mathcal{I}$; Load control over all GCs

Figure 3.5: Functionals $\mathcal{J}(\dot{\mathsf{q}}_1, \dot{\mathsf{q}}_2, \dot{\mathsf{P}} = 10^3)$ and $\mathcal{I}(\dot{\mathsf{q}}_1, \dot{\mathsf{q}}_2)$ evaluated on the undeflected equilibrium path at 110% of the primary bifurcation load P^{*0}. There are three stationary points, but only two correspond to a minimum. Note that a state like this can only be reached when additional constraints are enforced.

4 A preliminary, incompatible model

As a first approach to the problem, an infinite periodic arrangement of evenly spaced lamellae connected to the matrix only at evenly spaced individual points, rather then by a continuous bedding is considered. It is further assumed that the buckling-mode of these lamella is such that there is symmetry with respect to the midplane between two lamellae and the planes orthogonal to the lamellae passing through the connection points, hence the name symmetric mode. In this regular arrangement the domain spanning the space between two neighbouring symmetry planes, both horizontally and vertically, is representative of the entire assembly and is, therefore, called a unit cell (UC). Any UC can be made congruent with every other by suitable mirror transformations, and it is sufficient to deal only with one in order to describe the entire assembly.

The UC itself is rectangular and consists of the lamella connected at the top and bottom center and the matrix (Fig. 4.1). The main abstraction of the model is that in each UC the matrix itself is divided into four rectangular subdomains. At the interfaces the subdomains slide freely, they stay rectangular and do not separate or interpenetrate each other normal to the interfaces. However, the formation of voids and interpenetrations is otherwise allowed. For instance, an incompatibility will form at the UC center when the lamella buckles. The UC height spans the distance between two lamella-matrix connection points and corresponds to the half of the buckling-wavelength, which must be treated as an unknown and can be obtained from minimizing the buckling-load.

As becomes apparent from the numerous simplifications and assumptions stated so far the scope of the model is very limited. Due to the peculiar coupling the rectangular subdomains will only experience domain wide constant normal strains and either yield or unload as a whole, thus significantly simplifying the problem. This comes at the cost of being incompatible. Also, instead of the buckling-mode naturally arising from the theory it is a priory assumed to adhere to the symmetry conditions stated above, thus possibly suppressing relevant buckling-modes. However, the symmetry assumptions are necessary to allow for a meaningful coupling of the subdomains. While for these reasons the incompatible model is certainly not an accurate representation of an actual lamella-matrix arrangement it serves as a demonstrator of the properties of inelastic buckling of lamellar structures. It is, for instance, not obvious from the beginning whether there will be instant or gradual unloading in some of the subdomains during buckling, cf. section 4.4. The simplicity of the incompatible matrix segmentation allows for a more extensive mathematical treatment of the problem without leading to intractable equations. The purpose of this section is to relate the buckling-problem of a lamella embedded in an elastoplastic matrix to the general theory of inelastic buckling as discussed in chapter 3 rather than making accurate predictions for the actual lamella-structure. In the following chapters effort is

made to drop the crude simplifications applied here and to derive compelling reasons for many circumstances stated as assumptions here.

4.1 Kinematics and strain

The model width equals the lamella spacing and is denoted by $2A_1$, the height corresponds to half the buckling wavelength and is assigned the symbol A_2. The factor 2 is absent from the height for consistency with models discussed in the following chapters. A full buckling-period is obtained by mirroring the model at the top edge, and by repeated mirroring at the model edges the entire 2-dimensional plane can be filled. All quantities are considered per unit-depth.

Due to the abstractions introduced above, the model possesses only four GCs, q_1 to q_4. The amplitude of the buckling-mode is represented by q_1. The second GC, q_2 allows for unequal vertical expansion in the subdomains. The third and fourth GC relate to the horizontal and vertical overall deformation at the model boundary, respectively. The fourth GC q_4 includes both, the displacement which is due to the axial straining of the lamella, and the vertical displacement caused by the lateral deflection at constant axial lamella strain. All of the four GCs are considered free, i.e. not directly controlled, in the following. Conversely, the load P associated with $\dot{q}_4$ is supposedly controlled and the forces corresponding to the GCs one to three are controlled to zero.
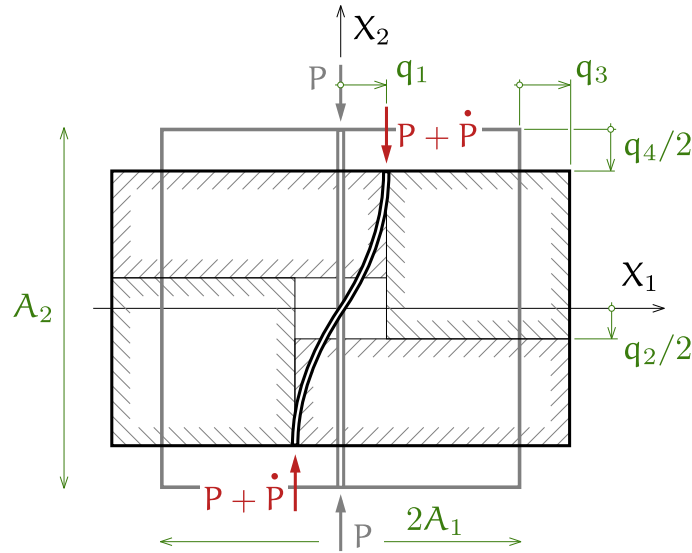

Figure 4.1: Generalized coordinates of the preliminary incompatible model

Symbols that relate to lamella-quantities are distinguished from matrix-quantities by a superscript α. Matrix-quantities, in turn, are furnished with a superscript γ. The lamella follows standard beam-theory kinematics and deflects in a sine-shape over the course of a half wavelength A_2. To account for the plane stress situation the Young's modulus in

the lamella is to be scaled by $1/(1-\nu^2)$, which is implicitly assumed whenever it appears and the symbol E^α stands for the scaled value. As has been mentioned above the lamella connects to (is pinned to) the matrix only at the top and bottom boundary of the model and freely interpenetrates the matrix in between.

$$v_1^\alpha = +\sin\left(\frac{\pi X_2}{A_2}\right)\dot{q}_1 \tag{4.1_1}$$

$$
\begin{aligned}
v_2^\alpha &= -\frac{X_2}{A_2}\dot{q}_4 - \frac{\partial v_1}{\partial X_2}X_1 \\
&= -\frac{X_2}{A_2}\dot{q}_4 - \frac{\pi X_1}{A_2}\cos\left(\frac{\pi X_2}{A_2}\right)\dot{q}_1
\end{aligned}
\tag{4.1_2}
$$

The matrix kinematics are setup to generate constant strain in each of the four respective subdomains. To avoid having four separate piecewise definitions the signum and absolute value functions are used and the velocity field for all four subdomains is given by a single expression:

$$v_1^\gamma = \left(1 - \frac{\operatorname{abs}(X_1)}{A_1}\right)\operatorname{sgn}(X_2)\dot{q}_1 + \frac{X_1}{A_1}\dot{q}_3 \tag{4.2_1}$$

$$v_2^\gamma = -\operatorname{sgn}(X_1)\left(\frac{1}{2} - \frac{\operatorname{abs}(X_2)}{A_2}\right)\dot{q}_2 - \frac{X_2}{A_2}\dot{q}_4 \tag{4.2_2}$$

The shape functions are obtained by extracting the coefficients from the velocity fields. The lamella shape functions are the same as those used in section 3.8 when L is replaced by A_2. The shape functions $\underline{\Phi}_2^\alpha = \underline{\Phi}_3^\alpha$ are zero.

$$\underline{\Phi}_1^\alpha = \begin{bmatrix} \sin\left(\frac{\pi X_2}{A_2}\right) \\ -\frac{\pi X_1}{A_2}\cos\left(\frac{\pi X_2}{A_2}\right) \end{bmatrix} \tag{4.3_1}$$

$$\underline{\Phi}_4^\alpha = \begin{bmatrix} 0 \\ -\frac{X_2}{A_2} \end{bmatrix} \tag{4.3_2}$$

Lamella shape function gradients:

$$\operatorname{Grad}\underline{\Phi}_1^\alpha = \begin{bmatrix} 0 & \frac{\pi}{A_2}\cos\left(\frac{\pi X_2}{A_2}\right) \\ -\frac{\pi}{A_2}\cos\left(\frac{\pi X_2}{A_2}\right) & \frac{\pi^2 X_1}{A_2^2}\sin\left(\frac{\pi X_2}{A_2}\right) \end{bmatrix} \tag{4.4_1}$$

$$\operatorname{Grad}\underline{\Phi}_4^\alpha = \begin{bmatrix} 0 & 0 \\ 0 & -\frac{1}{A_2} \end{bmatrix} \tag{4.4_2}$$

Matrix shape functions:

$$\underline{\Phi}_1^\gamma = \begin{bmatrix} +\operatorname{sgn}(X_2)\left(1 - \frac{\operatorname{abs}(X_1)}{A_1}\right) \\ 0 \end{bmatrix} \tag{4.5_1}$$

$$\underline{\Phi}_2^\gamma = \begin{bmatrix} 0 \\ -\operatorname{sgn}(X_1)\left(\frac{1}{2} - \frac{\operatorname{abs}(X_2)}{A_2}\right) \end{bmatrix} \qquad (4.5_2)$$

$$\underline{\Phi}_3^\gamma = \begin{bmatrix} \frac{X_1}{A_1} \\ 0 \end{bmatrix} \qquad (4.5_3)$$

$$\underline{\Phi}_4^\gamma = \begin{bmatrix} 0 \\ -\frac{X_2}{A_2} \end{bmatrix} \qquad (4.5_4)$$

Matrix shape function gradients

$$\operatorname{Grad} \underline{\Phi}_1^\alpha = \begin{bmatrix} -\frac{\operatorname{sgn}(X_1 X_2)}{A_1} & 0 \\ 0 & 0 \end{bmatrix} \qquad (4.6_1)$$

$$\operatorname{Grad} \underline{\Phi}_2^\alpha = \begin{bmatrix} 0 & 0 \\ 0 & +\frac{\operatorname{sgn}(X_1 X_2)}{A_2} \end{bmatrix} \qquad (4.6_2)$$

$$\operatorname{Grad} \underline{\Phi}_3^\alpha = \begin{bmatrix} +\frac{1}{A_1} & 0 \\ 0 & 0 \end{bmatrix} \qquad (4.6_3)$$

$$\operatorname{Grad} \underline{\Phi}_4^\alpha = \begin{bmatrix} 0 & 0 \\ 0 & -\frac{1}{A_2} \end{bmatrix} \qquad (4.6_4)$$

4.2 Incremental constitutive law

The normal stress in 2-direction present in the lamella and the matrix in the unbuckled configuration immediately prior to the instant of buckling is supposed to be known. The stresses and the external load are related by the equilibrium (4.7). This relation is used in the following to eliminate σ_{22}^α and give an expression in the known quantities P and σ_{22}^γ.

$$P + 2A_1 \sigma_{22}^\gamma + A^\alpha \sigma_{22}^\alpha = 0 \qquad (4.7)$$

The usual convention with regard to the sign of the stress components is observed, i.e., compressive stress is counted negative. The lamella is treated by beam-theory so the stress in an unbuckled configuration is simply σ_{22}^α. For the matrix plane strain was assumed and a biaxial stress state results from the loading in 2-direction. The out-of-plane component, however, does not contribute to the work of the internal forces because the corresponding strain is zero. Therefore, the components in 3-direction can be dropped.

$$\underset{\sim}{\sigma}^\gamma = \begin{bmatrix} 0 & 0 \\ 0 & \sigma_{22}^\gamma \end{bmatrix} \qquad (4.8)$$

4 A preliminary, incompatible model

The crude modeling of the matrix in the incompatible model has the virtue that it allows different loading/unloading-combinations in the subdomains to be considered. Four combinations can conceivably be triggered in the model: loading, respectively unloading, everywhere in the matrix and loading, respectively unloading, in two diagonally opposite matrix-subdomains. Each of these four combinations is assigned a subdomain-wise constant switch function $_L\xi(\underline{X})$. The function takes the value 1 in yielding regions and 0 in unloading regions. For ξ, and, when necessary, for other quantities, the loading-combination under consideration is indicated by using a left subscript $L \in \{ll, lu, ul, uu\}$. The switch functions $_L\xi$ are defined in (4.9) and Fig. 4.2 show how L relates to yielding or unloading in the subdomains.

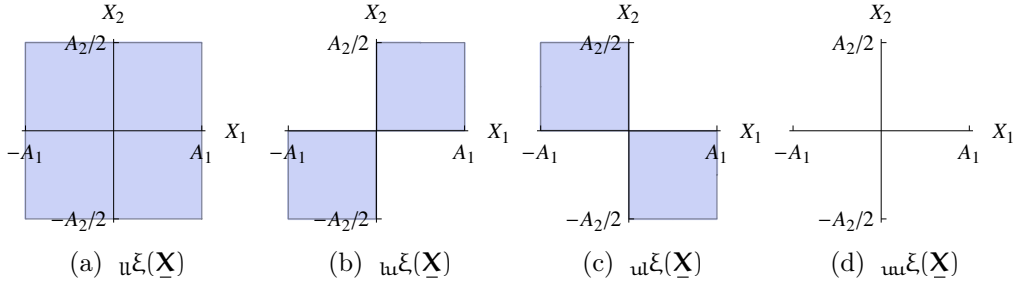(a) $_{ll}\xi(\underline{X})$ (b) $_{lu}\xi(\underline{X})$ (c) $_{ul}\xi(\underline{X})$ (d) $_{uu}\xi(\underline{X})$

Figure 4.2: Switch-function $_L\xi(\underline{X})$ for the loading situations under investigation, The function is 1 in the shaded areas and zero in the unshaded ones.

$$
\begin{aligned}
_{ll}\xi(\underline{X}) &= 1 \\
_{lu}\xi(\underline{X}) &= \tfrac{1}{2}\big(1 + \mathrm{sgn}(X_1 X_2)\big) \\
_{ul}\xi(\underline{X}) &= \tfrac{1}{2}\big(1 - \mathrm{sgn}(X_1 X_2)\big) \\
_{uu}\xi(\underline{X}) &= 0
\end{aligned}
\tag{4.9}
$$

The Eulerian elastoplastic tangent material stiffness tensor valid on the primary loading path is given by Eq. (2.37) as derived in section 2.4. To be able to handle all four loading-combinations mentioned above in a unified way, the switch function is incorporated into the tangent material stiffness tensor. For this purpose the definitions of the constitutive constants, F_i, as introduced in (2.35), are recalled, and the switch function ξ for a loading-combination L is considered therein.

$$
_LF_1(\underline{X}) = {}_L\underset{\approx}{\mathbb{L}}{}^{\gamma}_{1111} \qquad\qquad = \lambda - \frac{2\mu^2}{\theta + 2\mu}\,{}_L\xi(\underline{X}) + 2\mu
\tag{4.10$_1$}
$$

$$
_LF_2(\underline{X}) = {}_L\underset{\approx}{\mathbb{L}}{}^{\gamma}_{1122} = {}_L\underset{\approx}{\mathbb{L}}{}^{\gamma}_{2211} = \lambda + \frac{2\mu^2}{\theta + 2\mu}\,{}_L\xi(\underline{X})
\tag{4.10$_2$}
$$

The lamella is assumed to remain in an elastic state and only the elastic modulus is required:

$$\mathbb{\underset{\approx}{L}}^{\alpha}_{2222} = \mathsf{E}^{\alpha} \tag{4.11}$$

The mixed tangent material stiffness tensor are calculated from (2.26). It is subdomain-wise constant, but the material regime in the subdomains may be different.

$$\mathbb{\underset{\approx}{L}}^{\gamma} = \begin{bmatrix} \begin{bmatrix} {}_{\mathsf{L}}\mathsf{F}_1(\underline{\mathbf{X}}) & 0 \\ 0 & {}_{\mathsf{L}}\mathsf{F}_2(\underline{\mathbf{X}}) \end{bmatrix} & \begin{bmatrix} 0 & \mu + \frac{1}{2}\sigma^{\gamma}_{22} \\ \mu - \frac{1}{2}\sigma^{\gamma}_{22} & 0 \end{bmatrix} \\ \begin{bmatrix} 0 & \mu - \frac{1}{2}\sigma^{\gamma}_{22} \\ \mu - \frac{1}{2}\sigma^{\gamma}_{22} & 0 \end{bmatrix} & \begin{bmatrix} {}_{\mathsf{L}}\mathsf{F}_2(\underline{\mathbf{X}}) & 0 \\ 0 & {}_{\mathsf{L}}\mathsf{F}_1(\underline{\mathbf{X}}) - \sigma^{\gamma}_{22} \end{bmatrix} \end{bmatrix} \tag{4.12}$$

$$\mathbb{\underset{\approx}{C}}^{\alpha} = \begin{bmatrix} \begin{bmatrix} 0 & 0 \\ 0 & 0 \end{bmatrix} & \begin{bmatrix} 0 & +\frac{1}{2}\sigma^{\alpha}_{22} \\ -\frac{1}{2}\sigma^{\alpha}_{22} & 0 \end{bmatrix} \\ \begin{bmatrix} 0 & -\frac{1}{2}\sigma^{\alpha}_{22} \\ -\frac{1}{2}\sigma^{\alpha}_{22} & 0 \end{bmatrix} & \begin{bmatrix} 0 & 0 \\ 0 & \mathsf{E}^{\alpha} - \sigma^{\alpha}_{22} \end{bmatrix} \end{bmatrix} \tag{4.13}$$

4.3 Internal force rates and stiffness

Equation (3.34) provides the instructions to calculate the internal force rates for the present problem:

$$\begin{aligned} {}_{\mathsf{L}}\dot{\mathsf{Q}}_i = & + \sum_{j=1}^{n} \dot{\mathsf{q}}_j \int_{-\frac{1}{2}\mathsf{A}^{\alpha}}^{+\frac{1}{2}\mathsf{A}^{\alpha}} \int_{-\frac{1}{2}\mathsf{A}_2}^{+\frac{1}{2}\mathsf{A}_2} \operatorname{Grad} \underline{\boldsymbol{\phi}}^{\alpha}_j : \ \mathbb{\underset{\approx}{C}}^{\alpha} : \operatorname{Grad} \underline{\boldsymbol{\phi}}^{\alpha}_i \, d\mathsf{X}_1 d\mathsf{X}_2 \\ & + \sum_{j=1}^{n} \dot{\mathsf{q}}_j \int_{-\mathsf{A}_1}^{+\mathsf{A}_1} \int_{-\frac{1}{2}\mathsf{A}_2}^{+\frac{1}{2}\mathsf{A}_2} \operatorname{Grad} \underline{\boldsymbol{\phi}}^{\gamma}_j : {}_{\mathsf{L}}\mathbb{\underset{\approx}{C}}^{\gamma} : \operatorname{Grad} \underline{\boldsymbol{\phi}}^{\gamma}_i \, d\mathsf{X}_1 d\mathsf{X}_2 \end{aligned} \tag{4.14}$$

The necessity to specify the loading-combination in the matrix by the subscript L is present for the internal force rates as well. In order to specify the results in a concise manner, the parts that require reference to a certain loading-combination are consolidated into constants ${}_{\mathsf{L}}\mathsf{C}_i$ and ${}_{\mathsf{L}}\mathsf{D}_i$. The constants are defined below and are precalculated for further reference.

$$\mathsf{L}\mathsf{C}_i := \frac{1}{2\mathsf{A}_1\mathsf{A}_2} \int_{-\mathsf{A}_1}^{+\mathsf{A}_1} \int_{-\frac{1}{2}\mathsf{A}_2}^{+\frac{1}{2}\mathsf{A}_2} {}_{\mathsf{L}}\mathsf{F}_i(\underline{\mathbf{X}}) \, d\mathsf{X}_1 d\mathsf{X}_2 \tag{4.15}$$

$$\mathsf{L}\mathsf{D}_i := \frac{1}{2\mathsf{A}_1\mathsf{A}_2} \int_{-\mathsf{A}_1}^{+\mathsf{A}_1} \int_{-\frac{1}{2}\mathsf{A}_2}^{+\frac{1}{2}\mathsf{A}_2} {}_{\mathsf{L}}\mathsf{F}_i(\underline{\mathbf{X}}) \operatorname{sgn}(\mathsf{X}_1\mathsf{X}_2) \, d\mathsf{X}_1 d\mathsf{X}_2 \tag{4.16}$$

4 A preliminary, incompatible model

The constants are given in terms of the isotropic hardening factor and the Lamé-parameters:

$$_\text{ll}C_1 = \lambda + \frac{2\mu(\theta+\mu)}{\theta+2\mu} \qquad\qquad _\text{ll}D_1 = 0 \tag{4.17$_1$}$$

$$_\text{ll}C_2 = \lambda + \frac{2\mu^2}{\theta+2\mu} \qquad\qquad _\text{ll}D_2 = 0 \tag{4.17$_2$}$$

$$_\text{lu}C_1 = \lambda + \frac{\mu(2\theta+3\mu)}{\theta+2\mu} \qquad\qquad _\text{lu}D_1 = -\frac{\mu^2}{\theta+2\mu} \tag{4.17$_3$}$$

$$_\text{lu}C_2 = \lambda + \frac{\mu^2}{\theta+2\mu} \qquad\qquad _\text{lu}D_2 = -_\text{lu}D_1 \tag{4.17$_4$}$$

$$_\text{ul}C_1 = {}_\text{lu}C_1 \qquad\qquad _\text{ul}D_1 = -_\text{lu}D_1 \tag{4.17$_5$}$$

$$_\text{ul}C_2 = {}_\text{lu}C_2 \qquad\qquad _\text{ul}D_2 = {}_\text{lu}D_1 \tag{4.17$_6$}$$

$$_\text{uu}C_1 = (\lambda + 2\mu) \qquad\qquad _\text{uu}D_1 = 0 \tag{4.17$_7$}$$

$$_\text{uu}C_2 = \lambda \qquad\qquad _\text{uu}D_2 = 0 \tag{4.17$_8$}$$

This allows the internal force rates to be stated without the need to consider each loading-combination individually. Note that some of the D_i-constants might vanish for a particular loading-combination and further simplification might be possible.

$$_\text{L}\dot{Q}_1 = 2\frac{A_2}{A_1}\,_\text{L}C_1\dot{q}_1 - 2\,_\text{L}C_2\dot{q}_2 - 2\frac{A_2}{A_1}\,_\text{L}D_1\dot{q}_3 + 2\,_\text{L}D_2\dot{q}_4$$
$$+ \frac{\pi^4(A^\alpha)^3}{24A_2^3}(E^\alpha - \sigma_{22}^\alpha)\dot{q}_1 + \frac{\pi^2 A^\alpha}{2A_2}\sigma_{22}^\alpha\dot{q}_1 \tag{4.18$_1$}$$

$$_\text{L}\dot{Q}_2 = 2\frac{A_1}{A_2}\,_\text{L}C_1\dot{q}_2 - 2\,_\text{L}C_2\dot{q}_1 - 2\frac{A_1}{A_2}\,_\text{L}D_1\dot{q}_4 + 2\,_\text{L}D_2\dot{q}_3 - 2\frac{A_1}{A_2}\sigma_{22}^\gamma\dot{q}_2 \tag{4.18$_2$}$$

$$_\text{L}\dot{Q}_3 = 2\frac{A_2}{A_1}\,_\text{L}C_1\dot{q}_3 - 2\,_\text{L}C_2\dot{q}_4 - 2\frac{A_2}{A_1}\,_\text{L}D_1\dot{q}_1 + 2\,_\text{L}D_2\dot{q}_2 \tag{4.18$_3$}$$

$$_\text{L}\dot{Q}_4 = 2\frac{A_1}{A_2}\,_\text{L}C_1\dot{q}_4 - 2\,_\text{L}C_2\dot{q}_3 - 2\frac{A_1}{A_2}\,_\text{L}D_1\dot{q}_2 + 2\,_\text{L}D_2\dot{q}_1$$
$$+ \frac{A^\alpha}{A_2}(E^\alpha - \sigma_{22}^\alpha)\dot{q}_4 - 2\frac{A_1}{A_2}\sigma_{22}^\gamma\dot{q}_4 \tag{4.18$_4$}$$

In the equations above a direct subtraction of the lamella's stress from the lamella's Young's modulus occurs. It appears beneficial to assume that the *elastic* modulus in the lamella exceeds the stress by far, and the stress can be dropped without incurring a significant error. However, no such simplification should be made beforehand to the relation of the matrix tangent hardening modulus and the matrix stress, since they might be of similar scale when the matrix is hardening only little or not at all. The system stiffness matrix is calculated by (3.39). The result in terms of the constants tabulated in

(4.17) is stated below:

$$
{}_\text{L}\underset{\sim}{\mathbf{K}} = 2 \begin{bmatrix} \frac{A_2}{A_1}{}_\text{L}C_1 + \frac{\pi^2 A^\alpha}{4A_2}\sigma_{22}^\alpha + \frac{\pi^4 (A^\alpha)^3}{48 A_2^3}E^\alpha & -{}_\text{L}C_2 & -\frac{A_2}{A_1}{}_\text{L}D_1 & {}_\text{L}D_2 \\ -{}_\text{L}C_2 & \frac{A_1}{A_2}({}_\text{L}C_1 - \sigma_{22}^\gamma) & {}_\text{L}D_2 & -\frac{A_1}{A_2}{}_\text{L}D_1 \\ -\frac{A_2}{A_1}{}_\text{L}D_1 & {}_\text{L}D_2 & \frac{A_2}{A_1}{}_\text{L}C_1 & -{}_\text{L}C_2 \\ {}_\text{L}D_2 & -\frac{A_1}{A_2}{}_\text{L}D_1 & -{}_\text{L}C_2 & \frac{A_1}{A_2}({}_\text{L}C_1 - \sigma_{22}^\gamma) + \frac{A^\alpha}{2A_2}E^\alpha \end{bmatrix}
$$
$$(4.19)$$

4.4 Buckling

With the stiffness matrix on hand, the bifurcation point can be determined by invoking theorem 2 from [Petryk, 1991], cf. section 3.7. On the primary equilibrium path in the elastoplastic regime, all four subdomains are loading and the stiffness matrix is given by ${}_\text{u}\underset{\sim}{\mathbf{K}}$. The tangent stiffness matrix is assumed positive definite when entering the elasto-plastic regime, but turns positive semidefinite at some point with progressive loading. Any further loading on the primary path would render the stiffness matrix indefinite, violating (3.50). Hence, the uniqueness of the primary loading path ends when ${}_\text{u}\underset{\sim}{\mathbf{K}}$ becomes singular. Setting the determinant of ${}_\text{u}\underset{\sim}{\mathbf{K}}$ to zero leads to the expression (4.20) for the buckling load P^* where the lamella stress, σ_{22}^α has been eliminated by using (4.7).

$$
\mathsf{P}^* = \underbrace{\frac{\pi^2 E^\alpha (A^\alpha)^3}{12 A_2^2}}_{\text{Euler buckling load}} + \overbrace{\frac{4A_2^2({}_\text{u}C_1^2 - {}_\text{u}C_2^2 - {}_\text{u}C_1 \sigma_{22}^\gamma)}{\pi^2 A_1({}_\text{u}C_1 - \sigma_{22}^\gamma)}}^{\text{due to geometric and material matrix stiffness}} - \underbrace{2A_1 \sigma_{22}^\gamma}_{\text{load carried by matrix}}
$$
$$(4.20)$$

Examination of the expression (4.20) suggests a classification into three individual terms contributing to the bifurcation load: The left most term represents the Euler-buckling load of a laterally unsupported lamella with a buckling length A_2. The middle term reflects the effect of the lateral support exerted by the matrix on the lamella, and comprises the material constants C_i and the matrix stress, in addition to the model dimensions. The last term represents the load carried by the matrix directly. The matrix bedding affects all three terms, even the Euler buckling term, since buckling half-wavelength A_2 cannot be regarded as known, but must be obtained from minimizing P^*.

It is of interest to determine to which extend the matrix-preload affects the bifurcation load via the geometrical stiffness it causes. A simple way to do so is to replace ${}_\text{L}\underset{\approx}{\mathbb{C}}{}^\gamma$ by ${}_\text{L}\underset{\approx}{\mathbb{L}}{}^\gamma$ in (4.16). This approach is equivalent to setting σ_{22}^γ to zero in (4.18) and (4.19), but not in (4.7). For the lamella ${}_\text{L}\underset{\approx}{\mathbb{C}}{}^\alpha$ must be retained, of course, otherwise buckling would be completely suppressed. Any quantity derived under this simplification is marked by

4 A preliminary, incompatible model

an overscript háček (upside-down chevron). Comparison of the recalculated bifurcation load in (4.21) to (4.20) shows only the middle term is changed.

$$\check{P}^* = \underbrace{\frac{\pi^2 E^\alpha (A^\alpha)^3}{12 A_2^2}}_{\text{Euler buckling load}} + \overbrace{\frac{4A_2^2({}_u C_1^2 - {}_u C_2^2)}{\pi^2 A_1\, {}_u C_1}}^{\text{due material matrix stiffness only}} - \underbrace{2A_1 \sigma_{22}^\gamma}_{\text{load carried by matrix}} \tag{4.21}$$

$$\Delta P^* = P^* - \check{P}^* \tag{4.22}$$

$$\Delta P^* = -\frac{4A_2^2\, {}_u C_2^2 \sigma_{22}^\gamma}{\pi^2 A_1\, {}_u C_1\,({}_u C_1 - \sigma_{22}^\gamma)} \tag{4.23}$$

The half-wavelength, A_2, is calculated by minimizing for both, the buckling loads taking the matrix prestress into account, and the buckling load neglecting it.

$$A_2 = \sqrt[4]{\frac{\pi (A^\alpha)^3 E^\alpha A_1 ({}_u C_1 - \sigma_{22}^\gamma)}{48({}_u C_1^2 - {}_u C_2^2 - {}_u C_1 \sigma_{22}^\gamma)}} \tag{4.24_1}$$

$$\check{A}_2 = \sqrt[4]{\frac{\pi (A^\alpha)^3 E^\alpha A_1\, {}_u C_1}{48({}_u C_1^2 - {}_u C_2^2)}} \tag{4.24_2}$$

It is noteworthy that for the case of ideal plasticity ${}_u C_1$ equals ${}_u C_2$ and the wavelength and the buckling load tend to infinity and zero, respectively, for the simplified case. Ideal plasticity is revisited in chapter 5 for an improved model, and arguments are presented that point to a coupling of the wavelength to the lamella spacing.

Substituting the result for the buckling wavelength back into the expression for the bifurcation load shows that when the lamella thickness and spacing are scaled by a common factor the bifurcation load also scales with the same factor.

$$\check{P}^* = \frac{2\sqrt{E^\alpha}\sqrt{{}_u C_1^2 - {}_u C_2^2}\,(A^\alpha)^{3/2}}{\sqrt{3\, {}_u C_1 A_1}} - 2A_1 \sigma_{22}^\gamma \tag{4.25}$$

To reduce the algebraic complexity, only simplified quantities, neglecting the geometric matrix stiffness, are considered in the remainder of the chapter. The simplified $\mathcal{J}$-functional for the present model is:

$$\begin{aligned}
{}_L \check{\mathcal{J}} = {}&-\frac{\pi^2 A_1 \dot{q}_1^2}{2A_2}\sigma_{22}^\gamma + \frac{A_2\, {}_L C_1 \dot{q}_1^2}{A_1} + \frac{A_1\, {}_L C_1 \dot{q}_2^2}{A_2} + \frac{A_2\, {}_L C_1 \dot{q}_3^2}{A_1} + \frac{A_1\, {}_L C_1 \dot{q}_4^2}{A_2} \\
&-\frac{2A_2\, {}_L D_1 \dot{q}_1 \dot{q}_3}{A_1} - \frac{2A_1\, {}_L D_1 \dot{q}_2 \dot{q}_4}{A_2} - \frac{\pi^2 \dot{q}_1^2 P}{4A_2} + \frac{\pi^4 \dot{q}_1^2 E^\alpha (A^\alpha)^3}{48 A_2^3} \\
&+\frac{\dot{q}_4^2 E^\alpha A^\alpha}{2A_2} - 2\, {}_L C_2 \dot{q}_1 \dot{q}_2 - 2\, {}_L C_2 \dot{q}_3 \dot{q}_4 + 2\, {}_L D_2 \dot{q}_1 \dot{q}_4 + 2\, {}_L D_2 \dot{q}_2 \dot{q}_3 - \dot{q}_4 \dot{P} \quad (4.26)
\end{aligned}$$

The expression is valid for all loading-combinations on account of the constants ${}_L C_i$, ${}_L D_i$ taking different values for a given loading-combination. To examine the circumstances

under which buckling occurs, it is of interest when the functional attains a minimal value. In a contour plot similar to Figs. 3.3(a) to 3.5(a) only the dependence on two GCs can be displayed. The GC-rates $\dot{q}_1$ and $\dot{q}_4$ are best suited to describe the model behaviour, so $\dot{q}_2$ and $\dot{q}_3$ are eliminated by minimizing $\check{\mathcal{J}}$ with respect to them. They assume the value given below:

$$\dot{q}_2 = \frac{({}_L C_1 \, {}_L C_2 - {}_L D_1 \, {}_L D_2) A_2 \dot{q}_1 + ({}_L C_1 \, {}_L D_1 - {}_L C_2 \, {}_L D_2) A_1 \dot{q}_4}{({}_L C_1^2 - {}_L D_2^2) A_1} \tag{4.27}$$

$$\dot{q}_3 = \frac{({}_L C_1 \, {}_L D_1 - {}_L C_2 \, {}_L D_2) A_2 \dot{q}_1 + ({}_L C_1 \, {}_L C_2 - {}_L D_1 \, {}_L D_2) A_1 \dot{q}_4}{({}_L C_1^2 - {}_L D_2^2) A_2} \tag{4.28}$$

$$E^\alpha = E^\gamma = 200 \times 10^3 \, [\text{FL}^{-2}] \quad A^\alpha = 0.125 \, [\text{L}] \quad \nu = 0.45$$
$$E_t = 5 \times 10^3 \, [\text{FL}^{-2}] \quad\quad\quad A_1 = 1 \, [\text{L}]$$

Table 4.1: Parameters used to generate the plots in Fig. 4.3

The simplified $\mathcal{J}$-functional for a model that has been loaded up to of 80% of the bifurcation load is shown in Figure 4.3(a). There is a single, global minimum point on the $\dot{q}_4$-axis, thus demonstrating the uniqueness of the undeflected primary equilibrium path $\check{\underline{V}}_I$.

$$\check{\underline{V}}_I = {}_u\check{\underline{K}}^{-1} \begin{bmatrix} 0 \\ 0 \\ 0 \\ \dot{P} \end{bmatrix} = \frac{\dot{P}}{2\,{}_u C_1^2 A_1 - 2\,{}_u C_2^2 A_1 + {}_u C_1 E^\alpha A^\alpha} \begin{bmatrix} 0 \\ 0 \\ {}_u C_2 A_1 \\ {}_u C_1 A_2 \end{bmatrix} \tag{4.29}$$
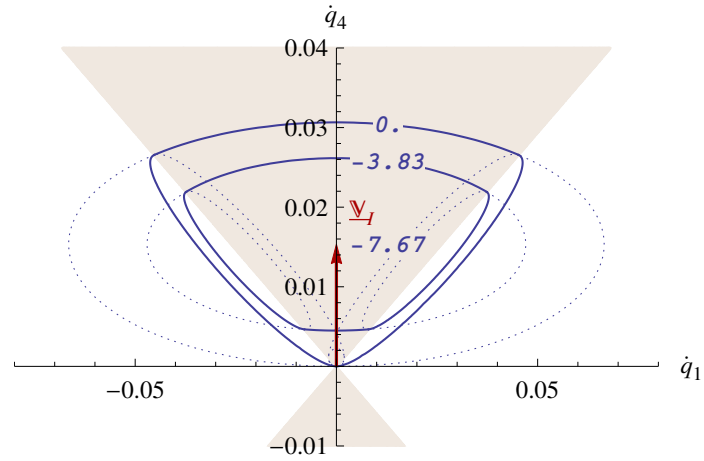
In the figure the different loading-combinations manifest themselves as sectors radiating from the origin. The ll-loading comprises the shaded sector on top, and the lu/ul-sectors lie to either side of it. The system's tangent stiffness matrix is positive definite in all sectors, as can be inferred from the circumstance that all contours of constant value of the functional are closed curves around the minimum.

When the load is increased to the bifurcation load, the ellipsoidal contours in the ll-sector degenerate to parallel lines, Fig. 4.3(b), as ${}_u\underline{K}$ becomes singular. The eigenvector $\check{\underline{W}}^*$, corresponding to the singular eigenvalue, is given in (4.30).

$$\underbrace{\begin{bmatrix} \frac{2\,{}_u C_2^2 A_2}{{}_u C_1 A_1} & -2\,{}_u C_2 & 0 & 0 \\ -2\,{}_u C_2 & \frac{2\,{}_u C_1 A_1}{A_2} & 0 & 0 \\ 0 & 0 & \frac{2\,{}_u C_1 A_2}{A_1} & -2\,{}_u C_2 \\ 0 & 0 & -2\,{}_u C_2 & \frac{2\,{}_u C_1 A_1 + A^\alpha E^\alpha}{A_2} \end{bmatrix}}_{{}_u\check{\underline{K}}(P = P^*)} \underbrace{\begin{bmatrix} {}_u C_1 A_1 \\ {}_u C_2 A_2 \\ 0 \\ 0 \end{bmatrix}}_{\check{\underline{W}}^*} = \begin{bmatrix} 0 \\ 0 \\ 0 \\ 0 \end{bmatrix} \tag{4.30}$$

Since $\dot{q}_4$ is zero in $\check{\underline{W}}^*$ any movement along the eigenvector immediately leaves the ll-sector for which it has been calculated. The sector boundaries suppress the pure eigen-
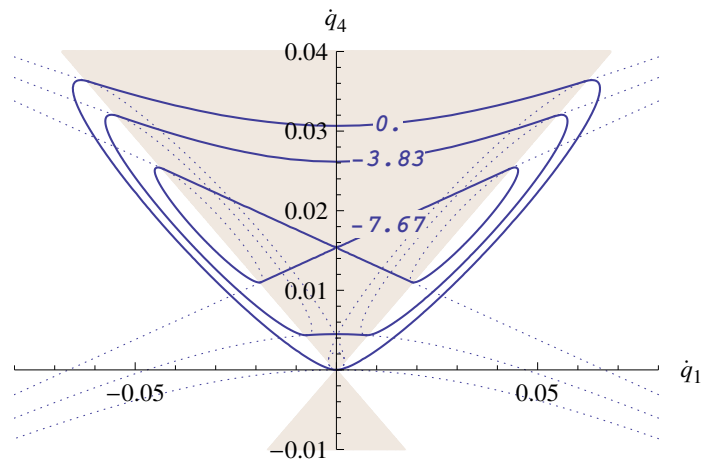
4 A preliminary, incompatible model

(a) $\check{\mathcal{J}}(\dot{q}_1, \dot{q}_4, \mathsf{P} = 0.8\check{\mathsf{P}}^*)$
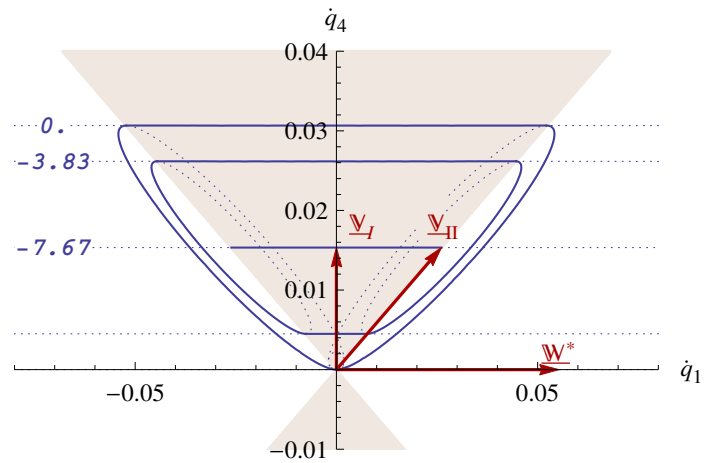
(b) $\check{\mathcal{J}}(\dot{q}_1, \dot{q}_4, \mathsf{P} = 1.0\check{\mathsf{P}}^*)$

(c) $\check{\mathcal{J}}(\dot{q}_1, \dot{q}_4, \mathsf{P} = 1.2\check{\mathsf{P}}^*)$

Figure 4.3: Evolution of the $\check{\mathcal{J}}$-function(al) evaluated at the primary equilibrium path with increasing loads, P; $\mathsf{P}^\bullet = 10^3\,[\mathrm{FT}^{-1}]$, $\sigma_{22}^\gamma = -100\,[\mathrm{FL}^{-2}]$

mode and maintain stability at constant load even when the stiffness matrix in the loading-only sector is singular. However, it is also apparent that some limited deflection-rate, confined by the sector boundaries, is possible when $\underline{\check{\boldsymbol{W}}}^*$ is superposed by some additional movement along the primary path $\underline{\check{\boldsymbol{V}}}_{\mathrm{I}}$. To minimize $\check{\mathcal{J}}$ the system indeed must continue to follow $\underline{\check{\boldsymbol{V}}}_{\mathrm{I}}$, and deflection by $\underline{\check{\boldsymbol{W}}}^*$ as permitted by the length of the line segment forming the minimum is possible at precisely the bifurcation load. Any ever so slight load increase, however, forces the minimum to the two end-points of the line segment. The former minimum point on the $\dot{\mathsf{q}}_4$-axis is then a saddle point, and $\underline{\check{\boldsymbol{V}}}_{\mathrm{I}}$ alone no longer minimizes $\check{\mathcal{J}}$. The actual GC-rate vector at this instance is given by $\underline{\check{\boldsymbol{V}}}_{\mathrm{II}}$ as a superposition of $\underline{\check{\boldsymbol{V}}}_{\mathrm{I}}$ and $\underline{\check{\boldsymbol{W}}}^*$ so that the system at the very instant of bifurcation moves along the border of the $\mathfrak{ll}$-sector and either one of the $\mathfrak{lu}$- or $\mathfrak{ul}$-sector. From this it is apparent that there is no sudden unloading in any of the four matrix sub-domains at the bifurcation point. The instant of bifurcation, that is the initiation of buckling, merely marks the transition from gradual loading to gradual unloading in two of the four subdomains as $\underline{\check{\boldsymbol{V}}}_{\mathrm{II}}$ initially follows exactly the sector boundary. The $\mathcal{J}$-functional continuously transitions from a sector activating one set of constitutional branches to another activating different branches. In the context of the current model this means that the transitions at the sector boundaries are continuous, in particular $\underline{\check{\boldsymbol{V}}}_{\mathrm{II}}$ coincides with the sector boundary in the instant of bifurcation and, therefore:

$$\mathfrak{u}\mathcal{J}(\underline{\check{\boldsymbol{V}}}_{\mathrm{II}}) = {}_{\mathfrak{lu}}\mathcal{J}(\underline{\check{\boldsymbol{V}}}_{\mathrm{II}}) \tag{4.31}$$

Since $\underline{\check{\boldsymbol{V}}}_{\mathrm{II}}$ follows an equilibrium path internal and external force rates must coincide, irrespective which loading-combination is used to calculate the force rate. The internal force rates are the partial derivatives of the respective $\mathcal{J}$ so the transition is not only continuous, but also has a continuous slope.

$$\frac{\partial \, {}_{\mathfrak{u}}\mathcal{J}(\underline{\check{\boldsymbol{V}}}_{\mathrm{II}})}{\partial \dot{\mathsf{q}}_i} = {}_{\mathfrak{u}}\dot{\mathsf{Q}}_i(\underline{\check{\boldsymbol{V}}}_{\mathrm{II}}) = \frac{\partial \, {}_{\mathfrak{lu}}\mathcal{J}(\underline{\check{\boldsymbol{V}}}_{\mathrm{II}})}{\partial \dot{\mathsf{q}}_i} = {}_{\mathfrak{lu}}\dot{\mathsf{Q}}_i(\underline{\check{\boldsymbol{V}}}_{\mathrm{II}}) = \dot{\mathsf{P}}_i \tag{4.32}$$

The stiffness, however, is not continuous and neither is the curvature of the $\mathcal{J}$-functional.

$$\frac{\partial^2 \, {}_{\mathfrak{u}}\mathcal{J}}{\partial \dot{\mathsf{q}}_i \partial \dot{\mathsf{q}}_j} = {}_{\mathfrak{u}}\mathsf{K}_{ij} \neq \frac{\partial^2 \, {}_{\mathfrak{lu}}\mathcal{J}}{\partial \dot{\mathsf{q}}_i \partial \dot{\mathsf{q}}_j} = {}_{\mathfrak{lu}}\mathsf{K}_{ij} \tag{4.33}$$

Using the continuity property gives a relation for the ray marking the sector boundary:

$$\dot{\mathsf{q}}_1 A_2 = \begin{cases} +\dot{\mathsf{q}}_4 A_1 : {}_{\mathfrak{u}}\check{\mathcal{J}} = {}_{\mathfrak{ul}}\check{\mathcal{J}} \\ -\dot{\mathsf{q}}_4 A_1 : {}_{\mathfrak{u}}\check{\mathcal{J}} = {}_{\mathfrak{lu}}\check{\mathcal{J}} \end{cases} \tag{4.34}$$

The bifurcating velocity solution $\underline{\check{\boldsymbol{V}}}_{\mathrm{II}}$ at the instant of buckling is a superposition of the primary velocity solution $\underline{\check{\boldsymbol{V}}}_{\mathrm{I}}$ and the eigenvector $\underline{\check{\boldsymbol{W}}}^*$ so that it exactly follows the sector boundary. The relation for the sector boundary can be used to determine a multiplier, k,

to be applied to $\underline{\check{\boldsymbol{W}}}^*$ to obtain $\underline{\check{\boldsymbol{V}}}_{\mathrm{II}}$, cf. Fig. 4.3(b).

$$\underline{\check{\boldsymbol{V}}}_{\mathrm{II}} = \underline{\check{\boldsymbol{V}}}_{\mathrm{I}} + \mathsf{k}\,\underline{\check{\boldsymbol{W}}}^*$$

$$\underline{\check{\boldsymbol{V}}}_{\mathrm{II}} = \frac{\dot{\mathsf{P}}}{2\,{}_{\mathrm{u}}\mathsf{C}_1^2\mathsf{A}_1 - 2\,{}_{\mathrm{u}}\mathsf{C}_2^2\mathsf{A}_1 + {}_{\mathrm{u}}\mathsf{C}_1\mathsf{E}^\alpha\mathsf{A}^\alpha} \begin{bmatrix} {}_{\mathrm{u}}\mathsf{C}_1\mathsf{A}_1 \\ {}_{\mathrm{u}}\mathsf{C}_2\mathsf{A}_2 \\ {}_{\mathrm{u}}\mathsf{C}_2\mathsf{A}_1 \\ {}_{\mathrm{u}}\mathsf{C}_1\mathsf{A}_2 \end{bmatrix} \tag{4.35}$$

Usually the bifurcation load can not be exceeded in a loading process without deflection, unless there are additional constraints in place. Such a situation could come up if the bifurcation load is smaller then the load required to cause yielding in the matrix. In that case no bifurcation occurs while the system is in the elastic regime, and deflection immediately starts upon yielding. The simplified $\mathcal{J}$-functional of the model for a load at 120% the bifurcation load is depicted in Fig. 4.3(c). The equilibrium is still stable. If the system is held in an undeflected state and loaded to even higher loads the equilibrium might become unstable when the additional constraint is released. In that case the deflection would occur in a dynamic rather then a quasi-static manner, cf. [Petryk, 1997] for a comprehensive classification of instability modes.

4.5 Numeric examples

As a verification, the results are compared to results obtained from a finite element method (FEM) analysis. The FEM-model is designed in analogy to Fig. 4.1 comprising four plane strain-elements for the subdomain and several beam-elements for the lamella. Coupling constraints enforce the same kinematic restrictions as (4.1) and (4.2). The simulations were done using the commercial FEM-software Abaqus, version 6.13. The matrix is modeled by four plane strain, reduced integration, hybrid formulation elements (CPE4RH). For the lamella two-node cubic beam-elements are used. The load-deflection path is calculated by an incremental static analysis. Both geometric and material nonlinearities are covered in the simulation. To ensure convergence on the bifurcated branch the model is provided with a slight geometric imperfection of 1×10^{-5} [L] at the top connection point. This imperfection transforms the bifurcation of the perfect model to a continuous loading path close to the bifurcated branch in the post-bifurcation segment of the path. Since the bifurcation load is not precisely calculated by this method, the numerical bifurcation load is defined here as the load where any matrix-element is unloaded for the first time. The increment of first unloading is highlighted by a blue circle marker in the graphs.

The results of two series of simulation runs for a uniaxial tangent modulus of zero (odd numbered parameter sets) and $5000\,[\mathrm{FL}^{-2}]$ (even numbered) are included below. Each series covers three different initial model-heights $\mathsf{A}_2 = 0.5/1.0/1.5\,[\mathrm{L}]$. All other parameters are taken from Table 4.1. In the hardening series the models deform significantly before bifurcation. Since the analytical results presented refer to quantities on the preloaded configuration, the prebuckling deformation needs to be taken into account when comparing numerical and analytical results. The matrix strain at the instant of bifurcation is far

$\mathsf{E_t} = 0\,[\mathrm{FL}^{-2}]$

parameter set 1
    initial values:
        $\mathsf{A}_1 = 1.000\,[\mathrm{L}]$ $\mathsf{A}_2 = \mathbf{0.500}\,[\mathrm{L}]$
    at buckling load:
        $\mathsf{A}_1 = 1.056\,[\mathrm{L}]$ $\mathsf{A}_2 = 0.473\,[\mathrm{L}]$ $\sigma_{22}^\gamma = -116\,[\mathrm{FL}^{-2}]$ $\sigma^\alpha = -11549\,[\mathrm{FL}^{-2}]$
    buckling loads:
        $\mathsf{P}^* = 1687\,[\mathrm{F}]$ $_\mathrm{u}\mathsf{\check{P}}^* = 1677\,[\mathrm{F}]$ $\mathsf{P}^*_\mathrm{num} = 1470\,[\mathrm{F}]$

parameter set 3
    initial values:
        $\mathsf{A}_1 = 1.000\,[\mathrm{L}]$ $\mathsf{A}_2 = \mathbf{1.000}\,[\mathrm{L}]$
    at buckling load:
        $\mathsf{A}_1 = 1.015\,[\mathrm{L}]$ $\mathsf{A}_2 = 0.985\,[\mathrm{L}]$ $\sigma_{22}^\gamma = -116\,[\mathrm{FL}^{-2}]$ $\sigma^\alpha = -3005\,[\mathrm{FL}^{-2}]$
    buckling loads:
        $\mathsf{P}^* = 610.2\,[\mathrm{F}]$ $\mathsf{\check{P}}^* = 565.4\,[\mathrm{F}]$ $\mathsf{P}^*_\mathrm{num} = 590\,[\mathrm{F}]$

parameter set 5
    initial values:
        $\mathsf{A}_1 = 1.000\,[\mathrm{L}]$ $\mathsf{A}_2 = \mathbf{1.500}\,[\mathrm{L}]$
    at buckling load:
        $\mathsf{A}_1 = 1.010\,[\mathrm{L}]$ $\mathsf{A}_2 = 1.485\,[\mathrm{L}]$ $\sigma_{22}^\gamma = -116\,[\mathrm{FL}^{-2}]$ $\sigma^\alpha = -1983\,[\mathrm{FL}^{-2}]$
    buckling loads:
        $\mathsf{P}^* = 481.2\,[\mathrm{F}]$ $\mathsf{\check{P}}^* = 379.0\,[\mathrm{F}]$ $\mathsf{P}^*_\mathrm{num} = 475\,[\mathrm{F}]$

Table 4.2: Parameters for the simulation series for ideal plastic case

beyond the strain for initial yielding and the assumptions made in section 2.4 can be considered fulfilled. The lamella stress at buckling generally very high and attains extreme values for the hardening case. In all cases the stable post buckling behaviour is apparent. The bifurcation loads P^* calculated from (4.20) or the simplification $\mathsf{\check{P}}^*$ by (4.21) differ only by a moderate amount. The geometric stiffness of the matrix has a stabilizing effect for the cases considered here. The analytical bifurcation load P^* is marked as a dashed line in the diagrams. Comparison to the numerical bifurcation load (blue circle) show an acceptable accordance for $\mathsf{A}_2 = 1.0\,[\mathrm{L}]$ and $\mathsf{A}_2 = 1.5\,[\mathrm{L}]$. A certain discrepancy is apparent for the shortest model height (parameter sets 1 and 2). Also the analytical result is not strictly over- or underestimating the numerical outcome.

$\mathsf{E_t} = 5000\,[\mathrm{FL}^{-2}]$

parameter set 2
  initial values:
      $\mathsf{A}_1 = 1.000\,[\mathrm{L}]$ $\mathsf{A}_2 = \mathbf{0.500}\,[\mathrm{L}]$
  at buckling load:
      $\mathsf{A}_1 = 1.086\,[\mathrm{L}]$ $\mathsf{A}_2 = 0.460\,[\mathrm{L}]$ $\sigma_{22}^{\gamma} = -664\,[\mathrm{FL}^{-2}]$ $\sigma^{\alpha} = -16760\,[\mathrm{FL}^{-2}]$
  buckling loads:
      $\mathsf{P}^* = 3537\,[\mathrm{F}]$ $\check{\mathsf{P}}^* = 3485\,[\mathrm{F}]$ $\mathsf{P}^*_{\mathrm{num}} = 3200\,[\mathrm{F}]$

parameter set 4
  initial values:
      $\mathsf{A}_1 = 1.000\,[\mathrm{L}]$ $\mathsf{A}_2 = \mathbf{1.000}\,[\mathrm{L}]$
  at buckling load:
      $\mathsf{A}_1 = 1.130\,[\mathrm{L}]$ $\mathsf{A}_2 = 0.884\,[\mathrm{L}]$ $\sigma_{22}^{\gamma} = -807\,[\mathrm{FL}^{-2}]$ $\sigma^{\alpha} = -20002\,[\mathrm{FL}^{-2}]$
  buckling loads:
      $\mathsf{P}^* = 4324\,[\mathrm{F}]$ $\check{\mathsf{P}}^* = 4100\,[\mathrm{F}]$ $\mathsf{P}^*_{\mathrm{num}} = 4490\,[\mathrm{F}]$

parameter set 6
  initial values:
      $\mathsf{A}_1 = 1.000\,[\mathrm{L}]$ $\mathsf{A}_2 = \mathbf{1.500}\,[\mathrm{L}]$
  at buckling load:
      $\mathsf{A}_1 = 1.276\,[\mathrm{L}]$ $\mathsf{A}_2 = 1.174\,[\mathrm{L}]$ $\sigma_{22}^{\gamma} = -1745\,[\mathrm{FL}^{-2}]$ $\sigma^{\alpha} = -31237\,[\mathrm{FL}^{-2}]$
  buckling loads:
      $\mathsf{P}^* = 8358\,[\mathrm{F}]$ $\check{\mathsf{P}}^* = 7602\,[\mathrm{F}]$ $\mathsf{P}^*_{\mathrm{num}} = 8230\,[\mathrm{F}]$

Table 4.3: Parameters for the simulation series for hardening case

4.6 Conclusions

It can be concluded that the behavior of the highly abstracted incompatible model discussed in this chapter is in line with the expectations from the theory of elastoplastic buckling presented in chapter 3. The prediction by the theory that the start of the lamella deflection, i.e. the bifurcation of the primary equilibrium path, does not imply loss of stability has been corroborated by analytical considerations in section 4.4. This finding is consistent with the numerical simulations in section 4.5 that show a stable post-buckling behaviour. At the bifurcation load there is no sudden unloading in the matrix, but a gradual transition from loading to neutral loading to unloading taking place.

The geometric stiffness in the matrix has been found of some influence on the bifurcation load in the incompatible model. The effects of initial matrix stress is investigated further in the following chapters.
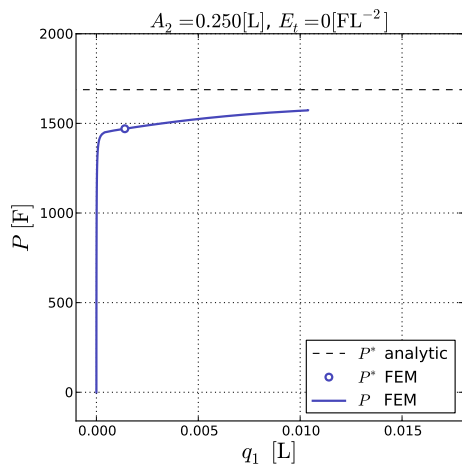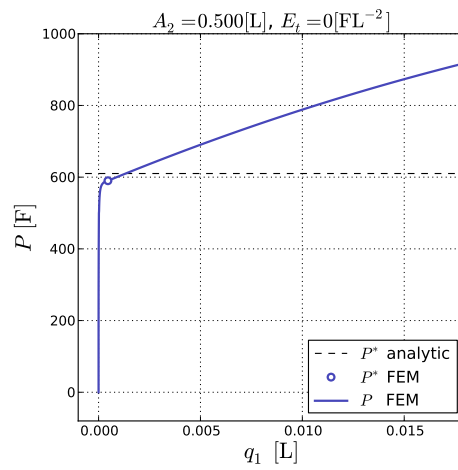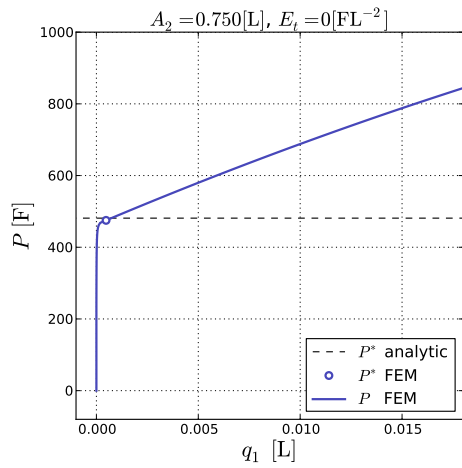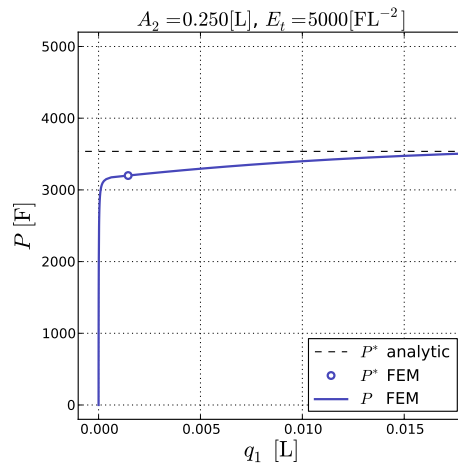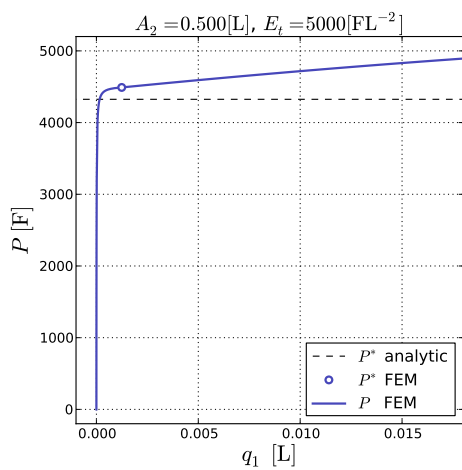
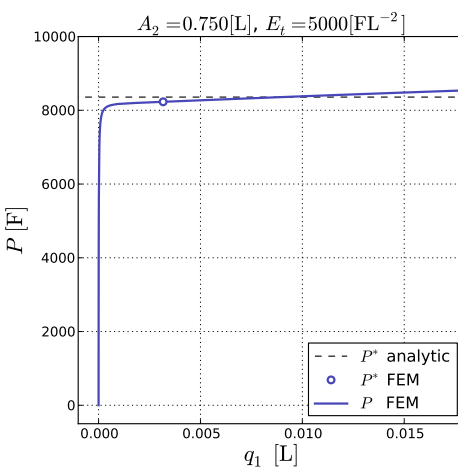(a) parameter set 1

(b) parameter set 3

(c) parameter set 5

(d) parameter set 2

(e) parameter set 4

(f) parameter set 6

Figure 4.4: Load-deflection diagrams

5 A compatible model for ideal plasticity

In order to obtain a model suited to accurately predict buckling loads the segmentation into incompatible subdomains used in chapter 4 needs to be dropped, thus abandoning the simplifications that allowed to handle simultaneous yielding and elastic unloading in the matrix. Instead, the matrix is modelled as a compatible continuum in this and the following chapters. The main assumption of chapter 4 that the buckling mode is symmetric is retained for most of this chapter, and is shown in section 5.5 to coincide with the buckling mode leading to the lowest buckling load. A unit cell approach is used to model both the symmetric and the generic periodic BCs.

To gain insight into the nature of the problem the development of an analytical model is attempted. The field equations that govern the behaviour of the elastoplastic matrix can be formulated with either the displacements or stresses (Airy-stress function) as unknown variables. For the special case of ideal plasticity a quite simple treatment of the problem is possible by the formulation in the displacements. The so obtained displacement field in the matrix is coupled to the assumed sinusoidal buckling mode of the lamella and, again, a system with a finite degree of freedom is obtained. This discrete model can be analyzed in analogy to the incompatible model. However, since the domains of active yielding or unloading are no longer rectangular, modeling of matrix unloading in the manner of chapter 4 is impractical.

5.1 Unit cells

For the case of evenly spaced lamellae the micro-structured material constitutes an inhomogeneous periodic medium. It can be efficiently described via a cut-out representing a whole period of the repeating arrangement, called a unit cell (UC) [Anthoine, 1995]. Such UCs are often utilized to calculate homogenized or smeared 'material'-properties of heterogeneous multi-scale materials that can be derived from the structural properties at a smaller length-scale [Böhm, 2004]. This approach gives meaningful results only if the length-scale at the micro-level and the length-scale of the macro scale are sufficiently different, so that the gradient of the macro-scale properties and field variables can be neglected on the micro-scale.

In the present case a plane strain situation was assumed which can be handled by a 2-dimensional UC. The periodicity results from the assumed evenly spaced lamellae in horizontal direction and the periodic buckling modeshape in vertical direction defining

two periodicity vectors $\underline{r}^A$ and $\underline{r}^B$. The periodicity vectors touch the boundary of the UC but its shape is otherwise arbitrary, provided it allows for compatible tiling of the medium when translated by $\underline{t}$, an integer multiple of the periodicity vectors, cf. Fig. 5.1 [Pahr, 2003].

$$\underline{t} = n^A \underline{r}^A + n^B \underline{r}^B \qquad n^A, n^B \in \mathbb{N} \tag{5.1}$$

Only quadrilateral UCs are considered here of which the lamella forms the left boundary. The periodicity vector $\underline{r}^B$ is locked to the buckling wavelength and must therefore be treated as an unknown. At this point it is also left open whether two neighboring lamellae buckle in-phase or with a phase-shift by allowing for a vertical component in the periodicity vector $\underline{r}^A$.

(a) Rhomboidal UC (b) Rectangular UC
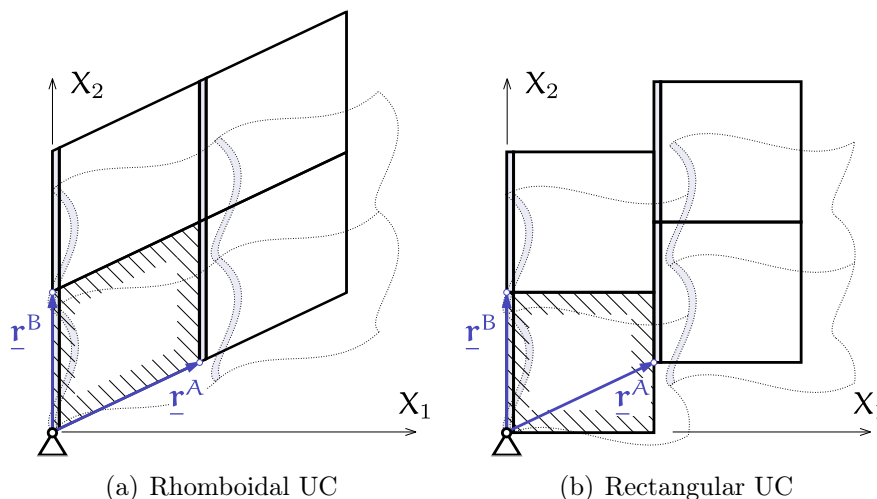
Figure 5.1: Two possible UC topologies. Both tile the 2-dimensional space in a compatible way in the unbuckled and buckled configuration.

The linear strain tensor at any particular point in the UC can be decomposed into contributions from the macroscopic strain and the local fluctuations on the length-scale of the UC [Anthoine, 1995]. It was assumed that the length scales are sufficiently different so that any gradient in the macroscopic strain is negligible on the scale of the UC. Under these circumstances the macroscopic strain can be considered homogeneous on the micro level and manifests it self as a mean or averaged strain in the UC. Any additional strain-rate fluctuations, on the other hand, are local to the UC and do not contribute to the strain apparent on the macro scale. Consequently, their average over the UC cancels out. In the present case the problem is formulated in velocities, i.e. displacement rates, rather than displacements, but the same principles apply to the rate of deformation tensor. Averaged quantities are denoted by an overscript bar while fluctuating quantities are furnished with

an overscript tilde.

$$\underline{\mathbf{d}}(\underline{\mathbf{X}}) = \bar{\underline{\mathbf{d}}} + \tilde{\underline{\mathbf{d}}}(\underline{\mathbf{X}}) \qquad\qquad \int_V \underline{\mathbf{d}}(\underline{\mathbf{X}})\,\mathrm{d}V = \bar{\underline{\mathbf{d}}}\int_V \mathrm{d}V + \underbrace{\int_V \tilde{\underline{\mathbf{d}}}(\underline{\mathbf{X}})\,\mathrm{d}V}_{=\,0}$$

$$\bar{\underline{\mathbf{d}}} = \frac{1}{V}\int_V \underline{\mathbf{d}}(\underline{\mathbf{X}})\,\mathrm{d}V \qquad\qquad \tilde{\underline{\mathbf{d}}}(\underline{\mathbf{X}}) = \underline{\mathbf{d}}(\underline{\mathbf{X}}) - \bar{\underline{\mathbf{d}}} \tag{5.2}$$

Disregarding rigid body motions the velocity field can be decomposed in a similar manner. By choosing the frame of reference so that $\underline{\mathbf{v}}(\underline{\mathbf{0}}) = \underline{\mathbf{0}}$ the mean velocity can be expressed by the mean rate of deformation, i.e. the macroscopic strain rates. Again, the fluctuations cancel out on average over the UC and give the same value if an integer multiple of the periodicity vectors, $\underline{\mathbf{t}}$, is added to the position $\underline{\mathbf{X}}$.

$$\underline{\mathbf{v}}(\underline{\mathbf{X}}) = \bar{\underline{\mathbf{d}}}\underline{\mathbf{X}} + \tilde{\underline{\mathbf{v}}}(\underline{\mathbf{X}})$$
$$\tilde{\underline{\mathbf{v}}}(\underline{\mathbf{X}}) = \tilde{\underline{\mathbf{v}}}(\underline{\mathbf{t}} + \underline{\mathbf{X}}) \tag{5.3}$$

The relative velocity between a certain point in a UC and the associated point in a UC translated by $\underline{\mathbf{t}}$ is given in terms of the mean rate of deformation tensor and the vector $\underline{\mathbf{t}}$:

$$\underline{\mathbf{v}}(\underline{\mathbf{X}} + \underline{\mathbf{t}}) = \bar{\underline{\mathbf{d}}}\,\underline{\mathbf{X}} + \bar{\underline{\mathbf{d}}}\,\underline{\mathbf{t}} + \tilde{\underline{\mathbf{v}}}(\underline{\mathbf{X}} + \underline{\mathbf{t}}) = \bar{\underline{\mathbf{d}}}\,\underline{\mathbf{X}} + \bar{\underline{\mathbf{d}}}\,\underline{\mathbf{t}} + \tilde{\underline{\mathbf{v}}}(\underline{\mathbf{X}})$$
$$\underline{\mathbf{v}}(\underline{\mathbf{X}} + \underline{\mathbf{t}}) - \underline{\mathbf{v}}(\underline{\mathbf{X}}) = \bar{\underline{\mathbf{d}}}\,\underline{\mathbf{t}} \tag{5.4}$$

Then the velocities in the points marked by the periodicity vectors is obtained by setting $n^A = 1 \wedge n^B = 0$ and $n^A = 0 \wedge n^B = 1$ respectively.

$$\underline{\mathbf{v}}^A = \bar{\underline{\mathbf{d}}}\,\underline{\mathbf{r}}^A \tag{5.5$_1$}$$
$$\underline{\mathbf{v}}^B = \bar{\underline{\mathbf{d}}}\,\underline{\mathbf{r}}^B \tag{5.5$_2$}$$

In a finite element implementation the BCs must be realized by coupling the *displacements* of two nodes on opposite sides of the quadrilateral UC and the displacements of the reference nodes at the locations $\underline{\mathbf{r}}^A$ and $\underline{\mathbf{r}}^B$. The relations given above also hold when velocities and rate of deformation tensor are exchanged for the displacements and linear strain. The mean strain is controlled by the displacement of the reference nodes and can be expressed by inverting a expression similar to (5.5) in terms of displacements.

$$\underbrace{\begin{bmatrix} u_1^A & u_1^B \\ u_2^A & u_2^B \end{bmatrix}}_{\underset{\sim}{\mathbf{V}}} = \begin{bmatrix} \bar{\varepsilon}_{11} & \bar{\varepsilon}_{12} \\ \bar{\varepsilon}_{21} & \bar{\varepsilon}_{22} \end{bmatrix} \underbrace{\begin{bmatrix} r_1^A & r_1^B \\ r_2^A & r_2^B \end{bmatrix}}_{\underset{\sim}{\mathbf{R}}}$$
$$\underset{\sim}{\mathbf{V}} = \bar{\underset{\sim}{\varepsilon}}\,\underset{\sim}{\mathbf{R}}$$
$$\bar{\underset{\sim}{\varepsilon}} = \underset{\sim}{\mathbf{V}}\,\underset{\sim}{\mathbf{R}}^{-1} \tag{5.6}$$

Using (5.6) the displacements at two opposite boundaries of the quadrilateral UC are related via the position and displacements of the periodicity vectors. This expression is

particularly useful for the formulation of the coupling constraints in a FEM-model since it only contains displacements as unknowns.

$$\underline{u}(\underline{X}_{\mathrm{rgt}}) = \underline{\underline{V}}\,\underline{\underline{R}}^{-1}\underline{X}_{\mathrm{rgt}} + \underline{u}(\underline{X}_{\mathrm{lft}}) \tag{5.7$_1$}$$

$$\underline{u}(\underline{X}_{\mathrm{top}}) = \underline{\underline{V}}\,\underline{\underline{R}}^{-1}\underline{X}_{\mathrm{rgt}} + \underline{u}(\underline{X}_{\mathrm{bot}}) \tag{5.7$_2$}$$

Combining stress and strain the decomposition can be extended to the work of the internal forces. Mixed terms will cancel out due to periodicity.

$$\mathcal{A} = -\int_V \underline{\underline{\sigma}} : \underline{\underline{d}}\,\mathrm{dV} = -\int_V (\bar{\underline{\underline{\sigma}}} + \tilde{\underline{\underline{\sigma}}}) : (\bar{\underline{\underline{d}}} + \tilde{\underline{\underline{d}}})\,\mathrm{dV}$$

$$= -\int_V (\bar{\underline{\underline{\sigma}}} : \bar{\underline{\underline{d}}} + \underbrace{\bar{\underline{\underline{\sigma}}} : \tilde{\underline{\underline{d}}}}_{=0} + \underbrace{\tilde{\underline{\underline{\sigma}}} : \bar{\underline{\underline{d}}}}_{=0} + \tilde{\underline{\underline{\sigma}}} : \tilde{\underline{\underline{d}}}\,\mathrm{dV} = \bar{\mathcal{A}} + \tilde{\mathcal{A}} \tag{5.8}$$

$$\bar{\mathcal{A}} := -\int_V \bar{\underline{\underline{\sigma}}} : \bar{\underline{\underline{d}}}\,\mathrm{dV} \tag{5.9}$$

$$\tilde{\mathcal{A}} := -\int_V \tilde{\underline{\underline{\sigma}}} : \tilde{\underline{\underline{d}}}\,\mathrm{dV} \tag{5.10}$$

5.2 Governing equations in terms of velocities

In the following the superscript γ to indicate matrix quantities will be dropped when there is no ambiguity.

The crude assumptions with regard to the matrix kinematics made so far are now replaced by kinematic assumptions that properly respect a set of governing equations, (5.11) to (5.14). The stress-rates in the matrix are required to satisfy the equation of continuing equilibrium. As a simplification, matrix body force densities are only admitted if their rate vanishes.

$$\mathrm{Div}\,\dot{\underline{\underline{\sigma}}} = \underline{0} \tag{5.11}$$

The assumptions that were made in section 2.1 with regard to the additive decomposition of rate of deformation tensor and the identification of the material and the spatial configuration in section 2.3 still apply.

$$\underline{\underline{F}} = \underline{\underline{1}}$$

$$\underline{\underline{d}} = \underline{\underline{d}}^{\mathrm{e}} + \underline{\underline{d}}^{\mathrm{p}} = \mathrm{sym}(v_{\mathrm{i,j}}) = \tfrac{1}{2}(v_{\mathrm{i,j}} + v_{\mathrm{j,i}}) \tag{5.12}$$

The elastic response is given by Hooke's law, cf. (2.3), and the plastic part of the deformation rates is isochoric.

$$\mathrm{tr}(\underline{\underline{d}}^{\mathrm{p}}) = 0 \tag{5.13}$$

$$\dot{\underline{\underline{\sigma}}} = \lambda \underline{\underline{1}}\,\mathrm{tr}(\underline{\underline{d}}) + 2\mu\underline{\underline{d}} - 2\mu\underline{\underline{d}}^{\mathrm{p}} \tag{5.14}$$

5 A compatible model for ideal plasticity

For ease of manipulation the governing equations are restated in index-notation:

$$\dot{\sigma}_{ij,i} = 0 \qquad\qquad\qquad\qquad\qquad\qquad \dot{\sigma}_{ij} = \dot{\sigma}_{ji} \qquad\qquad (5.15_1)$$

$$d_{ij} = d^e_{ij} + d^p_{ij} = 1/2(v_{i,j} + v_{j,i}) \qquad\qquad\qquad\qquad\qquad\qquad (5.15_2)$$

$$d^p_{kk} = 0 \qquad\qquad\qquad\qquad\qquad\qquad d^p_{ij} = d^p_{ji} \qquad\qquad (5.15_3)$$

$$\dot{\sigma}_{ij} = \lambda\delta_{ij}d_{kk} + 2\mu d_{ij} - 2\mu d^p_{ij} \qquad\qquad\qquad\qquad\qquad\qquad (5.15_4)$$

In an adaption from [Mendelson, 1968] or [Srinivasa and Srinivasan, 2009], the equations are be combined and restated as a partial differential equation (PDE) in terms of the velocity:

$$\dot{\sigma}_{ij} = \lambda\delta_{ij}v_{k,k} + \mu\left(v_{i,j} + v_{j,i}\right) - 2\mu d^p_{ij}$$

$$\dot{\sigma}_{ij,i} = \dot{\sigma}_{ij,j} = 0$$

$$\dot{\sigma}_{ij,j} = \lambda\underbrace{\delta_{ij}v_{k,kj}}_{v_{k,kj} = v_{j,ji} = v_{j,ij}} + \mu\left(v_{i,jj} + v_{j,ij}\right) - 2\mu\underbrace{d^p_{ij,j}}_{d^p_{ij,j} = d^p_{ij,i}} = 0$$

$$\lambda v_{j,ij} + \mu(v_{i,jj} + v_{j,ij}) = 2\mu d^p_{ij,j}$$

$$(\lambda + \mu)v_{j,ij} + \mu v_{i,jj} = 2\mu d^p_{ij,j}$$

The second derivatives can be concisely written in terms of the nabla and Laplace differential-operators.

$$v_{j,ij}\ \underline{e}_i = \operatorname{Grad}\operatorname{Div}(\underline{v}) = \boldsymbol{\nabla}(\boldsymbol{\nabla}\cdot\underline{v})$$

$$v_{i,jj}\ \underline{e}_i = \operatorname{Div}\operatorname{Grad}(\underline{v}) = \boldsymbol{\Delta}(\underline{v})$$

Returning to direct notation, the PDE governing the matrix deformation is given by (5.16)

$$(\lambda + \mu)\operatorname{Grad}\operatorname{Div}(\underline{v}) + \mu\operatorname{Div}\operatorname{Grad}(\underline{v}) = 2\mu\operatorname{Div}(\underset{\sim}{\mathbf{d}}^p)$$

$$(\lambda + \mu)\boldsymbol{\nabla}(\boldsymbol{\nabla}\cdot\underline{v}) + \mu\boldsymbol{\Delta}(\underline{v}) = 2\mu\boldsymbol{\nabla}\cdot\underset{\sim}{\mathbf{d}}^p \qquad\qquad (5.16)$$

In the equation above, no reference to a particular state of initial stress has been made. However, the plastic part of the deformation tensor on right-hand side of the equation needs to be expressed in terms of the velocity as well, and for this purpose it is necessary to reference the conditions that were introduced in section 2.4. Utilizing the assumptions made with regard to the initial deviatoric stress on the primary loading path in (2.30) yields an expression for the right-hand side in derivations of the velocity.

$$\hat{\underset{\sim}{\sigma}} = \frac{\kappa}{\sqrt{2}}\begin{bmatrix} +1 & 0 \\ 0 & -1 \end{bmatrix}$$

$$\phi = \frac{\hat{\underset{\sim}{\sigma}} : \underset{\approx}{\mathbb{E}} : \underset{\sim}{\mathbf{d}}}{\hat{\underset{\sim}{\sigma}} : \underset{\approx}{\mathbb{E}} : \hat{\underset{\sim}{\sigma}} + \kappa^2\theta} = \frac{\sqrt{2}\,\mu}{\kappa(\theta + 2\mu)}(v_{2,2} - v_{1,1})$$

$$\underset{\sim}{\mathbf{d}}^p = \phi\hat{\underset{\sim}{\sigma}} = \frac{\mu}{\theta + 2\mu}\begin{bmatrix} v_{1,1} - v_{2,2} & 0 \\ 0 & v_{2,2} - v_{1,1} \end{bmatrix}$$

$$\underline{\nabla} \cdot \underline{\underline{d}}^p = \frac{\mu}{\theta + 2\mu} \begin{bmatrix} v_{1,11} - v_{2,21} \\ v_{2,22} - v_{1,12} \end{bmatrix}$$

The general equation in (5.16) is thus restated for the problem of elastoplastic lamella buckling:

$$(\lambda + \mu) \begin{bmatrix} v_{1,11} + v_{2,12} \\ v_{1,12} + v_{2,22} \end{bmatrix} + \mu \begin{bmatrix} v_{1,11} + v_{1,22} \\ v_{2,11} + v_{2,22} \end{bmatrix} = \frac{2\mu^2}{\theta + 2\mu} \begin{bmatrix} v_{1,11} - v_{2,21} \\ v_{2,22} - v_{1,12} \end{bmatrix}$$

$$(\lambda + 2\mu - \frac{2\mu^2}{\theta + 2\mu}) \begin{bmatrix} v_{1,11} \\ v_{2,22} \end{bmatrix} + (\lambda + \mu + \frac{2\mu^2}{\theta + 2\mu}) \begin{bmatrix} v_{2,12} \\ v_{1,12} \end{bmatrix} + \mu \begin{bmatrix} v_{1,22} \\ v_{2,11} \end{bmatrix} = \underline{0} \quad (5.17)$$

5.3 The symmetric unit cell

A solution to (5.17) can be guessed using a 'ansatz'-function. One such function that solves the PDE is given by (5.18). The fluctuation part of the ansatz is symmetric about the axis $X_1 = A_1$ and is compatible with the symmetry of the UC assumed so far, thus it can be seen as a compatible analogon to the model discussed in chapter 4.

$$\begin{bmatrix} v_1 \\ v_2 \end{bmatrix} = \begin{bmatrix} c \cos(aX_1/A_1)\sin(bX_2/A_2) + fX_1/A_1 \\ d \sin(aX_1/A_1)\cos(bX_2/A_2) + eX_2/A_2 \end{bmatrix} \quad (5.18)$$

$$\begin{bmatrix} v_{1,11} \\ v_{2,22} \end{bmatrix} = \begin{bmatrix} -\frac{a^2 c}{A_1^2} \cos(aX_1/A_1)\sin(bX_2/A_2) \\ -\frac{b^2 d}{A_2^2} \sin(aX_1/A_1)\cos(bX_2/A_2) \end{bmatrix}$$

$$\begin{bmatrix} v_{2,12} \\ v_{1,12} \end{bmatrix} = \begin{bmatrix} -\frac{abd}{A_1 A_2} \cos(aX_1/A_1)\sin(bX_2/A_2) \\ -\frac{abc}{A_1 A_2} \sin(aX_1/A_1)\cos(bX_2/A_2) \end{bmatrix}$$

$$\begin{bmatrix} v_{1,22} \\ v_{2,11} \end{bmatrix} = \begin{bmatrix} -\frac{b^2 c}{A_2^2} \cos(aX_1/A_1)\sin(bX_2/A_2) \\ -\frac{a^2 d}{A_1^2} \sin(aX_1/A_1)\cos(bX_2/A_2) \end{bmatrix}$$

The guessed solution to the PDE is of course not necessarily exhaustive, and a more generic solution could be obtained, e.g. , by adding the expression (5.19) below. However, in this section only (5.18) is considered as a solution, and in the course of the chapter arguments are put forward that it is sufficient for the present purpose.

$$\begin{bmatrix} g \sin(aX_1/A_1)\cos(bX_2/A_2) \\ h \cos(aX_1/A_1)\sin(bX_2/A_2) \end{bmatrix} \quad (5.19)$$

The solution under consideration does not allow for shear strain in the matrix. Whether this constitutes an oversimplification or not needs to be investigated in the following. The investigations presented in this section and thereafter, however, show that the function captures the buckling mode under certain circumstances, i.e. no hardening, well as will be elaborated below. Since the fluctuation in the displacement field is reminiscent to a checkerboard it will be referred to as 'checkerboard pattern', cf. Fig. 5.4 and Fig. 5.5.

Inserting the ansatz into the PDE and canceling the trigonometric functions gives two equations:

$$-(\lambda + 2\mu - \frac{2\mu^2}{\theta + 2\mu}) \begin{bmatrix} \frac{a^2c}{A_1^2} \\ \frac{b^2d}{A_2^2} \end{bmatrix} - (\lambda + \mu + \frac{2\mu^2}{\theta + 2\mu}) \begin{bmatrix} \frac{abd}{A_1 A_2} \\ \frac{abc}{A_1 A_2} \end{bmatrix} - \mu \begin{bmatrix} \frac{b^2c}{A_2^2} \\ \frac{a^2d}{A_1^2} \end{bmatrix} = \underline{0}$$

Solving for a and c results in a complex solution for any real valued b and c, unless $\theta = 0$, i.e. the ansatz solves the differential equation only for the special case of *ideal plasticity*. The case of ideal plasticity has been briefly considered in chapter 4. It has been found problematic for the incompatible model insofar as the buckling length was unbounded. For the compatible model, however, it is demonstrated in the following that the buckling length is related to the lamella spacing and no complication arises for $\theta \to 0$. Solving for a and b gives:

$$-(\lambda + \mu) \begin{bmatrix} \frac{a^2c}{A_1^2} \\ \frac{b^2d}{A_2^2} \end{bmatrix} - (\lambda + 2\mu) \begin{bmatrix} \frac{abd}{A_1 A_2} \\ \frac{abc}{A_1 A_2} \end{bmatrix} - \mu \begin{bmatrix} \frac{b^2c}{A_2^2} \\ \frac{a^2d}{A_1^2} \end{bmatrix} = \underline{0}$$

$$a = \pm b A_1 / A_2 \qquad c = \mp d \tag{5.20}$$

The two solutions in (5.20) represent the possibility to deflect to the left or the right. The derivation continues with $a = +b A_1 / A_2$ and $c = -d$.

$$v_1^\gamma(X_1, X_2) = -d \cos(b X_1 / A_2) \sin(b X_2 / A_2) + f X_1 / A_1 \tag{5.21_1}$$
$$v_2^\gamma(X_1, X_2) = +d \sin(b X_1 / A_2) \cos(b X_2 / A_2) + e X_2 / A_2 \tag{5.21_2}$$
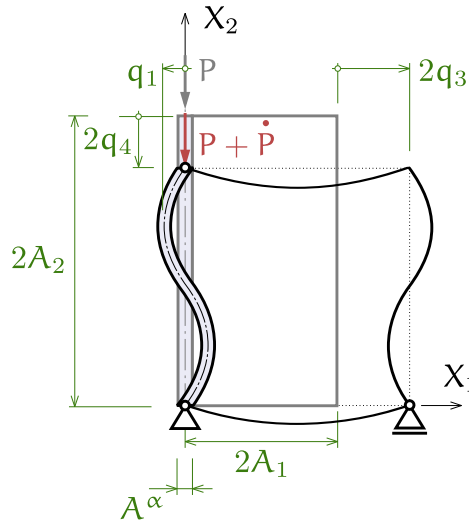

Figure 5.2: Generalized coordinates of the symmetric UC.

In order to determine the remaining constants in (5.21) BCs need to be specified. The UC-height is defined by the buckling wavelength $2A_2$ and contains, therefore, by definition,

exactly one buckling period. The mean shortening-rate per half-wavelength is $\dot{q}_4$, and by comparison to (5.21) it follows that $f = \dot{q}_4$. Likewise, for the horizontal direction e can be determined as equal to $\dot{q}_3$. The remaining constants b and d are obtained by matching the lamella displacements at the left boundary. For simplicity, the lamella thickness is neglected and coupling is thought to occur at the lamella centerline. Then $v_1^\gamma(0, X_2) = v_1^\alpha(0, X_2)$ and $-d = \dot{q}_1$, $b = \pi$. All constants have thus been determined, and the velocity field can be stated in terms of the GC-rates as follows:

$$
\underline{\boldsymbol{v}}^\gamma(\underline{\mathbf{X}}) = \underbrace{\left[\begin{array}{c} +\dot{q}_1 \cos(\pi X_1/A_2) \sin(\pi X_2/A_2) \\ -\dot{q}_1 \sin(\pi X_1/A_2) \cos(\pi X_2/A_2) \end{array} \right]}_{\tilde{\underline{v}}^\gamma(\underline{\mathbf{X}})} + \underbrace{\left[\begin{array}{c} +\dot{q}_3 X_1/A_1 \\ -\dot{q}_4 X_2/A_2 \end{array} \right]}_{\bar{\underline{v}}^\gamma(\underline{\mathbf{X}})}
\tag{5.22}
$$
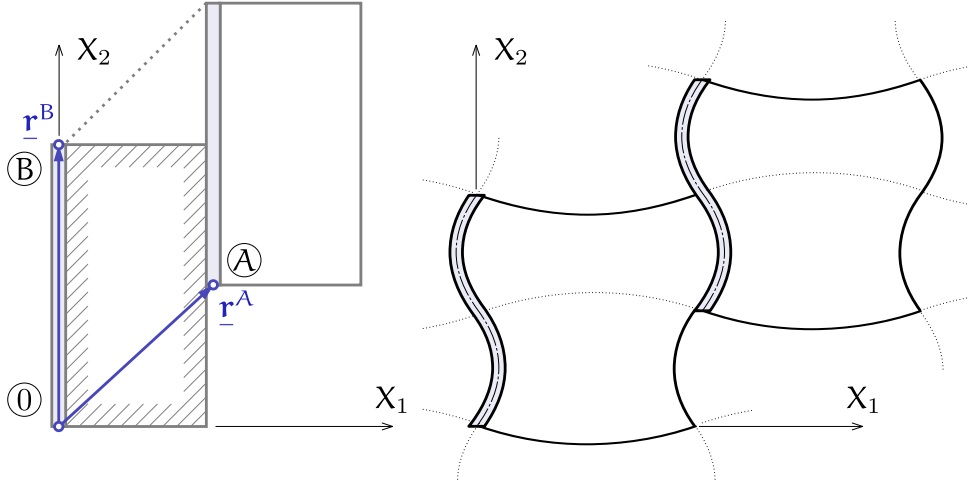
Figure 5.3: Tiling of the symmetric UC.

With all constants determined, the BC on the right side still needs to be accounted for. It is met when the velocity fluctuations are periodic as required by (5.3). Taking notice that the periodicity vectors of the current model are given by (5.23) the periodicity of the velocity fluctuations is checked in (5.24).

$$
\underline{\mathbf{r}}^A = \left[\begin{array}{c} 2A_1 \\ A_2 \end{array} \right]
\tag{5.23_1}
$$

$$
\underline{\mathbf{r}}^B = \left[\begin{array}{c} 0 \\ 2A_2 \end{array} \right]
\tag{5.23_2}
$$

Expanding $\tilde{\underline{v}}^\gamma(\underline{\mathbf{X}} + \underline{\mathbf{t}})$ for $n^A = 1$ and $n^B = 0$ via trigonometric identities:

$$
\begin{aligned}
+\frac{1}{\dot{q}_1} \tilde{v}_1^\gamma(\underline{\mathbf{X}} + \underline{\mathbf{r}}^A) &= \cos\left(\pi \frac{X_1 + 2A_1}{A_2} \right) \sin\left(\pi \frac{X_2 + A_2}{A_2} \right) \\
&= -\left[\cos\left(\pi \frac{X_1}{A_2} \right) \cos\left(\pi \frac{2A_1}{A_2} \right) - \sin\left(\pi \frac{X_1}{A_2} \right) \sin\left(\pi \frac{2A_1}{A_2} \right) \right] \sin\left(\pi \frac{X_2}{A_2} \right)
\end{aligned}
\tag{5.24_1}
$$

$$-\frac{1}{\dot{q}_1}\tilde{v}_2^\gamma(\underline{X}+\underline{r}^A) = \sin\left(\pi\frac{X_1+2A_1}{A_2}\right)\cos\left(\pi\frac{X_2+A_2}{A_2}\right)$$

$$= -\left[\sin\left(\pi\frac{X_1}{A_2}\right)\cos\left(\pi\frac{2A_1}{A_2}\right) + \cos\left(\pi\frac{X_1}{A_2}\right)\sin\left(\pi\frac{2A_1}{A_2}\right)\right]\cos\left(\pi\frac{X_2}{A_2}\right) \qquad (5.24_2)$$

To reconcile the fluctuating part of (5.22) and (5.24) a certain ratio of the buckling wavelength to the lamella spacing is required. The UC-width can, in principle, contain more than one fluctuation half-period in horizontal direction. For the present model, however, it is thought that only one half-period in the fluctuations occurs over the space between two lamellae. The more general case is investigated in section 5.5. So the relation A_1 to A_2 is:

$$A_2 = 2A_1 \qquad (5.25)$$

It is notable that, unlike the situation in chapter 4, the buckling wavelength for the present model is not determined by some minimization procedure, but arises from the relations governing the matrix displacement.

With the matrix velocity field determined, the matrix shape functions and their gradients are given below. The lamella shape functions are unchanged from (4.3) and (4.4).

$$\underline{\Phi}_1^\gamma = \begin{bmatrix} +\cos\left(\frac{\pi X_1}{A_2}\right)\sin\left(\frac{\pi X_2}{A_2}\right) \\ -\sin\left(\frac{\pi X_1}{A_2}\right)\cos\left(\frac{\pi X_2}{A_2}\right) \end{bmatrix} \qquad (5.26_1)$$

$$\underline{\Phi}_3^\gamma = \begin{bmatrix} +\frac{X_1}{A_1} \\ 0 \end{bmatrix} \qquad (5.26_2)$$

$$\underline{\Phi}_4^\gamma = \begin{bmatrix} 0 \\ -\frac{X_2}{A_2} \end{bmatrix} \qquad (5.26_3)$$

$$\text{Grad } \underline{\Phi}_1^\gamma = \frac{\pi}{A_2}\begin{bmatrix} -\sin\left(\frac{\pi X_1}{A_2}\right)\sin\left(\frac{\pi X_2}{A_2}\right) & +\cos\left(\frac{\pi X_1}{A_2}\right)\cos\left(\frac{\pi X_2}{A_2}\right) \\ -\cos\left(\frac{\pi X_1}{A_2}\right)\cos\left(\frac{\pi X_2}{A_2}\right) & +\sin\left(\frac{\pi X_1}{A_2}\right)\sin\left(\frac{\pi X_2}{A_2}\right) \end{bmatrix} \qquad (5.27_1)$$

$$\text{Grad } \underline{\Phi}_3^\gamma = \begin{bmatrix} +\frac{1}{A_1} & 0 \\ 0 & 0 \end{bmatrix} \qquad (5.27_2)$$

$$\text{Grad } \underline{\Phi}_4^\gamma = \begin{bmatrix} 0 & 0 \\ 0 & -\frac{1}{A_2} \end{bmatrix} \qquad (5.27_3)$$

No shear strain is present in the matrix, because the ansatz in Eq. (5.18) does not allow for shear deformation. By using it, the tacit assumption is made that any shear related buckling modes are not relevant.

$$\underline{\underline{d}}^\gamma = \text{sym}(\dot{\underline{\underline{F}}}^\gamma(\underline{\underline{1}})^{-1}) = \text{sym}(\textstyle\sum_{i=1,3,4}\dot{q}_i\,\text{Grad }\underline{\Phi}_i^\gamma)$$

(a) v_1^γ (b) v_2^γ (c) ϕ
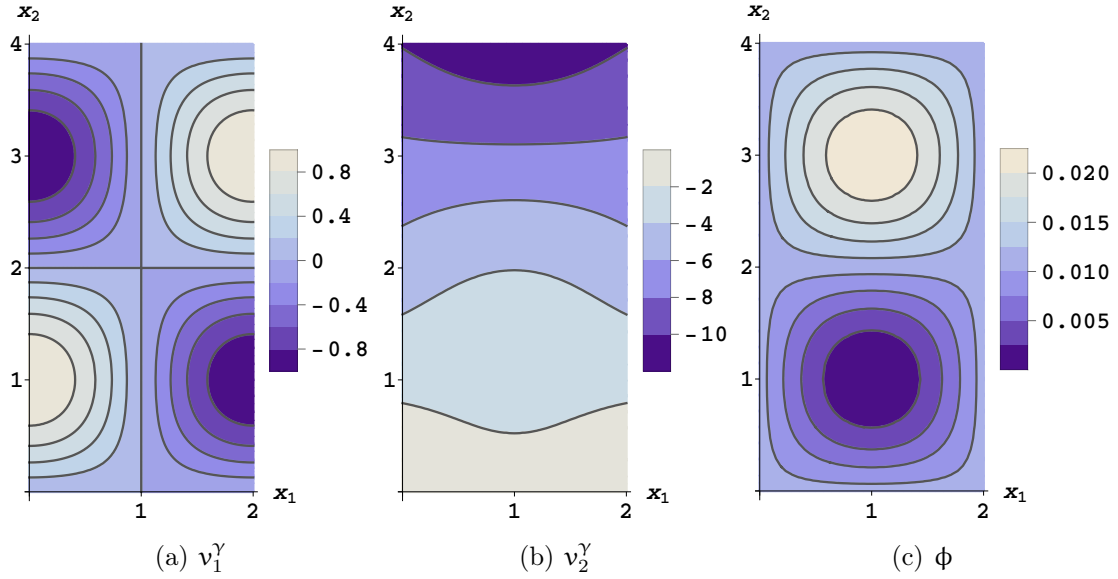
Figure 5.4: Contour plot of the components of the displacement field $\underline{v}^\gamma$ plus a contour plot of the plastic consistency parameter ϕ. The GC-rate $\dot{q}_4$ has been adjusted so that $\phi \geqslant 0$ everywhere.
$A_1 = 1\,[\mathrm{L}], A_2 = 2\,[\mathrm{L}], \dot{q}_1 = 1\,[\mathrm{LT}^{-1}], \dot{q}_3 = 0, \dot{q}_4 = (\pi/2 - \pi^2/16)\,[\mathrm{LT}^{-1}]$

(a) d_{11}^γ (b) d_{22}^γ (c) d_{12}^γ
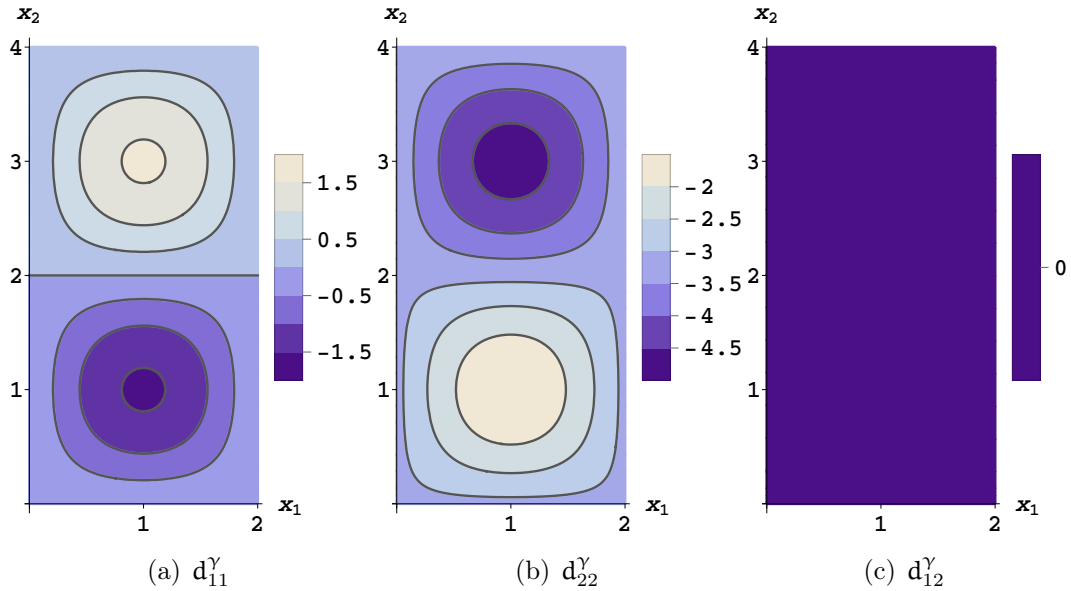
Figure 5.5: Contour plot of the components of the strain-rate $\underline{\underline{d}}^\gamma$. A single column of the 'checkerboard pattern' can be seen in 5.5(a) and 5.5(b).
$A_1 = 1\,[\mathrm{L}], A_2 = 2\,[\mathrm{L}], \dot{q}_1 = 1\,[\mathrm{LT}^{-1}], \dot{q}_3 = 0, \dot{q}_4 = (\pi/2 - \pi^2/16)\,[\mathrm{LT}^{-1}]$

$$\underset{\sim}{\mathbf{d}}^\gamma = \underbrace{\frac{\pi \dot{q}_1}{A_2} \sin\left(\frac{\pi X_1}{A_2}\right) \sin\left(\frac{\pi X_2}{A_2}\right) \begin{bmatrix} -1 & 0 \\ 0 & +1 \end{bmatrix}}_{\tilde{\underset{\sim}{\mathbf{d}}}^\gamma} + \underbrace{\begin{bmatrix} \frac{\dot{q}_3}{A_1} & 0 \\ 0 & -\frac{\dot{q}_4}{A_2} \end{bmatrix}}_{\bar{\underset{\sim}{\mathbf{d}}}^\gamma} \tag{5.28}$$

The difficulties of properly separating the matrix into yielding and nonyielding subdomains effectively preclude the consideration of simultaneous loading and unloading in the matrix. Only the 'loading everywhere'-situation can be modeled easily. This is sufficient, however, for the purpose of a comparison solid in the sense of section 3.5, and it can be used to derive the bifurcation load. The matrix load is again given as the homogeneous stress σ_{22}^γ and the constants $_{ll}F_1$ and $_{ll}F_2$ from (4.10) can be reused in the expression for the mixed material stiffness. The left subscript ll can be dropped here, since no other loading situation is considered. Because (5.18) is a solution for the case of ideal plasticity only, the hardening factor θ takes the value zero, and both constants simplify to $\lambda + \mu$. The hardening factor is retained, however, in the formulae to investigate if the so obtained results can serve as an approximation for slight hardening. The lamella material stiffness is adopted from (4.13).

$$\underset{\approx}{\mathbb{L}}^\gamma = \begin{bmatrix} \begin{bmatrix} F_1 & 0 \\ 0 & F_2 \end{bmatrix} & \begin{bmatrix} 0 & \mu \\ \mu & 0 \end{bmatrix} \\ \begin{bmatrix} 0 & \mu \\ \mu & 0 \end{bmatrix} & \begin{bmatrix} F_2 & 0 \\ 0 & F_1 \end{bmatrix} \end{bmatrix} \tag{5.29}$$

$$\underset{\approx}{\mathbb{C}}^\gamma = \begin{bmatrix} \begin{bmatrix} F_1 & 0 \\ 0 & F_2 \end{bmatrix} & \begin{bmatrix} 0 & \mu + \frac{1}{2}\sigma_{22}^\gamma \\ \mu - \frac{1}{2}\sigma_{22}^\gamma & 0 \end{bmatrix} \\ \begin{bmatrix} 0 & \mu - \frac{1}{2}\sigma_{22}^\gamma \\ \mu - \frac{1}{2}\sigma_{22}^\gamma & 0 \end{bmatrix} & \begin{bmatrix} F_2 & 0 \\ 0 & F_1 - \sigma_{22}^\gamma \end{bmatrix} \end{bmatrix} \tag{5.30}$$

It is noteworthy that for ideal plasticity, i.e. $F_1 = F_2$, no change in Cauchy-stress is associated with the GC-rate $\dot{q}_1$. The lateral support stiffness exerted by the matrix on the lamella vanishes.

$$\underset{\approx}{\mathbb{L}} : \tilde{\underset{\sim}{\mathbf{d}}}^\gamma = \frac{\pi \dot{q}_1}{A_2}(F_1 - F_2)\sin\left(\frac{\pi X_1}{A_2}\right)\sin\left(\frac{\pi X_2}{A_2}\right)\begin{bmatrix} -1 & 0 \\ 0 & +1 \end{bmatrix}$$

The internal force rates are calculated in the same way as specified by (4.14), the integration limits need to be updated to reflect the changed model size, however. The left subscript is not used, all forces are calculated for the 'loading everywhere'-case. Again, the lamella stress is neglected in relation to the elastic modulus in direct subtraction.

$$\dot{Q}_1 = \left(\frac{2\pi^2(F_1 - F_2)A_1}{A_2} + \frac{\pi^2 A^\alpha \sigma_{22}^\alpha}{A_2} + \frac{\pi^4(A^\alpha)^3(E^\alpha - \cancel{\sigma_{22}^\alpha})}{12 A_2^3}\right)\dot{q}_1 \tag{5.31_1}$$

$$\dot{Q}_3 = +4F_1 \frac{A_2}{A_1}\dot{q}_3 - 4F_2 \dot{q}_4 \tag{5.31_2}$$

$$\dot{Q}_4 = +\left(4\frac{A_1}{A_2}(F_1 - \sigma_{22}^\gamma) + 2\frac{A^\alpha}{A_2}(E^\alpha - \cancel{\sigma_{22}^\alpha})\right)\dot{q}_4 - 4F_2\dot{q}_3 \tag{5.31$_3$}$$

$$\underset{\sim}{\mathbf{K}} = \begin{bmatrix} \frac{\pi^4(A^\alpha)^3}{12A_2^3}E^\alpha + 2\frac{\pi^2 A_1}{A_2}(F_1 - F_2) + \frac{\pi^2 A^\alpha}{A_2}\sigma_{22}^\alpha & 0 & 0 \\ 0 & 4\frac{A_2}{A_1}F_1 & -4F_2 \\ 0 & -4F_2 & 4\frac{A_1}{A_2}(F_1 - \sigma_{22}^\gamma) + 2\frac{A^\alpha}{A_2}E^\alpha \end{bmatrix} \tag{5.32}$$

The load P can be introduced to (5.32) via the equilibrium condition (4.7), and the bifurcation load is obtained as the load for which $\det(\underset{\sim}{\mathbf{K}})$ vanishes. The K_{11} element is completely uncoupled from the other matrix elements, and the bifurcation load is reached when it attains the value zero. The terms determining the bifurcation load P^* of the current model can be arranged in a way that allows to give them an interpretation, as was done for the incompatible model. The first and the last term are identical to (4.20). The middle term representing the matrix support does not depend on the matrix prestress and is zero for ideal plasticity. This is in contrast to the result for the incompatible model that showed a certain influence of the geometric matrix-stiffness on the bifurcation load. Unlike for the incompatible model, the half-wavelength A_2 for the current model is not to be determined by a minimization procedure, but is directly related to the lamella spacing by (5.25).

$$P^* = \underbrace{\frac{\pi^2 E^\alpha(A^\alpha)^3}{12A_2^2}}_{\text{Euler-buckling load}} + \overbrace{\frac{4\theta\mu}{\theta + 2\mu}}^{\text{due to matrix stiffness}} - \underbrace{2A_1\sigma_{22}^\gamma}_{\text{load carried by matrix}} \tag{5.33}$$

When P^* is reached, one point in the UC experiences neutral loading, i.e. The plastic consistency factor ϕ is zero there, cf. Fig. 5.4(c). When the load increases further on the bifurcated equilibrium path this point becomes the nucleus of an expanding, elastically unloading zone.

5.4 Symmetric finite element model

To verify the results for the symmetric UC a new compatible FEM-model is used. The simulations are setup in the manner described in section 4.5, i.e. the bifurcating loading-path is transformed into a continuous path by a small geometric imperfection, and the path is followed by a quasi static analysis. Since the model is compatible, the matrix is properly discretized by second order interpolating elements (Elements CPE8RH in Abaqus). Again, the increment of first unloading in any previously yielding element is used as a definition to extract the buckling load from the numerical data. The elastic moduli, matrix Poisson's ratio and the lamella thickness are the same for all models here

and unchanged from the values given in Table 4.1. The matrix tangent modulus in the plastic regime is set to zero, however.

It is one of the objectives of the FEM-model to verify the finding that the buckling wavelength is determined by the lamella spacing. To this end, care has to be taken that the wavelength can develop freely in the FEM-model. However, the FEM-model also constitutes a UC of some sort and needs boundary constraints as specified by (5.7_2). They suppress deflection at the corners, and only integer numbers of lamella fluctuation periods can be accommodated in the FEM-model. To keep errors resulting from this effect to a minimum the FEM-model height is 10 wavelengths or more. Horizontally the FEM-model spans the distance between two lamellae, $2A_1$, in accordance with the UC used in the analytical computations. The FEM-model, therefore, can be seen as a series of UCs stacked in vertical direction.

To enforce symmetry, the fluctuations at the model boundary are subject to the constraint:

$$\tilde{v}_1(0, X_2) = -\tilde{v}_1(2A_1, X_2) \tag{5.34_1}$$
$$\tilde{v}_2(0, X_2) = +\tilde{v}_2(2A_1, X_2) \tag{5.34_2}$$

This condition is in general not equivalent to the periodicity of the fluctuations, as specified by (5.3). Equation (5.34) does not strictly enforce compatibility. For the sinusoidal lamella deflection postulated for this model compatibility is maintained, however. The mode-shape of the lamella deflection is investigated below. The mean strain of the FEM-model is controlled by the displacement of the node located at the periodicity vectors via (5.6).

Figure 5.7 shows the evolution of the displacement at the left boundary $(X_1 = 0)$ over increasing loads. Only a small part of the lower FEM-model boundary is shown. The lamella spacing, $2A_1$, for the shown simulation is $2\,[L]$. The figure shows that the half-wavelength is also equal to $2\,[L]$ and this is in accordance with the prediction by Equation (5.25). A total of 20 UCs is accommodated in the FEM-model with a total height of $80\,[L]$. For the load increments near the buckling load a sinusoidal deflection-mode becomes evident. This mode-shape is present even in the prebuckling steps since the equilibrium-path of an imperfect system is followed. However, only when approaching the buckling load the amplitude becomes significant.

Results for the buckling load from FEM-analysis are displayed in Fig. 5.6 and compared to the analytical results by Eq. (5.33). To eliminate the effect of the prebuckling deformations, the actual value of A_1 at the instant of buckling in the FEM-model is used in the analytical formula rather than the initial, unloaded value. The initial values of A_1 range from $0.5\,[L]$ to $2.0\,[L]$. The data-points are positioned horizontally according to A_1 at the instant of buckling. For lamella spacings $A_1 > 1.1\,[L]$ a certain scatter in the distribution of the buckling loads, as calculated by FEM-analysis, appears. This is likely caused by the low number of half-waves accommodated in the FEM-model (12 to 10). When only few half-waves are contained within the FEM-model mismatch to the ideal buckling wavelength is possibly larger, since the step size between integer wavelengths increases.
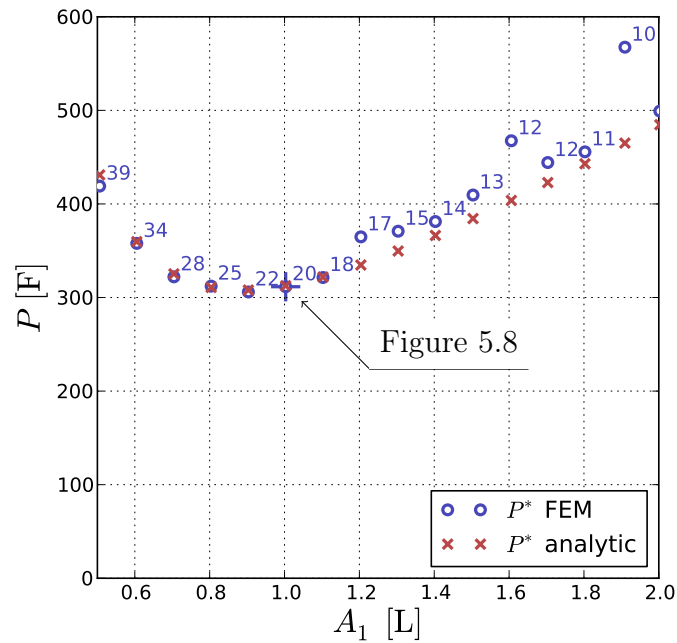
Figure 5.6: Comparison of buckling loads as calculated from (5.33) to results from FEM-analysis. The numbers next to the data points indicate the number of buckling waves over the FEM-model height.
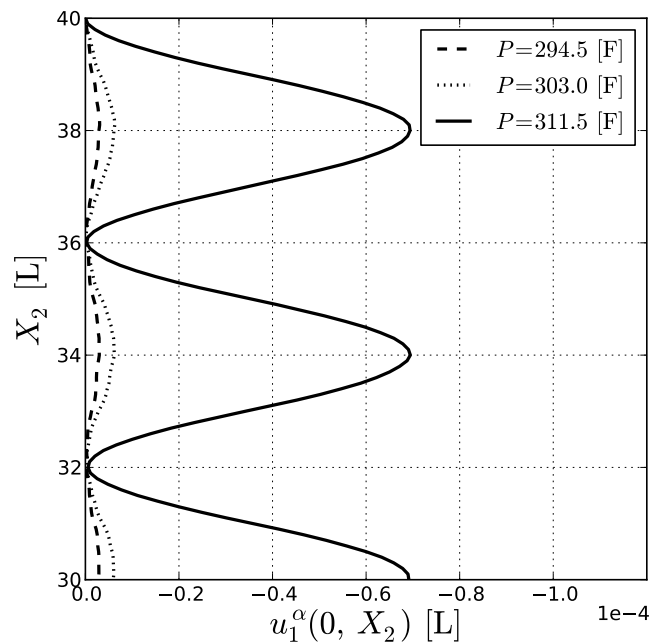

Figure 5.7: Wavelength and eigenmode at the left FEM-model boundary, $X_1 = -A_1$, for the lamella spacing $2A_1 = 2\,[\mathrm{L}]$

The matrix strain as obtained from the simulation and expressed by the logarithmic strain measure LE is shown in Fig. 5.8. It shows the checkerboard pattern predicted by (5.28). A closer look to the amplitudes of the components of normal strain $LE_{11}^{max} - LE_{11}^{min} = 8.00 \times 10^{-5}$ and $LE_{22}^{max} - LE_{22}^{min} = 8.00 \times 10^{-5}$ reveals that they have an equal amplitude but are phase shifted by a half-period. The shear strain, on the other hand is mostly due to noise generated by the imperfection and only slightly hint at a checkerboard shifted by a quarter period in both horizontal and vertical direction.
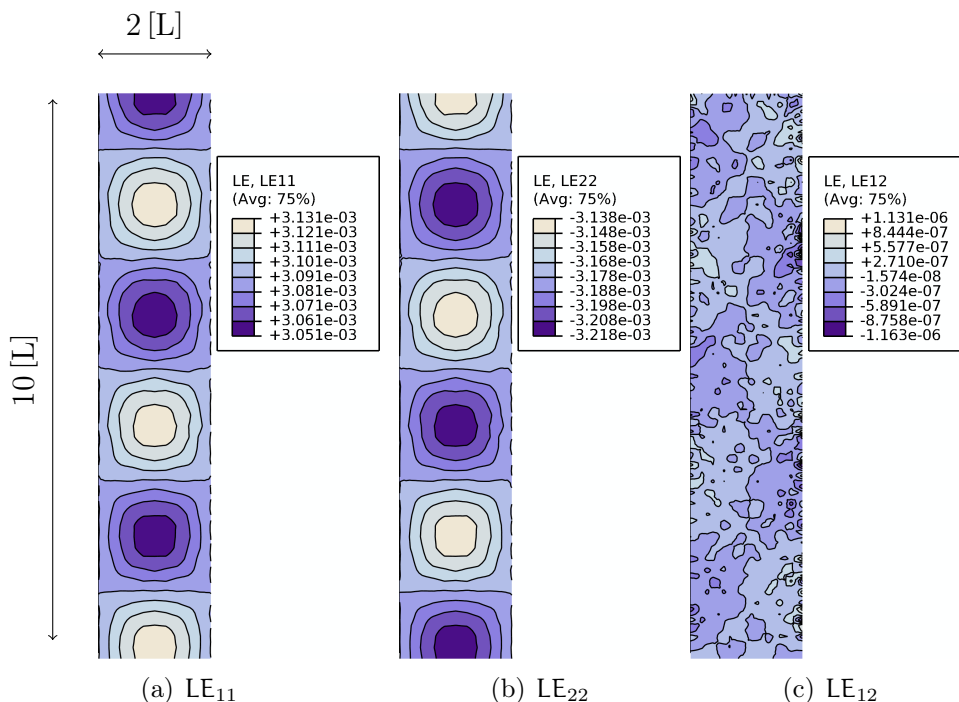
Figure 5.8: Logarithmic total strains, LE, as obtained from FEM-analysis for $2A_1 = 2\,[L]$ at the increment of first unloading in the matrix ($P = 311.5\,[F]$).

For completeness, the effect of the size of the initial imperfection on the buckling load is investigated as well. However, due to the stable postbuckling behaviour no significant effect is expected. As is evident from Fig. 5.9 the effect is indeed very small.

5.5 The periodic unit cell

In the previous sections several assumptions on the mean strain and the periodicity of the displacements at the boundary are made. These assumptions impose artificial constraints on the system, so the obtained results can not on their own be taken as representative of the unconstrained case. Providing a motivation for the assumption of displacement symmetry is the objective of the present section. For this purpose the UC is redefined to allow for greater generality.
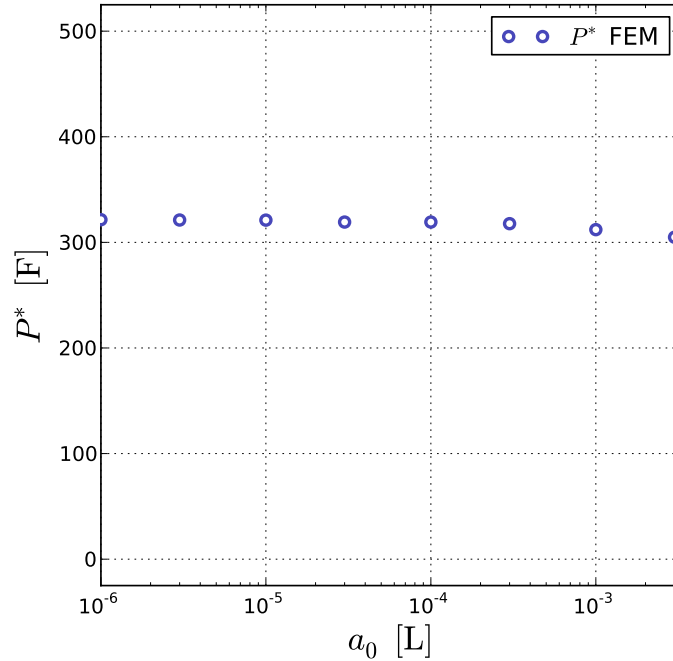
Figure 5.9: The buckling load as a function of the initial amplitude of the random imperfection $\mathfrak{a}_0$; An amplitude of 10^{-5} [L] was used in all simulations.

The UC used in section 5.3 required that there is exactly one half-period in the fluctuation of the displacements over the horizontal width of the unit cell so the fluctuating part of the deformation is symmetric with respect to the UC midplane. The question addressed here is if there is a different periodic solution that allows for periodic compatible tiling and if this results in a lower buckling load lower than (5.33).

For periodicity it is required that $\tilde{v}_1^\gamma(\underline{\mathbf{X}}) = \tilde{v}_1^\gamma(\underline{\mathbf{X}} + \underline{\mathbf{t}})$. The periodicity vector $\underline{\mathbf{r}}^B$ is related to the buckling wavelength and remains unchanged from (5.23_2). There is an ambiguity in the definition of $\underline{\mathbf{r}}^A$, however, as more than one half-period can occur in horizontal direction, and $\underline{\mathbf{r}}^A$ is more generally given by (5.35). The symmetric UC is recovered for $\mathfrak{m} = 1$ and $\mathfrak{n} = 0$.

$$\underline{\mathbf{r}}^A = \begin{bmatrix} 2A_1 \\ (2\mathfrak{n} + \mathfrak{m})A_2 \end{bmatrix} \quad \mathfrak{m} \in \mathbb{N}^+, \quad \mathfrak{n} \in \mathbb{N} \tag{5.35}$$

Figure 5.10 shows $\underline{\mathbf{r}}^A$ for a range of integers $\mathfrak{m}$ and $\mathfrak{n}$. UCs for $\mathfrak{m}$ from 1 to 4 are outlined by alternating hatching in 45° and 135°. In the figure the buckling wavelength is held constant to avoid clutter and the lamella spacing is adapted for different values of $\mathfrak{m}$. The actual situation is in reverse, however, with the lamella spacing fixed and the wavelength resulting from the UC definition. From this observation it is apparent that $\mathfrak{m} > 1$ enforces a shorter buckling length than the symmetric UC, and will result in a higher buckling load. The general periodic relation between lamella spacing and buckling length follows from
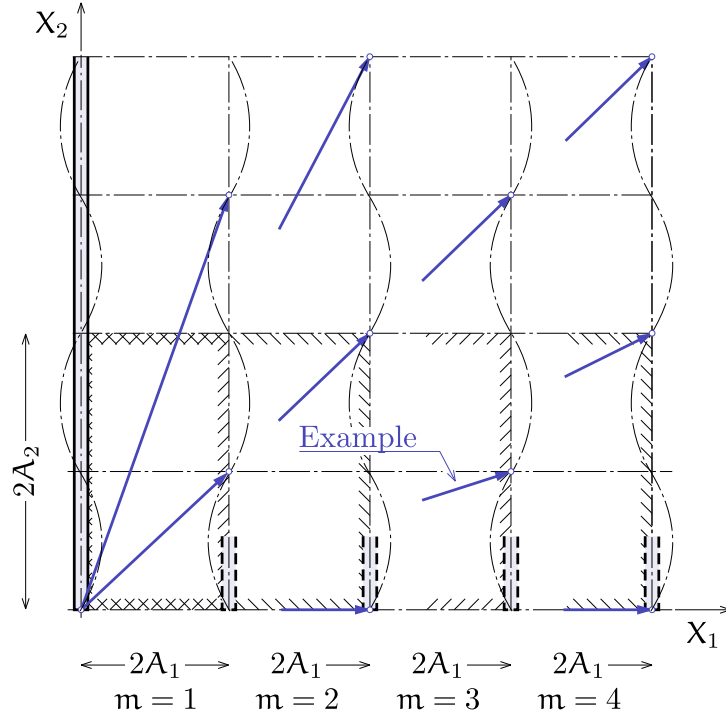
Figure 5.10: Possible periodic unit cell definitions and periodicity vectors $\underline{r}^A$ for various parameters m and n. N.b. the lamella spacing is always $2A_1$, regardless of m, even though, it is adjusted *in the figure* for each m to maintain a common scale in vertical direction. The actual situation is in reverse with A_2 adjusting to match $(2/m)A_1$.

comparing the velocity fluctuations in (5.22) to the fluctuations shifted by one period.

$$+\frac{1}{\dot{q}_1}\tilde{v}_1^\gamma(\underline{X}+\underline{r}^A) = \cos\left(\pi\frac{X_1+2A_1}{A_2}\right)\sin\left(\pi\frac{X_2+(2n+m)A_2}{A_2}\right)$$

$$= (-1)^m\left[\cos\left(\pi\frac{X_1}{A_2}\right)\cos\left(\pi\frac{2A_1}{A_2}\right) - \sin\left(\pi\frac{X_1}{A_2}\right)\sin\left(\pi\frac{2A_1}{A_2}\right)\right]\sin\left(\pi\frac{X_2}{A_2}\right) \quad (5.36_1)$$

$$-\frac{1}{\dot{q}_1}\tilde{v}_2^\gamma(\underline{X}+\underline{r}^A) = \sin\left(\pi\frac{X_1+2A_1}{A_2}\right)\cos\left(\pi\frac{X_2+(2n+m)A_2}{A_2}\right)$$

$$= (-1)^m\left[\sin\left(\pi\frac{X_1}{A_2}\right)\cos\left(\pi\frac{2A_1}{A_2}\right) + \cos\left(\pi\frac{X_1}{A_2}\right)\sin\left(\pi\frac{2A_1}{A_2}\right)\right]\cos\left(\pi\frac{X_2}{A_2}\right) \quad (5.36_2)$$

Equations (5.22) and (5.36) coincide when:

$$A_2 = \frac{2}{m}A_1 \tag{5.37}$$

Substituting into (5.33) confirms that $m = 1$ for the symmetric UC gives the lowest buckling load.

5.6 Periodic finite element model, phase angle

To obtain buckling load for different phase angles a FEM-model is used that allows for different values for φ in (5.38). For $\varphi = \pi/4$ the periodicity vector coincides with (5.23$_1$) and the model constitutes a symmetric UC.

$$\underline{r}^A = \begin{bmatrix} 2A_1 \\ 2A_1 \tan\varphi \end{bmatrix} \tag{5.38}$$

The boundary of the UC forms a rhomboidal quadrilateral like in Fig. 5.1(a). Nodal displacements on the boundary are constraint in the manner of (5.7$_2$) and the mean strain is controlled by the displacements of control nodes at $\underline{r}^A$ and $\underline{r}^B$ via (5.6). Figure
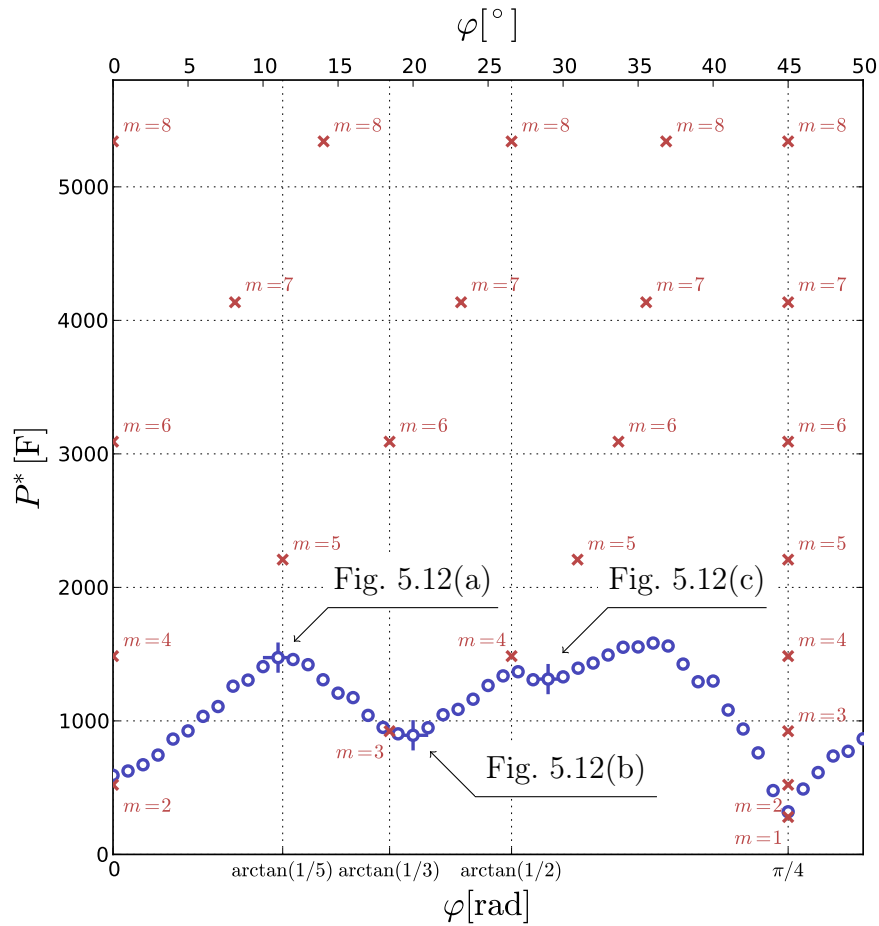

Figure 5.11: Buckling loads P^* as a function of the phase shift angle φ. The red cross markers are buckling loads calculated by (5.33) assuming a rectangular checkerboard-type deformation. The relation of wavelength to lamella spacing is given by (5.37), and values for m up to 8 are included in the figure. The blue circles represent FEM-analysis results.

5.11 shows buckling loads obtained analytically from (5.33) (red crosses) and buckling loads extracted from the FEM-model (blue circles) at different phase angles φ. The lamella spacing $2A_1$ is set to $2\,[\mathrm{L}]$ for all calculations. The phase angle in the FEM-model is controlled via $\underline{\mathbf{r}}^A$ in (5.38) and is evaluated at increments of $1°$. The FEM-model extends for more than $\underline{\mathbf{r}}^B$ in vertical direction, like the one used in section 5.4 so that the model size does not interfere to much with the buckling length. Superposed are the analytically calculated buckling loads with the buckling length given by (5.37). The analytical buckling load for a given integer $\mathfrak{m}$ applies to multiple angles φ, because $2\mathfrak{n}$ can be added arbitrarily, so more than one data point is present for $\mathfrak{m} > 1$. The phase angle in the analytical model is related to $\mathfrak{m}$ and $\mathfrak{n}$ via equation (5.6). For instance, the phase angle $\varphi = \arctan 1/3$ is obtained for $\mathfrak{m} = 3$ and $\mathfrak{n} = -1$. The corresponding periodicity vector is marked as 'Example' in Fig. 5.10.

$$\varphi = \arctan\left(\frac{(\mathfrak{m} + 2\mathfrak{n})A_2}{2A_1}\right) = \arctan\left(\frac{(\mathfrak{m} + 2\mathfrak{n})}{\mathfrak{m}}\right)$$

It is apparent from Figure 5.10 that the FEM-analysis results approach the analytical results for low values of $\mathfrak{m}$. A source of discrepancy is due to the circumstance that undeformed values for A_1 are used in (5.33) and prebuckling deformation is neglected. Also, the periodic BCs in (5.7_2) for the FEM-model can only be specified in terms of undeformed coordinates, rather than coordinates at the instance of buckling. Prebuckling shortening of the FEM-model will therefore cause the actual phase angle be less than the nominal value. Taking these limitations into account, it can be seen that the FEM-buckling loads attain local minima near data points for small values of $\mathfrak{m}$ at the angles $0, \arctan 1/5, \arctan 1/3$ and $\arctan 1/2$ radian, although the minima are visibly shifted to the right because of the effects mentioned. The absolute minimum is attained at $\pi/4$ for the symmetric UC.

In Fig. 5.12 the strain distribution at the increment of buckling is examined at the phase angles $11°$, $20°$ and $29°$, also marked in Fig. 5.11. The last two angles have a rather undisturbed, 'checkerboard'-style strain pattern for $\mathfrak{m} = 3$ and $\mathfrak{m} = 4$, respectively, as they are located near a local minimum of the buckling load. The angle $\varphi = 6°$, however, coincides with a local maximum and the strain pattern is distorted as a mode change from $\mathfrak{m} = 2$ to $\mathfrak{m} = 3$ is about to occur.

5.7 Array

All the models presented so far refer to a UC representation of the periodic medium and necessarily introduce kinematic constraints. As a safeguard against possible over-constraining by the UC-BCs it seems desirable to compare the UC-models against an unconstrained, enlarged model comprising an entire array of lamellae.

The array-model used for this purpose consists of a block containing ten lamellae, which are modelled by continuum elements rather than by the beam-elements used in the previous models. Like the models in sections 5.3 and 5.6 this model extends $40\,[\mathrm{L}]$
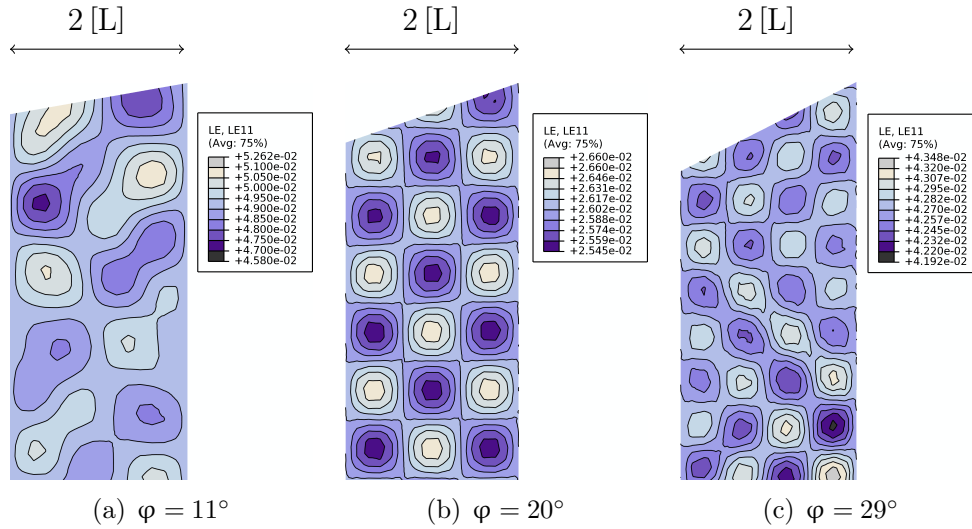
Figure 5.12: Matrix-LE$_{11}$ for selected phase-shift angles φ.

in vertical direction to limit interference with the buckling length. It is compressed in vertical direction by free horizontal sliding BCs at the top and the bottom. At the left and right boundary the zero traction conditions is imposed and the block can expand freely. Figure Fig. 5.13 displays the 11-components of the stress and strain fields in the matrix at the instant of buckling for a lamella spacing of $2A_1 = 2.0$ [L]. Lamella elements are hidden in the figure. The UC-BCs where developed for an infinite array and the free edge in the array-model poses a discrepancy, but the effect is relatively minor and the situation at the center of the array is close to the assumptions made for the UC-kinematics as can bee seen in Fig. 5.13(a). Also comparing the matrix strain in a slice of matrix between two lamellae in Fig. 5.13(b) to Fig. 5.8 shows a good match. The buckling load of 3681 [F] obtained for the array-model, however, exceeds the tenfold value of the prediction by (5.33) for the single slice 316.4 [F] . Repeating the simulation for a series of lamella spacings in the manner of Fig. 5.6 reveals that the analytical prediction, red cross-marker, corrected for prebuckling deformation, is met only for some lamella spacings. The software used did not report any negative eigenvalues for the system stiffness matrix preceding the numerical buckling load. Nevertheless, the enlarged array model seems to be more prone to numerical difficulties than the UC-models. For some other lamella spacings the FEM-model failed to converge at all, those data points are omitted in Fig. 5.14.

5.8 Periodic finite element model, post buckling

The symmetric UC definition with the periodicity vectors given by (5.23), put forward as an assumption in section 5.3 and subsequently verified, allows for very efficient numerical simulations. Since it has been found that the buckling wavelength is twice the lamella spacing, (5.25), the vertical oversize that allowed for free adjustment of the wavelength
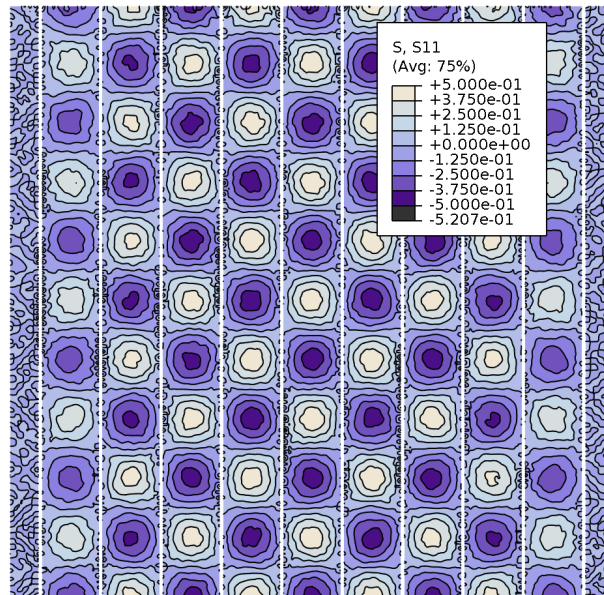
(a) True normal stress σ_{11}; The effect of the free boundary decays over roughly 3 lamellae
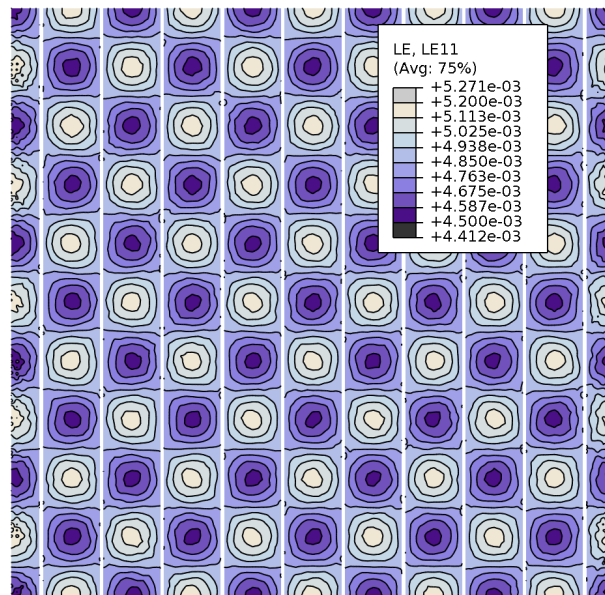
(b) Logarithmic normal strain in horizontal direction LE_{11}; only a fluctuation period occurs over the space between two lamellae

Figure 5.13: Strain and stress distribution of an extended model containing 10 lamellae and a total width of $20A_1 = 1.0 \times 20\,[\mathrm{L}]$. The total height is $40\,[\mathrm{L}]$. Only a small section of the height is shown. Both images show the model at the increment of buckling. The total load acting on the array is $3681\,[\mathrm{F}]$
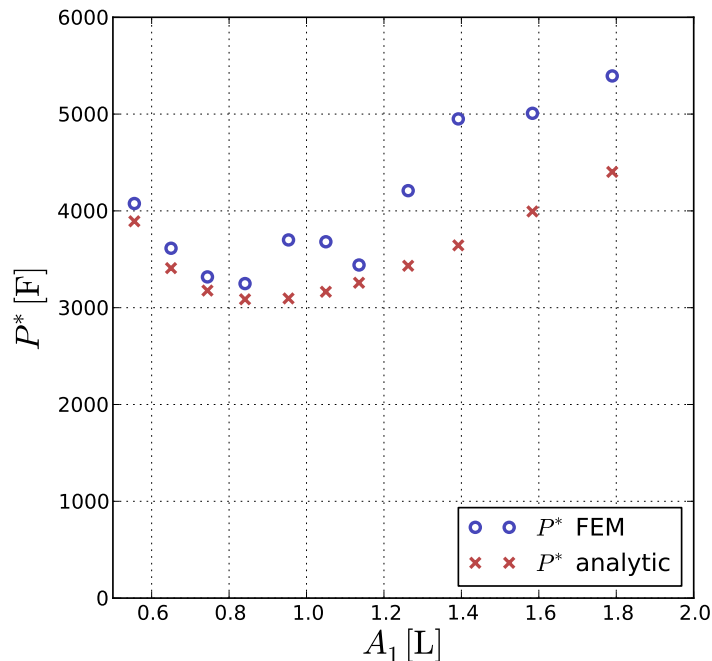
Figure 5.14: Comparison of the numerical buckling loads of the ten lamella array-model to the ten-fold of the analytic result from (5.33). For some lamella spacings the model failed to converge, those data points are omitted in the figure;

at the cost of inflating the model can be dropped. A minimum FEM-model comprising only one period in both directions is used here.

It has been shown for the incompatible model that the bifurcation load is not a limit load and the loading can be increased further in the postbuckling regime. This is the case even for ideal plasticity, cf. Fig. 4.4. This raises the question whether the same applies to the compatible model. This is investigated using the minimum FEM-model as described above.

Figure 5.15 displays the load carried per UC as a function of the UCs shortening for the lamella spacing $2A_1 = 2\,[\mathrm{L}]$. The buckling load, marked by the circle-marker, coincides with the buckling loads obtained for the other models so far. At the instant of buckling no significant discontinuity in stiffness is apparent, and the buckling load can be exceeded about four times without any noticeable softening. The limit load, indicated by the cross-marker, is reached in a rather abrupt manner at about five times the buckling load. Using the arc-length method the simulation could be extended slightly beyond the limit load before it fails to converge. It can be seen in the inset of the figure that the model is about to assume a 'snap-back'-type behaviour, with both the load and the shortening decreasing.

The strain-field at the limit load is shown in Fig. 5.16. The displacements are still quite moderate and they are displayed true-to-scale in the Figure. The unloaded area of the

matrix expands in the postbuckling regime and for some configurations the unloading can even cause reyielding under tension in the unloaded areas.

Figure 5.16 shows the limit load for different lamella spacings. For the range of values considered the limit load is typically three to four times the buckling load.
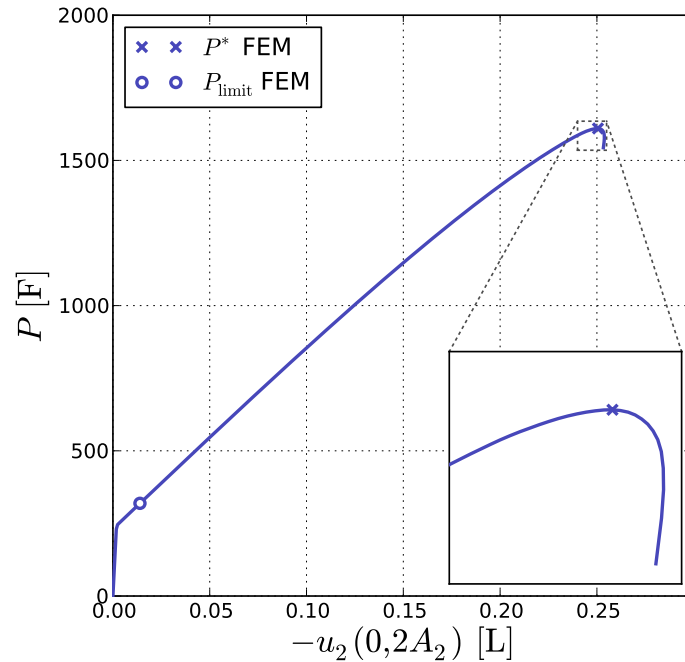

Figure 5.15: The load P carried by the UC as a function of the vertical displacement at $\underline{r}^B$ (shortening of the UC); The lamella spacing $2A_1$ is equal to 2 [L];

5.9 Conclusions

The case of ideal plasticity allowed for the derivation of an analytical prediction for the buckling load. It has been concluded from analytical arguments and observed in numerical simulations that the symmetric buckling mode corresponds to the lowest buckling load. The symmetric buckling mode was also assumed for the incompatible model in chapter 4. The qualitative behaviour with respect to bifurcation and stability can be reasonably expected to be similar, even though a detailed examination in the manner of section 4.4 is not possible for the compatible model. For the incompatible model the wavelength depends on the hardening behaviour of the matrix. For ideal plasticity it tends towards infinity. In the compatible model, however, the wavelength is tied to the lamella spacing and is finite even for the ideal plastic case. As expected, the buckling load is not the limit load, which is typically three to four times as large.

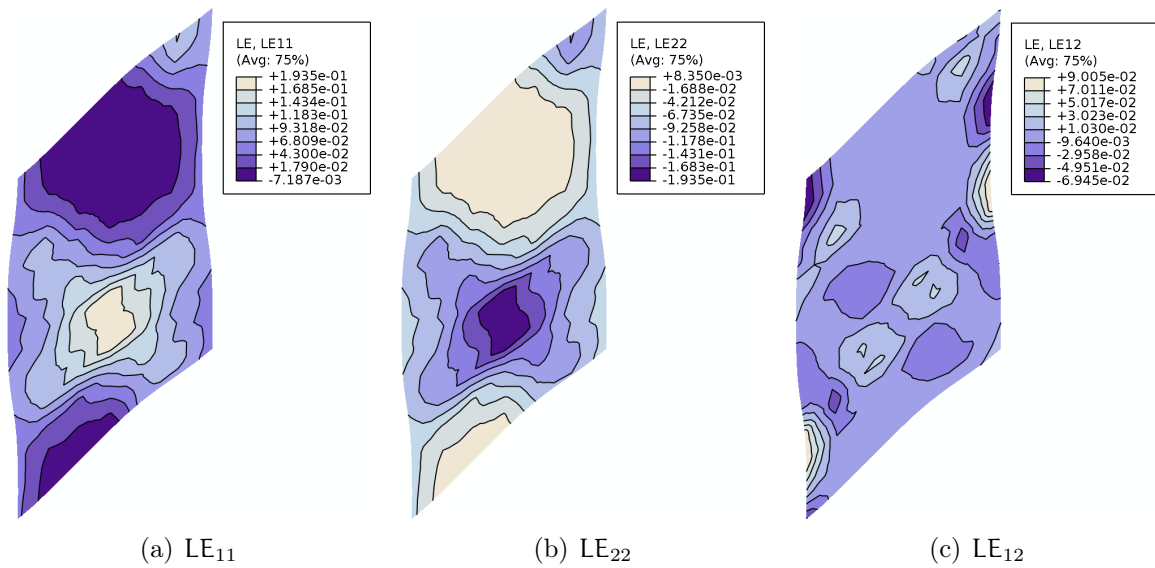(a) LE$_{11}$ (b) LE$_{22}$ (c) LE$_{12}$

Figure 5.16: Logarithmic strain, LE, at the limit load; The displacements in the plot are to scale;
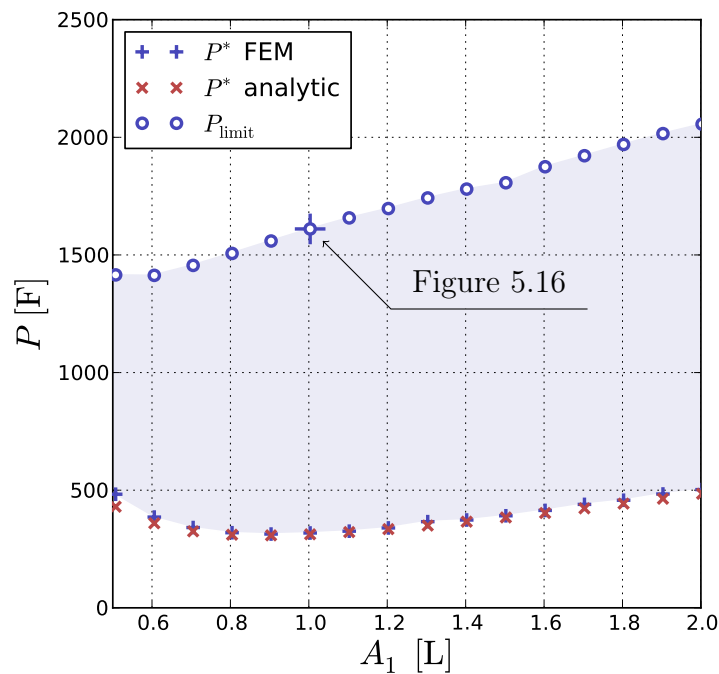

Figure 5.17: Buckling load and limit load in the postbuckling regime. In the shaded area the UC is buckled, but the loading can increase further

6 Matrix hardening

In the previous chapter it has been found that for the case of ideal plasticity the matrix does not provide any direct lateral support to the lamella as the middle term in (5.33) vanishes. The buckling mode was symmetrical, thus the deformation in neighbouring lamellae is coupled and they cannot deform independently, regardless of their distance.

In this chapter, however, it is shown that matrix hardening is linked to an exponential decay in the magnitude of stress and strain rates. For configurations with high tangent hardening modulus and/or large lamella spacings the fluctuations due to buckling of one lamella might fade out before reaching the other. In that case buckling of the lamella only affects the immediate surrounding matrix-areas and this scenario is dubbed buckling of noninteracting lamella. So within the range of increasing hardening modulus, the fully coupled buckling mode encountered in chapter 5, and the noninteracting limit case there exist a spectrum of varying degrees of mutual influence between the lamella. The intermediate situations are rather complex, but for situations that fall near the two limit cases certain approximations can be made. The buckling of lamellae embedded in a matrix with a relatively low hardening modulus is investigated in section 6.1, and in section 6.3 the non interacting limit case is examined.

6.1 Interacting lamellae

Before the governing equations for a hardening matrix are discussed in section 6.2, the strain field at the buckling load obtained from FEM-simulations of two different hardening parameters is presented as an introduction. The results where obtained from a model comprising an entire array of lamellae, like in section 5.7.

In Fig. 6.1(a) the strain field for a rather low tangent hardening modulus of $500\,[\mathrm{FL}^{-2}]$ is shown, and it can be seen to be very similar the pattern obtained for the ideal plastic case cf. Fig. 5.13(b). Only one fluctuation half-period occurs in horizontal direction and the lamellae are interacting in the same way as for the ideal plastic case. For Fig. 6.1(b) the tangent modulus has been increased threefold, and a completely new strain pattern emerges. Instead of only one there are three half-periods and a noticeable decreased amplitude in the middle between the two lamellae. Even so, the fluctuations do not completely decay and the lamellae can still be considered interacting, but this reveals the trend that for increased hardening and increased spacing a limit case ensues that allows to treat the lamellae isolated from each other.

An analytical description of a general interacting situation in the manner of Fig. 6.1(b) seems to be a daunting task as even the noninteracting limit case is quite complicated as is

shown in section 6.3. In principle the same methods as used in section 6.3 could be applied, but no such attempt is made here. On the other hand a simple estimate for situations with a very low tangent hardening modulus as depicted in Fig. 6.1(a) can be obtained by assuming that the velocity field (5.22), solving the governing equations for the ideal plastic case, is maintained as an approximation. Although (5.22) strictly applies only when the hardening parameter θ is set to zero, cf. (5.20), it still has been retained in the subsequent derivation of the buckling load (5.33). This conveniently allows (5.33) to be reused as an estimate for the slightly hardening case considered here. A plot comparing the estimate to FEM-results is depicted in Fig. 6.2. The figure reveals a rather high sensitivity of the buckling load to even moderate hardening, and the estimate provided by (5.33) is somewhat accurate for very small hardening moduli. The assumption that the velocity field is given by (5.22) obviously does not hold for hardening moduli of $1500\,[\mathrm{FL}^{-2}]$ as can be seen from Fig. 6.1(b) as the strain distribution is very different.

(a) $\mathsf{E}_t = 500\,[\mathrm{FL}^{-2}]$ (b) $\mathsf{E}_t = 1500\,[\mathrm{FL}^{-2}]$
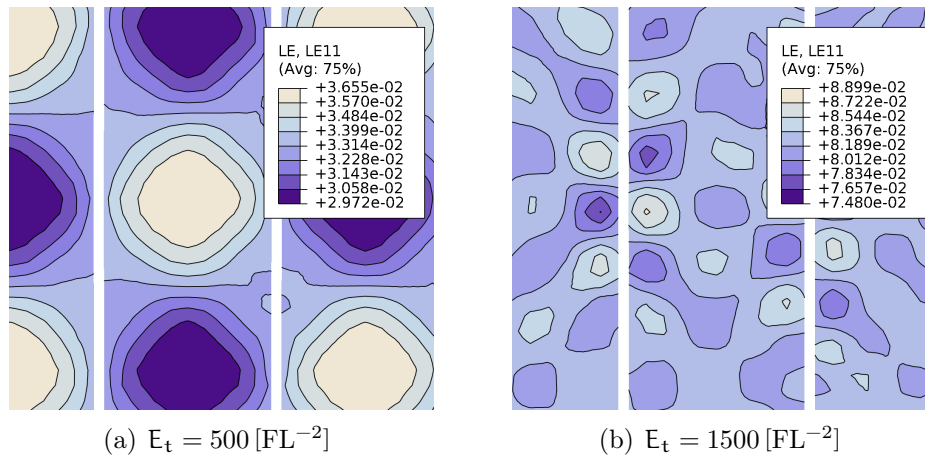
Figure 6.1: Strain distribution in the postbuckling regime, Lamella not shown; Fig. 6.1(a) maintains a strong similarity to the ideal plastic case, i.e. a similar strain distribution to Fig. 5.13(b). In Fig. 6.1(b) the strain pattern is completely different and the amplitude varies in horizontal and somewhat less in vertical direction.

6.2 Governing equations in terms of a stress function

In section 5.2 the governing equations were formulated in displacements resulting in a system of two second order PDEs. Simplification for ideal plasticity allowed a possible solution to be found by an educated guess (ansatz). However, the problem can also be formulated in terms of a stress function, denoted as A in the following. The in-plane
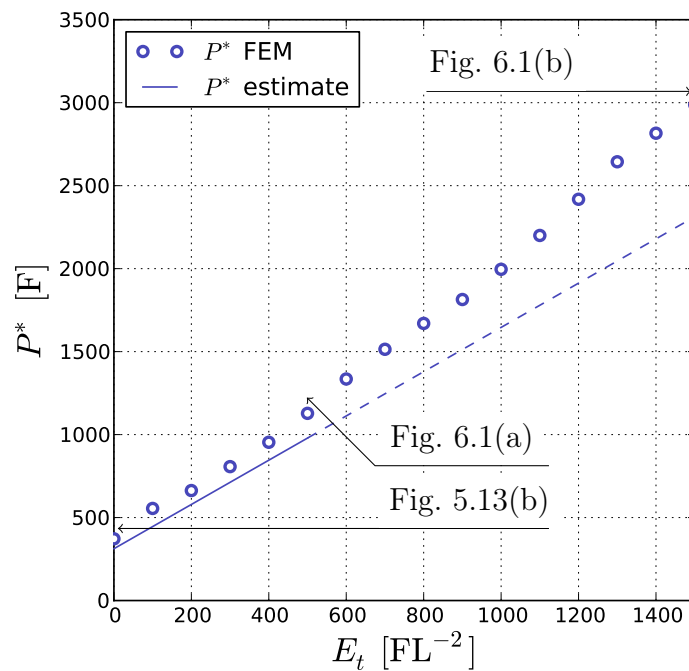
Figure 6.2: Comparison of FEM-analysis buckling loads to estimates obtained from (5.33); The lamella spacing $2A_1 = 2.0\,[\mathrm{L}]$ the other parameters are given in Table 4.1; The unconstrained multiple lamella model from section 5.7 is used with 10 lamellae, and FEM-analysis buckling loads are per slice. Equation 5.33 was derived for ideal plasticity, but can also give a rough estimate for the slightly hardening case. At about $E_t = 1000\,[\mathrm{FL}^{-2}]$ however the velocity field deviates substantially from (5.22), and the number of half-periods per unit cell in horizontal direction, m, increases from 1 to 3

stress-rates are derived from the stress function in a manner that ensures equilibrium:

$$
\left.\begin{aligned}
\dot{\sigma}_{11}^{\gamma} &= +A_{,22} \\
\dot{\sigma}_{12}^{\gamma} &= -A_{,12} \\
\dot{\sigma}_{22}^{\gamma} &= +A_{,11}
\end{aligned}\right\}
\Rightarrow \operatorname{div}(\dot{\underline{\sigma}}^{\gamma}) =
\begin{bmatrix}
+A_{,221} - A_{,122} \\
+A_{,112} - A_{,121} \\
\dot{\sigma}_{33,3}^{\gamma}
\end{bmatrix}
= \underline{0}
\tag{6.1}
$$

The superscript γ will be dropped for the remainder of the section. The elastic response in the matrix is taken into account by substituting the stress function into the Prandtl-Reuss equations for plane strain (2.6). It is more convenient here to replace the Lamé-parameters by the Young's modulus and the Poisson-ratio. The out-of-plane component d_{33}^{p} of the plastic strain rate could be expressed by the in-plane components since the trace of $\underline{d}^{p}$ is zero. It is retained, however, and the same assumption with regard to the out-of-plane strain rate as in section 2.4 is made further down when the equations are specialized for the problem at hand.

$$
d_{11} = \frac{1}{E}\left[+(1+\nu)A_{,22} - \nu\left(A_{,11} + A_{,22} + \dot{\sigma}_{33}\right)\right] + d_{11}^{p}
\tag{6.2$_1$}
$$

$$
d_{12} = \frac{1}{E}\left[-(1+\nu)A_{,12} \qquad\qquad\right] + d_{12}^{p}
\tag{6.2$_2$}
$$

$$
d_{22} = \frac{1}{E}\left[+(1+\nu)A_{,11} - \nu\left(A_{,11} + A_{,22} + \dot{\sigma}_{33}\right)\right] + d_{22}^{p}
\tag{6.2$_3$}
$$

$$
0 = \frac{1}{E}\left[+(1+\nu)\dot{\sigma}_{33} - \nu\left(A_{,11} + A_{,22} + \dot{\sigma}_{33}\right)\right] + d_{33}^{p}
\tag{6.2$_4$}
$$

The last equation can be used to eliminate the out-of-plane stress-rate.

$$
d_{11} = \frac{1+\nu}{E}\left[+A_{,22} - \nu\left(A_{,11} + A_{,22}\right)\right] + d_{11}^{p} + \nu d_{33}^{p}
\tag{6.3$_1$}
$$

$$
d_{12} = \frac{1+\nu}{E}\left[-A_{,12} \qquad\qquad\right] + d_{12}^{p}
\tag{6.3$_2$}
$$

$$
d_{22} = \frac{1+\nu}{E}\left[+A_{,11} - \nu\left(A_{,11} + A_{,22}\right)\right] + d_{22}^{p} + \nu d_{33}^{p}
\tag{6.3$_3$}
$$

In chapter 5 the governing equation was formulated directly in velocities, and compatibility is automatically ensured. Here, however, the governing equation is formulated in terms of the stress function, and the requirement of compatibility provides an additional equation.

$$
2d_{12,12} - d_{11,22} - d_{22,11} = 0
\tag{6.4}
$$

The stress-strain relation (6.3) and compatibility condition (6.4) result in the PDE (6.5) that relates the stress function and the plastic strain rates for the plane strain case, cf. [Srinivasa and Srinivasan, 2009, Mendelson, 1968]. The symbol $\mathbf{\Delta}$ stands for the Laplace-operator. Because the plastic strain rates depend on the stress function via the stress rates it is an implicit relation. The equation describes a general plane strain

situation and is not limited to the problems under investigation in this work.

$$2\mathsf{d}^\mathrm{p}_{12,12} - \mathsf{d}^\mathrm{p}_{11,22} - \mathsf{d}^\mathrm{p}_{22,11} + \nu\boldsymbol{\Delta}\mathsf{d}^\mathrm{p}_{33} = \frac{(1-\nu^2)}{\mathsf{E}}\boldsymbol{\Delta}\boldsymbol{\Delta}A \tag{6.5}$$

6.3 Non-interacting lamellae

In order to point out, at least in principle, the mechanisms behind buckling of elastic lamellae embedded in a hardening plastic matrix the governing equations (6.5) are specialized using the assumptions introduced in section 2.4 and already used in section 5.2. Together with the additional assumption that the strain rate is dominated by plastic strain this allows the derivation of a rather crude estimate of the buckling load.
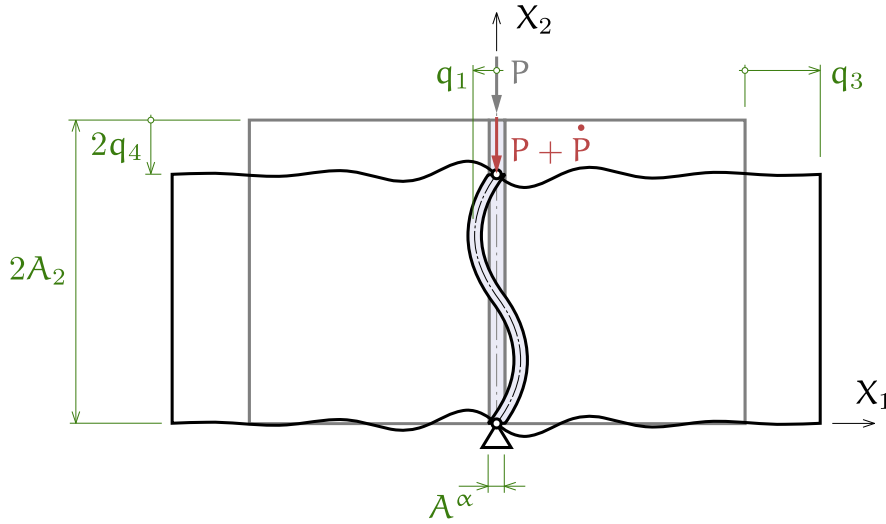

Figure 6.3: Generalized coordinates of the slice model

The problem is analyzed by considering a vertically repeating slice with a height of one buckling wavelength, $2\mathsf{A}_2$. The lamella lies at the center of the slice, and the horizontal extension on both sides is supposed to be wide enough so that any fluctuations resulting from lamella buckling have decayed at the boundary. Then the left and right boundary remain vertical and multiple slices can be arranged side by side. The complete decay of fluctuations means that, contrary to all other cases considered so far, buckling of one lamella does not have any effect on its neighbours, and each slice can be considered individually. Hence, the attribute 'non-interacting' is assigned to this situation.

The lamella velocity and the mean part of the matrix velocity field remain unchanged from chapter 5 and are not repeated here to avoid redundancy. Moreover, the GCs $\dot{\mathsf{q}}_3$ and $\dot{\mathsf{q}}_4$ contribute only to the mean stress/strain rates and have no effect on the buckling load which can be inferred from the circumstance that the element K_{11} in (5.32) is uncoupled from the rest of the stiffness matrix, i.e. the internal force rate $(\mathsf{Q})^{\bullet}_1$ does depend on $\dot{\mathsf{q}}_1$ only because $\mathsf{K}_{12} = \mathsf{K}_{13} = 0$. The stiffness matrix becomes singular for the first time

when element K_{11} vanishes. The GC-rate $\dot{\mathsf{q}}_1$, on the other hand, is associated only with fluctuations and does not contribute to the mean stress rates. Because $(\mathsf{Q})_1^{\bullet}$ is given as the partial derivative of the rate potential of the internal forces with respect to $\dot{\mathsf{q}}_1$ the mean part of the rate potential can be dropped and does not affect the buckling load. Consequently it suffices to deal with the fluctuating fields, and the buckling load can be derived from the condition $\mathsf{K}_{11} = 0$.

$$\mathcal{U}(\dot{\mathsf{q}}_1, \dot{\mathsf{q}}_3, \dot{\mathsf{q}}_4) = \tilde{\mathcal{U}}(\dot{\mathsf{q}}_1) + \bar{\mathcal{U}}(\dot{\mathsf{q}}_3, \dot{\mathsf{q}}_4) \tag{6.6}$$

$$\dot{\mathsf{Q}}_1(\dot{\mathsf{q}}_1) = \frac{\partial}{\partial \dot{\mathsf{q}}_1} \int_V \mathcal{U}(\dot{\mathsf{q}}_1, \dot{\mathsf{q}}_3, \dot{\mathsf{q}}_4) \, \mathrm{d}V = \frac{\partial}{\partial \dot{\mathsf{q}}_1} \int_V \tilde{\mathcal{U}}(\dot{\mathsf{q}}_1) \, \mathrm{d}V \tag{6.7}$$

$$\mathsf{K}_{11} = \frac{\partial \dot{\mathsf{Q}}_1(\dot{\mathsf{q}}_1)}{\partial \dot{\mathsf{q}}_1} \tag{6.8}$$

The investigations in section 4.4 have shown that the geometric stiffness of the matrix has little effect on the buckling load, and only the geometric stiffness of the lamella is essential. It, therefore, seems appropriate to neglect the effect of initial stresses due to the pre-loading in the matrix rate potential, and the material time derivative rather than the objective rate is used in the rate potential as a simplification.

$$\tilde{\mathcal{U}}^{\gamma} \doteq \frac{1}{2} \dot{\tilde{\sigma}} : \tilde{\underline{d}} \tag{6.9}$$

The mean stress rates are uniform everywhere so the fluctuations need to be in balance among themselves. Thus the stress function is introduced in terms of the fluctuating stress rates only:

$$\left. \begin{array}{l} \dot{\tilde{\sigma}}_{11}^{\gamma} = +A_{,22} \\ \dot{\tilde{\sigma}}_{12}^{\gamma} = -A_{,12} \\ \dot{\tilde{\sigma}}_{22}^{\gamma} = +A_{,11} \end{array} \right\} \Rightarrow \mathrm{div}(\dot{\tilde{\underline{\sigma}}}^{\gamma}) = \left[\begin{array}{c} +A_{,221} - A_{,122} \\ +A_{,112} - A_{,121} \\ \dot{\tilde{\sigma}}_{33,3}^{\gamma} \end{array} \right] = \underline{0} \tag{6.10}$$

In order to make (6.5) explicit in A, the plastic strain rates are to be expressed in terms of the stress function. For this purpose the relations between plastic and total strain rates, specific for the preloaded, but unbuckled state, are used. These relations were derived in section 2.4 and were used in section 5.2. Applying the procedure to separate mean and fluctuating contributions stated in (5.2) to (2.33) yields:

$$\tilde{\mathsf{d}}_{11}^{\mathrm{p}} = -\tilde{\mathsf{d}}_{22}^{\mathrm{p}} = \frac{E(\tilde{\mathsf{d}}_{11} - \tilde{\mathsf{d}}_{22})}{2E + 2\theta(1 + \nu)} \tag{6.11_1}$$

$$\tilde{\mathsf{d}}_{12}^{\mathrm{p}} = 0 \tag{6.11_2}$$

$$\tilde{\mathsf{d}}_{33}^{\mathrm{p}} = 0 \tag{6.11_3}$$

Applying the separation procedure again to (6.3) gives $\tilde{d}_{11}$ and $\tilde{d}_{22}$ which can be substituted into (6.11_1) to obtain an expression for $\tilde{d}_{11}^p$:

$$\tilde{d}_{11} - \tilde{d}_{22} = \frac{1 + \nu}{E}\left[A_{,22} - A_{,11}\right] + 2\tilde{d}_{11}^p$$

$$\tilde{d}_{11}^p = \frac{A_{,22} - A_{,11}}{2\theta} = -\tilde{d}_{22}^p \tag{6.12}$$

With the plastic strain rates d_{12}^p and d_{33}^p equal to zero and d_{11}^p and d_{22}^p given explicitly in terms of the stress function the governing equation can be specialized for the case at hand. For this purpose it is pertinent to introduce the dimensionless ratio H as an abbreviation:

$$H := \frac{E}{2\theta(1 - \nu^2)} \tag{6.13}$$

Substituting (6.11_2), (6.11_3) and (6.12) into (6.5) and making use of (6.13) yields a linear homogeneous fourth order PDE in $A(X_1, X_2)$:

$$(1 + H)A_{,1111} + 2(1 - H)A_{,1122} + (1 + H)A_{,2222} = 0 \tag{6.14}$$

At this point it is helpful to take a look at a stress distribution obtained from a FEM-simulation, as it provides a clue for a possible solution to (6.14). The contour plot of σ_{11} depicted in Fig. 6.4 was obtained from a model of a single lamella embedded in a matrix patch extending for 5 [LU] on both sides of the lamella horizontally and 20 [LU] vertically. The lamella is situated at the center and is not shown in the plot. The amplitude of the fluctuations decreases with horizontal distance from the lamella and has almost completely decayed at the left and right border, respectively, where a zero traction BC is imposed. Some parts of the model are not shown in the figure. In vertical direction there is also a certain variation in the amplitude. If this vertical amplitude variation is disregarded for the moment the stress field can be interpreted as a variant of the 'checkerboard' pattern that emerged in the ideal plastic case. Unlike before, however, the patterns evolution in horizontal direction seems to resemble a damped oscillation here rather than an undamped one. This observation motivates a separation of variables approach to (6.14) as stated in (6.15)

$$A(X_1, X_2) = B(X_1)\sin(\frac{\pi X_2}{A_2}) \tag{6.15}$$

With regard to the uneven amplitude in vertical direction it is not apparent whether this constitutes an artifact of the numerical simulations or not. It could, for instance, be a result of the finite model height. On the other hand it is present even for rather large FEM-models. Regardless, the separation approach with the term $\sin(\pi X_2/A_2)$ representing the dependence of the stress function on the vertical position is pursued here.

The separation results in a linear homogeneous fourth order ordinary differential equation (ODE) for $B(X_1)$. It can be solved in the usual manner by taking B as a linear

Figure 6.4: $E_t = 1000\,[FL^{-2}]$, $\sigma^\alpha = (\sigma^\alpha)^* = 17300\,FL^{-2}$
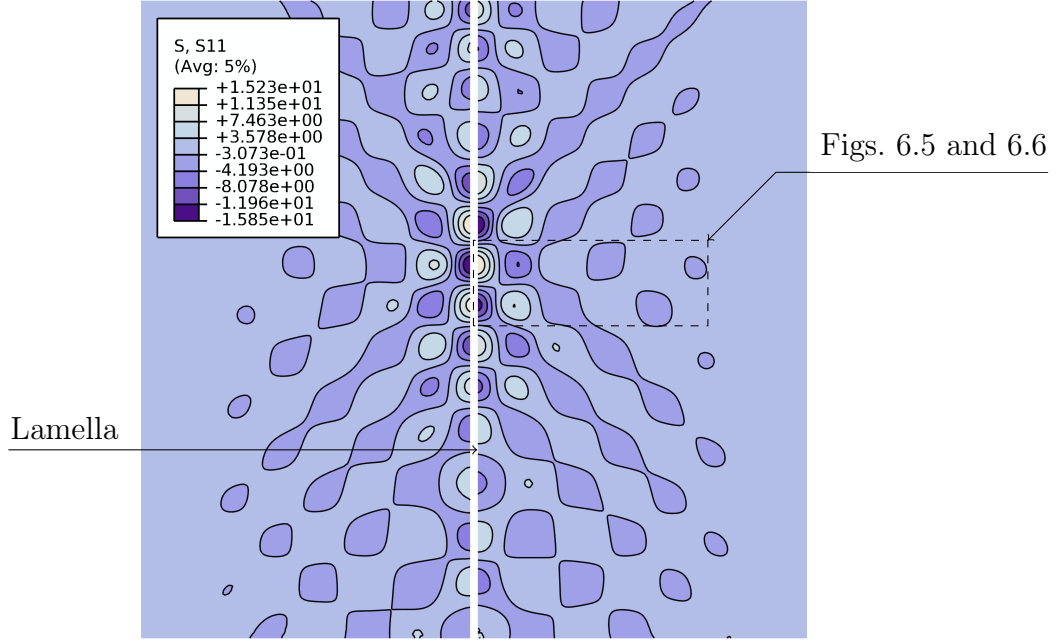
combination of exponential functions.

$$\left[(1+H)\frac{d^4B}{dX_1^4} + 2(1-H)\frac{d^2B}{dX_1^2}\left(-\frac{\pi^2}{A_2^2}\right) + (1+H)B(X_1)\left(+\frac{\pi^4}{A_2^4}\right)\right] = 0 \tag{6.16}$$

$$\left[(1+H)r^4 + 2(1-H)r^2\left(-\frac{\pi^2}{A_2^2}\right) + (1+H)\left(+\frac{\pi^4}{A_2^4}\right)\right] = 0 \tag{6.17}$$

Equation (6.17) has two pairs of respectively conjugate complex numbers:

$$r_1 = \frac{(+1 - i\sqrt{H})}{\sqrt{H+1}}\frac{\pi}{A_2} \qquad\qquad \bar{r}_1 = \frac{(+1 + i\sqrt{H})}{\sqrt{H+1}}\frac{\pi}{A_2}$$

$$r_2 = \frac{(-1 - i\sqrt{H})}{\sqrt{H+1}}\frac{\pi}{A_2} \qquad\qquad \bar{r}_2 = \frac{(-1 + i\sqrt{H})}{\sqrt{H+1}}\frac{\pi}{A_2} \tag{6.18}$$

Observing Euler's identity, the four roots can be combined to a solution to the ODE (6.16) with the real coefficients G_1 to G_4.

$$B(X_1) = e^{+\frac{1}{\sqrt{H+1}}\frac{\pi X_1}{A_2}}\left(G_1 \sin\left(\sqrt{\frac{H}{1+H}}\frac{\pi X_1}{A_2}\right) + G_3 \cos\left(\sqrt{\frac{H}{1+H}}\frac{\pi X_1}{A_2}\right)\right)$$

$$+ e^{-\frac{1}{\sqrt{H+1}}\frac{\pi X_1}{A_2}}\left(G_4 \sin\left(\sqrt{\frac{H}{1+H}}\frac{\pi X_1}{A_2}\right) + G_2 \cos\left(\sqrt{\frac{H}{1+H}}\frac{\pi X_1}{A_2}\right)\right) \tag{6.19}$$

From here on only the half-plane $X_1 > 0$ is considered, so that the first term in (6.19) is exponentially increasing. Because only the non interacting case is considered here, the increasing term can be dropped. Another simplification could be introduced here:

The ratio H, as defined by (6.13), is typically large compared to one even for moderate hardening. For instance taking $E_t = 5000\,[FL^{-2}]$, $E = 200 \times 10^3\,[FL^{-2}]$ and $\nu = 0.3$ the ratio H is approximately 32 and $\sqrt{H+1}$ could be replaced by $\sqrt{H}$ without incurring a significant error.

$$A(X_1, X_2) = e^{-\frac{\pi X_1}{\sqrt{1+H}\,A_2}} \sin\left(\tfrac{\pi X_2}{A_2}\right) \left(G_4 \sin\left(\sqrt{\tfrac{H}{1+H}}\,\tfrac{\pi X_1}{A_2}\right) + G_2 \cos\left(\sqrt{\tfrac{H}{1+H}}\,\tfrac{\pi X_1}{A_2}\right)\right)$$
$$(6.20)$$

The two remaining constants are determined from BCs at $X_1 = 0$. The condition that the fluctuations must fade out on the right boundary, which is idealized to be infinitely remote, has already been used to eliminate the constants G_1 and G_3. It can be seen from Fig. 6.4 that the fluctuations decay rather rapidly if the tangent hardening modulus is not too low. On the left boundary, $X_1 = 0$, the velocity fluctuations of matrix and lamella must match. Like in the previous chapters the coupling between lamella and matrix is thought to occur at the lamella centerline and its velocity is:

$$\underset{\sim}{v}^\alpha = \left[\begin{array}{c} \dot{q}_1 \sin\left(\tfrac{\pi X_2}{A_2}\right) \\ 0 \end{array} \right]$$

The matrix velocity field has to be integrated from the rate of deformation tensor which in turn could be determined from (6.3). This results in rather involved expressions, however, so a different approach is followed here. The expression for the plastic strain rates given by (6.12) is much simpler, and the total strain rates are dominated by their plastic part for a wide range of tangent hardening moduli, cf. Fig. 6.6. Therefore, the simplification that the total strain rates $\underset{\sim}{d}$ are approximately the same as the plastic strain rates $\underset{\sim}{d}^p$ seems reasonable. Evaluating (6.12) for A given by (6.20) yields:

$$\tilde{d}_{11}^p = -\tilde{d}_{22}^p = -\frac{\pi^2 e^{-\frac{\pi X_1}{\sqrt{H+1}\,A_2}} \sin\left(\tfrac{\pi X_2}{A_2}\right)}{(H+1)A_2^2 \theta} \left(\left(\sqrt{H}\,G_2 + G_4\right)\sin\left(\sqrt{\tfrac{H}{H+1}}\,\tfrac{\pi X_1}{A_2}\right) + \right.$$
$$\left. \left(G_2 - \sqrt{H}\,G_4\right)\cos\left(\sqrt{\tfrac{H}{H+1}}\,\tfrac{\pi X_1}{A_2}\right)\right) \quad (6.21)$$

The matrix fluctuating velocity field is thus approximated by (6.22_1) and (6.22_2):

$$\tilde{v}_1 \doteq \int \tilde{d}_{11}^p \, dX_1$$
$$= \frac{\pi e^{-\frac{\pi X_1}{A_2\sqrt{H+1}}} \sin\left(\tfrac{\pi X_2}{A_2}\right)}{\sqrt{H+1}\,A_2\theta} \left(G_4 \sin\left(\sqrt{\tfrac{H}{H+1}}\,\tfrac{\pi X_1}{A_2}\right) + G_2 \cos\left(\sqrt{\tfrac{H}{H+1}}\,\tfrac{\pi X_1}{A_2}\right)\right) \qquad (6.22_1)$$

$$\tilde{v}_2 \doteq \int \tilde{d}_{22}^p \, dX_2$$

$$= \frac{\pi e^{-\frac{\pi X_1}{A_2\sqrt{H+1}}} \cos\left(\frac{\pi X_2}{A_2}\right)}{(H+1)A_2\theta} \left(\left(\sqrt{H}G_2 + G_4\right) \sin\left(\sqrt{\frac{H}{H+1}}\frac{\pi X_1}{A_2}\right) + \right.$$
$$\left. \left(G_2 - \sqrt{H}G_4\right) \cos\left(\sqrt{\frac{H}{H+1}}\frac{\pi X_1}{A_2}\right)\right) \quad (6.22_2)$$

Because $\tilde{v}_2$ depends on X_2 via $\cos(\pi X_2/A_2)$ only, compatible tiling at the top and bottom of the slice is ensured. The equations obtained from setting $\tilde{\underline{v}}^\alpha(X_2) = \tilde{\underline{v}}^\gamma(0, X_2)$ yield the two remaining constants:

$$G_2 = \frac{\sqrt{H+1}\,\theta A_2}{\pi}\dot{q}_1 \quad (6.23_1)$$

$$G_4 = \frac{\sqrt{H+1}\,\theta A_2}{\pi\sqrt{H}}\dot{q}_1 \quad (6.23_2)$$

The plastic part of the strain rate is given by:

$$\tilde{d}_{11}^p = -\dot{q}_1\sqrt{\frac{H+1}{H}}\frac{\pi}{A_2}e^{-\frac{1}{\sqrt{H+1}}\frac{\pi X_1}{A_2}}\sin\left(\frac{\pi X_2}{A_2}\right)\sin\left(\sqrt{\frac{H}{H+1}}\frac{\pi X_1}{A_2}\right) \quad (6.24_1)$$

$$\tilde{d}_{22}^p = -\tilde{d}_{11}^p \quad (6.24_2)$$

$$\tilde{d}_{12}^p = 0 \quad (6.24_3)$$

The normal stress rates are:

$$\dot{\tilde{\sigma}}_{11} = -\dot{q}_1\sqrt{\frac{H+1}{H}}\frac{\pi\theta}{A_2}e^{-\frac{1}{\sqrt{H+1}}\frac{\pi X_1}{A_2}}\sin\left(\frac{\pi X_2}{A_2}\right)\left(+\sqrt{H}\cos\left(\sqrt{\frac{H}{H+1}}\frac{\pi X_1}{A_2}\right) \right.$$
$$\left. + \sin\left(\sqrt{\frac{H}{H+1}}\frac{\pi X_1}{A_2}\right)\right) \quad (6.25)$$

$$\dot{\tilde{\sigma}}_{22} = +\dot{q}_1\sqrt{\frac{H+1}{H}}\frac{\pi\theta}{A_2}e^{-\frac{1}{\sqrt{H+1}}\frac{\pi X_1}{A_2}}\sin\left(\frac{\pi X_2}{A_2}\right)\left(-\sqrt{H}\cos\left(\sqrt{\frac{H}{H+1}}\frac{\pi X_1}{A_2}\right) \right.$$
$$\left. + \sin\left(\sqrt{\frac{H}{H+1}}\frac{\pi X_1}{A_2}\right)\right) \quad (6.26)$$

For the purposes of calculating the rate potential of the fluctuations the slice is considered to extend indefinitely in horizontal direction from both sides of the lamella. However, because of the exponential decay the integral remains finite. The negative half-plane is taken into account by multiplying the expression with a factor of 2. For the reasons mentioned above, the internal force rate $(Q_1^\gamma)^\bullet$ does not depend on mean quantities and

can be calculated from the fluctuating quantities alone:

$$\dot{Q}_1^{\gamma} = 2\frac{\partial}{\partial \dot{q}_1}\int_0^{2A_2}\int_0^{\infty}\frac{1}{2}\dot{\tilde{\sigma}} : \tilde{\dot{d}}\, dX_1 dX_2 = \pi\sqrt{H+1}\,\theta\dot{q}_1 = \frac{\pi}{\sqrt{2\theta}}\sqrt{\frac{E+2\theta(1-\nu^2)}{(1-\nu^2)}}\,\dot{q}_1$$

(6.27)

The internal force rate of the lamella can be taken as the result from (3.57_1) multiplied by two with A_2, A^{α} and E^{α} replacing L, H and E_t respectively.

$$\dot{Q}_1^{\alpha} = \frac{\pi^2 A^{\alpha}(\pi^2(A^{\alpha})^2 E^{\alpha} + 12\sigma^{\alpha}A_2^2)}{12A_2^3}\dot{q}_1$$

(6.28)

The critical lamella stress $(\sigma^{\alpha})^*$ that will lead to buckling can be obtained from setting the matrix element K_{11} to zero:

$$K_{11} = \frac{\partial(\dot{Q}_1^{\alpha} + \dot{Q}_1^{\gamma})}{\partial \dot{q}_1} = \pi\sqrt{H+1}\,\theta + \frac{\pi^2 A^{\alpha}(\pi^2(A^{\alpha})^2 E^{\alpha} + 12\sigma^{\alpha}A_2^2)}{6A_2^3}$$

(6.29)

$$(\sigma^{\alpha})^* = -\frac{\pi^3(A^{\alpha})^3 E^{\alpha} + 12\sqrt{H+1}\,\theta A_2^3}{12\pi A^{\alpha}A_2^2}$$

(6.30)

The limit case for a vanishing hardening parameter θ in (6.30) is the Euler buckling load of the lamella alone. The wavelength is obtained from minimizing the critical lamella stress with respect to A_2 and the only real-valued solution is:

$$A_2 = \pi A^{\alpha}\left(\frac{E^{\alpha}}{6\sqrt{H+1}\,\theta}\right)^{\frac{1}{3}}$$

(6.31)

Combining (6.30) and (6.31) yields an expression for the buckling lamella stress with the wavelength eliminated. The lamella width drops from the expression as well:

$$(\sigma^{\alpha})^* = -\frac{1}{2}\left(\frac{9}{2}(1+H)E^{\alpha}\theta^2\right)^{\frac{1}{3}}$$

(6.32)

Comparing this result to results from FEM-analysis shows that the critical lamella stress can be predicted approximately, cf. Table 6.1. Stress rate and strain rate distributions are compared in Fig. 6.5 for $E_t = 1000\,[\text{Fl}^{-2}]$ and match qualitatively. Noticeable differences are the more rapid decay and a larger wavelength in the numerical results.

6.4 Conclusions

Stating an accurate analytical prediction for the buckling load for the general case of a hardening matrix is prevented by the complexity of the problem. Even the expression found for the limit case of an isolated lamella is very inaccurate. However, some conclusions about the qualitative behaviour can be made: It can be seen that a nonzero

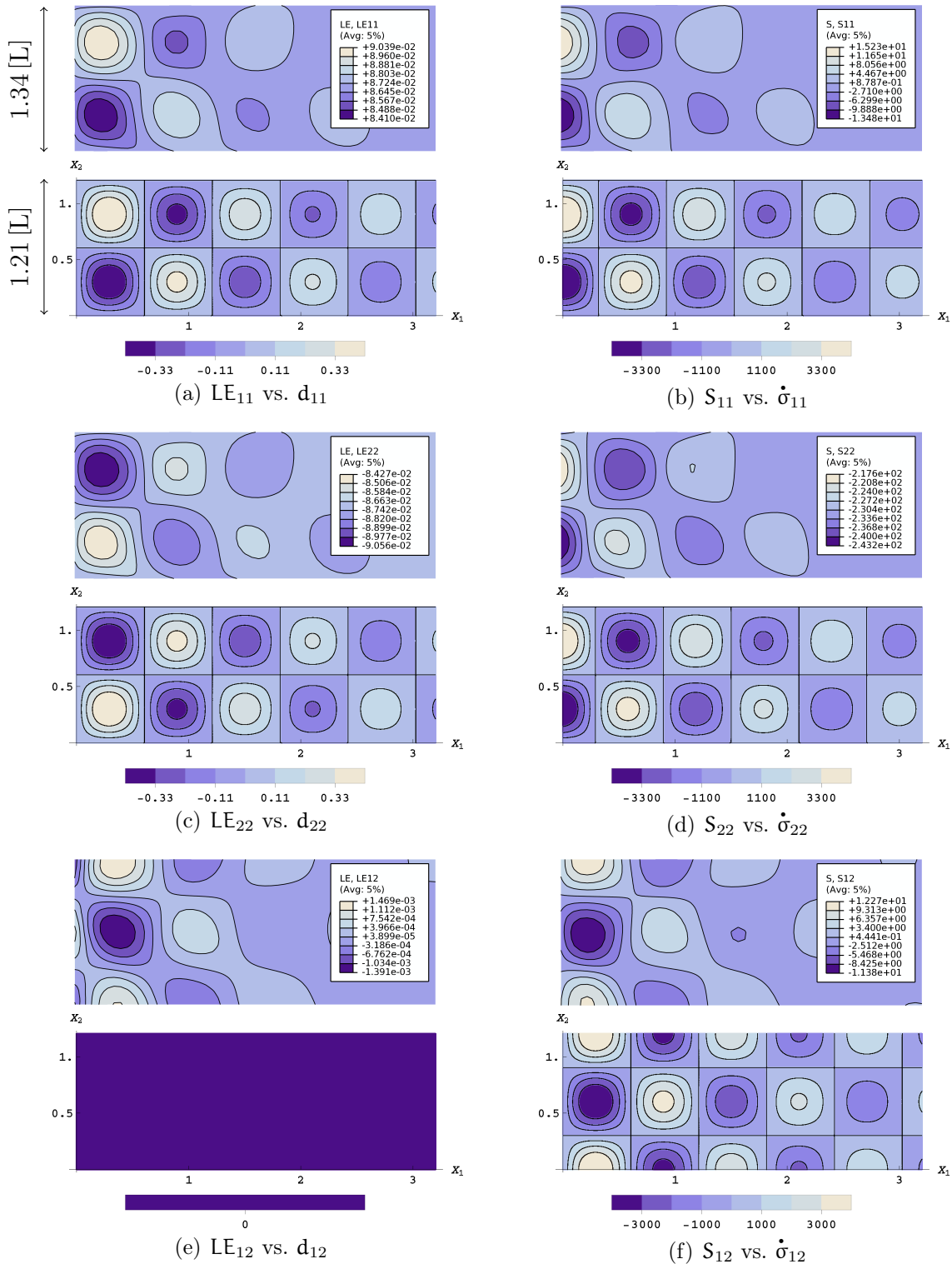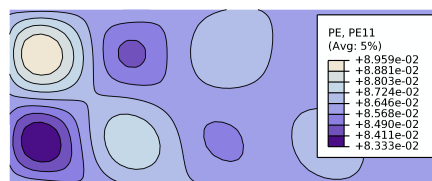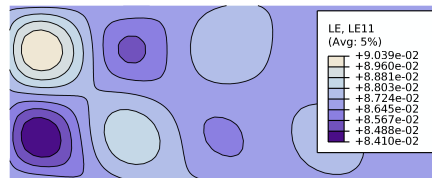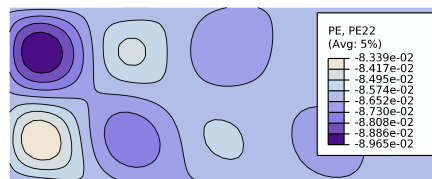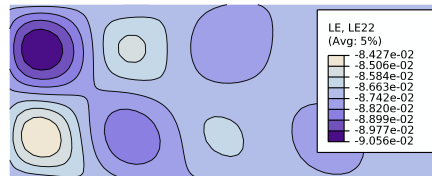Figure 6.5: Comparison of numerical(above) and analytical(below) strain rate distributions for $E_t = 1000\,[\mathrm{FL}^{-2}]$ along the slice marked in Fig. 6.4. Note that the scale is slightly different in the analytical and numerical results.
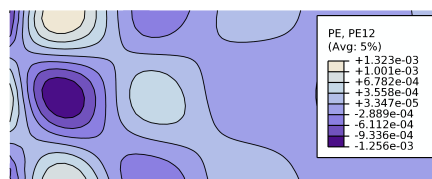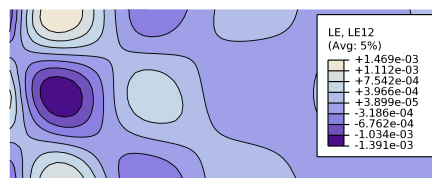
(a) LE$_{11}$ vs. PE$_{11}$

(b) LE$_{22}$ vs. PE$_{22}$

(c) LE$_{12}$ vs. PE$_{12}$

Figure 6.6: Comparison of total(above) and plastic(below) strain at the same instance as Figure 6.5. The strain state is dominated by plastic deformations

$E/1000$	E_t	$(\sigma^\alpha)^*$ by (6.32)	$(\sigma^\alpha)^*$ from FEM-analysis
200	500	-16782	-13490
200	1000	-21180	-17300
200	2000	-26778	-23850
200	5000	-36727	-38770

Table 6.1: Comparison of the approximate analytical prediction to results from FEM-analysis. Parameters other then E_t are given in Table 4.1. All numbers refer to the generic units $[\mathsf{FL}^{-2}]$.

tangent hardening modulus provides lateral support to the lamella and leads to a shorter buckling wavelength and a higher buckling load then ideal plasticity. It also constrains the wavelength to a finite value even if only an isolated lamella in an infinitely extending matrix is considered.

7 Appendix

7.1 Tensor analysis

First order tensors (vectors):

$$\underline{a} = \begin{bmatrix} a_1 \\ a_2 \end{bmatrix} = a_i \; \underline{e}_i \tag{7.1}$$

$$\underline{a} \cdot \underline{b} = \begin{bmatrix} a_1 & a_2 \end{bmatrix} \begin{bmatrix} b_1 \\ b_2 \end{bmatrix} = a_i b_j \; \underline{e}_i \cdot \underline{e}_j = a_i b_i \tag{7.2}$$

$$\underline{a} \otimes \underline{b} = \begin{bmatrix} a_1 \\ a_2 \end{bmatrix} \begin{bmatrix} b_1 & b_2 \end{bmatrix} = a_i b_j \; \underline{e}_i \otimes \underline{e}_j \tag{7.3}$$

Second order tensors:

$$\underline{\underline{a}} = \begin{bmatrix} a_{11} & a_{12} \\ a_{21} & a_{22} \end{bmatrix} = a_{ij} \; \underline{e}_i \otimes \underline{e}_j \tag{7.4}$$

$$\underline{\underline{a}} \cdot \underline{b} = \begin{bmatrix} a_{11} & a_{12} \\ a_{21} & a_{22} \end{bmatrix} \cdot \begin{bmatrix} b_1 \\ b_2 \end{bmatrix} = a_{ij} b_k \; \underline{e}_i \otimes \underline{e}_j \cdot \underline{e}_k = a_{ij} b_j \; \underline{e}_i \tag{7.5}$$

$$\underline{\underline{a}} : \underline{\underline{b}} = \begin{bmatrix} a_{11} & a_{12} \\ a_{21} & a_{22} \end{bmatrix} : \begin{bmatrix} b_{11} & b_{12} \\ b_{21} & b_{22} \end{bmatrix} = a_{ij} b_{kl} \; \underline{e}_i \cdot \underline{e}_j \otimes \underline{e}_k \cdot \underline{e}_l = a_{ij} b_{ij} \tag{7.6}$$

Fourth order tensors:

$$\underline{\underline{\underline{a}}} = \begin{bmatrix} \begin{bmatrix} a_{1111} & a_{1112} \\ a_{1121} & a_{1122} \end{bmatrix} & \begin{bmatrix} a_{1211} & a_{1212} \\ a_{1221} & a_{1222} \end{bmatrix} \\ \begin{bmatrix} a_{2111} & a_{2112} \\ a_{2121} & a_{2122} \end{bmatrix} & \begin{bmatrix} a_{2211} & a_{2212} \\ a_{2221} & a_{2222} \end{bmatrix} \end{bmatrix} = a_{ijkl} \; \underline{e}_i \otimes \underline{e}_j \otimes \underline{e}_k \otimes \underline{e}_l \tag{7.7}$$

$$\underline{\underline{\underline{a}}} : \underline{\underline{b}} = a_{ijkl} b_{mn} \; \underline{e}_i \otimes \underline{e}_j \otimes \underline{e}_k \cdot \underline{e}_m \otimes \underline{e}_l \cdot \underline{e}_n = a_{ijkl} b_{kl} \; \underline{e}_i \otimes \underline{e}_j \tag{7.8}$$

Differential operators:

$$\underline{\nabla} := \underline{\nabla}_{\underline{x}} = \begin{bmatrix} \dfrac{\partial}{\partial x_1} & \dfrac{\partial}{\partial x_2} \end{bmatrix}^\mathsf{T} \tag{7.9}$$

$$\underline{\Delta} := \underline{\nabla} \cdot \underline{\nabla} = \mathrm{div\,grad} = \frac{\partial^2}{\partial x_1^2} + \frac{\partial^2}{\partial x_2^2} \tag{7.10}$$

$$\underline{\Delta}\underline{\Delta} := \frac{\partial^4}{\partial x_1^4} + 2\frac{\partial^4}{\partial x_1^2 x_2^2} + \frac{\partial^4}{\partial x_2^4} \tag{7.11}$$

7.2 Index notation

$$\underset{\sim}{F} \quad = \sum_{i,j=1}^{3} \frac{\partial x_i}{\partial X_I} \underline{e}_i \otimes \underline{E}_I \overset{\text{index notation}}{\longrightarrow} F_{iI} \qquad (7.12)$$

$$\underset{\sim}{F}^{-1} = \sum_{I,j=1}^{3} \frac{\partial X_I}{\partial x_i} \underline{E}_I \otimes \underline{e}_i \overset{\text{index notation}}{\longrightarrow} F_{Ii}^{-1} \qquad (7.13)$$

$$\text{grad}(\underline{v}) = \sum_{i,j=1}^{3} \frac{\partial v_i}{\partial x_j} \underline{e}_i \otimes \underline{e}_j \overset{\text{index notation}}{\longrightarrow} v_{i,j} \qquad (7.14)$$

$$\text{Grad}(\underline{v}) = \sum_{i,J=1}^{3} \frac{\partial v_i}{\partial X_J} \underline{e}_i \otimes \underline{E}_J \overset{\text{index notation}}{\longrightarrow} v_{i,J} \qquad (7.15)$$

7.3 Homogeneous functions

A function $f(\underline{x})$ is said to be positive homogeneous of degree k if it satisfies the relation [Bartsch, 2001]:

$$\begin{aligned} &\alpha^k f(\underline{x}) = f(\alpha \underline{x}) \qquad &&\text{i.e.:} \quad \alpha^k f(x_1, \dots, x_n) = f(\alpha x_i, \dots, \alpha x_n) \\ &k \in \mathbb{R}, \ \alpha \in \mathbb{R}^+ && \end{aligned} \qquad (7.16)$$

Euler's theorem for a positive homogeneous function $f(x_1, \dots, x_n)$ of degree k states:

$$k \cdot f(\underline{x}) = \frac{\partial f}{\partial \underline{x}} \cdot \underline{x} \qquad \text{i.e.:} \quad k \cdot f(x_1, \dots, x_n) = \sum_{i=1}^{n} \frac{\partial f}{\partial x_i} x_i \qquad (7.17)$$

Bibliography

[Anthoine, 1995] Anthoine, A. (1995). Derivation of the in-plane elastic characteristics of masonry through homogenization theory. International Journal of Solids and Structures, 32(2):137 – 163.

[Bartsch, 2001] Bartsch, H.-J. (2001). Taschenbuch mathematischer Formeln. Fachbuchverl. Leipzig im Carl-Hanser-Verl., München ; Wien, 19., neu bearb. aufl. edition.

[Bažant and Cedolin, 2010] Bažant, Z. P. and Cedolin, L. (2010). Stability of structures : elastic, inelastic, fracture and damage theories. Hackensack, NJ : World Scientific.

[Böhm, 2004] Böhm, H. J. (2004). A short introduction to continuum micromechanics. In Böhm, H. J., editor, Mechanics of Microstructured Materials, volume 464 of International Centre for Mechanical Sciences, pages 1–40. Springer Vienna.

[Clemens et al., 2006] Clemens, H., Bartels, A., Bystrzanowski, S., Chladil, H., Leitner, H., Dehm, G., Gerling, R., and Schimansky, F. (2006). Grain refinement in gammatial-based alloys by solid state phase transformations. Intermetallics, 14(12):1380 – 1385.

[Daum et al., 2013] Daum, B., Dehm, G., Clemens, H., Rester, M., Fischer, F. D., and Rammerstorfer, F. G. (2013). Elastoplastic buckling as source of misinterpretation of micropillar tests. Acta Materialia, 61(13):4996 – 5007.

[Edalati et al., 2012] Edalati, K., Toh, S., Iwaoka, H., Watanabe, M., Horita, Z., Kashioka, D., Kishida, K., and Inui, H. (2012). Ultrahigh strength and high plasticity in tial intermetallics with bimodal grain structure and nanotwins. Scripta Materialia, 67(10):814 – 817.

[Hibbitt et al., 1997] Hibbitt, Karlsson, and Sorensen (1997). ABAQUS: Theory Manual, volume 2. Hibbitt, Karlsson and Sorensen.

[Hill, 1958] Hill, R. (1958). A general theory of uniqueness and stability in elastic-plastic solids. Journal of the Mechanics and Physics of Solids, 6(3):236 – 249.

[Hill, 1959] Hill, R. (1959). Some basic principles in the mechanics of solids without a natural time. Journal of the Mechanics and Physics of Solids, 7(3):209–225.

[Hill, 1978] Hill, R. (1978). Aspects of invariance in solid mechanics. In Yih, C.-S., editor, Advances in Applied Mechanics, volume 18 of Advances in Applied Mechanics, pages 1 – 75. Elsevier.

Bibliography

[Johnston, 1983] Johnston, B. G. (1983). Column buckling theory: historic highlights. Journal of Structural Engineering, 109(9):2086–2096.

[Kiener et al., 2009] Kiener, D., Motz, C., and G., D. (2009). Micro-compression testing: A critical discussion of experimental constraints. Materials Science and Engineering A, 505:79–87.

[Lee, 1981] Lee, E. (1981). Some comments on elastic-plastic analysis. International Journal of Solids and Structures, 17(9):859 – 872.

[Leine, 2010] Leine, R. (2010). The historical development of classical stability concepts: Lagrange, poisson and lyapunov stability. Nonlinear Dynamics, 59(1-2):173–182.

[Lubarda, 2002] Lubarda, V. A. (2002). Elastoplasticity Theory. CRC Press.

[Lubliner, 2008] Lubliner, J. (2008). Plasticity theory. Courier Dover Publications.

[Maruyama et al., 2004] Maruyama, K., Yamaguchi, M., Suzuki, G., Zhu, H., Kim, H. Y., and Yoo, M. (2004). Effects of lamellar boundary structural change on lamellar size hardening in tial alloy. Acta Materialia, 52(17):5185 – 5194.

[McMeeking and Rice, 1975] McMeeking, R. M. and Rice, J. (1975). Finite-element formulations for problems of large elastic-plastic deformation. International Journal of Solids and Structures, 11(5):601–616.

[Mendelson, 1968] Mendelson, A. (1968). Plasticity: theory and application. Macmillan series in applied mechanics. R.E. Krieger Pub. Co.

[Pahr, 2003] Pahr, D. H. (2003). Experimental and Numerical Investigations of Perforated FRP-Laminates. PhD thesis, Institute of Lightweight Structures and Aerospace Engineering, Vienna University of Technology.

[Petryk, 1985] Petryk, H. (1985). On energy criteria of plastic instability. Plastic Instability, Proc. Considere Memorial, pages 215–226.

[Petryk, 1991] Petryk, H. (1991). The energy criteria of instability in time-independent inelastic solids. Arch Mech, 43:519–545.

[Petryk, 1997] Petryk, H. (1997). Plastic instability: Criteria and computational approaches. Archives of Computational Methods in Engineering, 4:111–151.

[Petryk and Thermann, 1992] Petryk, H. and Thermann, K. (1992). On discretized plasticity problems with bifurcations. International Journal of Solids and Structures, 29(6):745 – 765.

[Rester et al., 2011] Rester, M., Fischer, F. D., Kirchlechner, C., Schmoelzer, T., Clemens, H., and Dehm, G. (2011). Deformation mechanisms in micron-sized pst tial compression samples: Experiment and model. Acta Materialia, 59:3313–3758.

Bibliography

[Srinivasa and Srinivasan, 2009] Srinivasa, A. R. and Srinivasan, S. M. (2009). Inelasticity of Materials. World Scientific Publishing Co. Pte. Ldt.

[Wu, 2004] Wu, H.-C. (2004). Continuum mechanics and plasticity. CRC Press.

[Zhang et al., 2006] Zhang, H., Schuster, B., Wei, Q., and Ramesh, K. (2006). The design of accurate micro-compression experiments. Scripta Materialia, 54(2):181 – 186.

Curriculum Vitae

Personal details:

Name	Benedikt Daum
Date of birth	October 6, 1980
Citizenship	Austrian

Education and professional development

09.1995 - 06.2000	HTL (Secondary College of Engineering) Anichstraße 26-28, 6020 Innsbruck; Specialization in mechanical engineering
02.2001 - 08.2001	Compulsory military service
11.2001 - 08.2005	Employed by Johann Rathgeber GmbH, Trientlgasse 45, 6020 Innsbruck
09.2005 - 10.2010	Diplomstudium (Master level studies) of mechanical engineering at the Graz university of technology
since 02.2011	Doctoral studies at the Vienna university of technology, employed as "Universitätsassistent" at the Institute of Lightweight Design and Structural Biomechanics from 02.2010 to 02.2015;